TUNABLE FEMTOSECOND PULSE GENERATION AND APPLICATIONS IN RAMAN MICRO-SPECTROSCOPY

A Dissertation

by

JIAHUI PENG

Submitted to the Office of Graduate Studies of
Texas A&M University
in partial fulfillment of the requirements for the degree of

DOCTOR OF PHILOSOPHY

August 2009

Major Subject: Physics

TUNABLE FEMTOSECOND PULSE GENERATION AND APPLICATIONS IN RAMAN MICRO-SPECTROSCOPY

A Dissertation

by

JIAHUI PENG

Submitted to the Office of Graduate Studies of
Texas A&M University
in partial fulfillment of the requirements for the degree of

DOCTOR OF PHILOSOPHY

Approved by:

Chair of Committee,	Alexei V. Sokolov
Committee Members,	Leonid V. Keldysh
	Christi K. Madsen
	George R. Welch
Head of Department,	Edward S. Fry

August 2009

Major Subject: Physics

ABSTRACT

Tunable Femtosecond Pulse Generation and Applications in Raman Micro-Spectroscopy.
(August 2009)
Jiahui Peng, B.S., Nankai University;
M.S., Shanghai Institute of Optics and Fine Mechanics, Chinese Academy of Science
Chair of Advisory Committee: Dr. Alexei V. Sokolov

The ability to perceive the dynamics of nature is ultimately limited by the temporal resolution of the instruments available. With the help of the ultrashort optical pulse, people now are able to observe and steer the electronic dynamics on the atomic scale. Meanwhile, high power attainable in such short time scale helps to boost the study of nonlinear physics.

Most commercial femtosecond lasers are based on Ti:sapphire, but such systems can only be tuned in a spectral range around 800 nm. Few applications need only a single wavelength in this spectral region and pulses tunable from the UV to the IR are highly desirable.

Based on the soliton characteristics of ultrashort laser pulses, we are the first ones who propose to make use of resonant dispersive waves, which are phase-matched non-solitonic linear waves, to extend the spectral tuning range of ultrashort laser without involving complicated amplifiers. Experimentally, we achieve the tuning of dispersive wave wavelengths by changing the dispersion parameters of the laser cavity, and confirm dispersive waves are ultrashort pulses under appropriate conditions. We successfully apply such a system into a multi-wavelength operation Ti:sapphire laser. The proposed idea is general, and can be applied to systems where solitons dominate, for example fiber lasers. Thanks to the newly developed novel fiber -photonic crystal fiber- we obtain widely tunable and gap-free femtosecond pulse by extending this mechanism to waveguides. This is the largest reported tuning range for efficient nonlinear optical frequency conversion obtained with such a simple and low energy laser.

We apply such a Ti:sapphire laser to Raman micro-spectroscopy. Because of the different temporal behaviors of the Raman process and other parametric processes, we can efficiently separate the coherent Raman signal from the unwanted background, and obtain a high chemical contrast and high resolution image. This high repetition rate and low energy laser oscillator makes it very suitable for biological Raman micro-spectroscopy, especially living samples for which damage is a big concern.

ACKNOWLEDGEMENTS

It is unforgettable experience for me of the studying in Texas A&M University. The unique people and unique culture of this university make these long seven years short. Since the first day I arrived Aggieland, I have been given lots help on both my research and my life. There are so many people to whom I am grateful.

I would like to thank my committee chair, Dr. A. V. Sokolov, for his guidance, help, and continuous support through the years, as my mentor and friend. I really appreciate the generous and kind help by my committee member, Dr. L. V. Keldysh offered to me. I feel lucky that I was able to learn physics from such a great physicist. I also want to thank my committee members Dr. C. K. Madsen and Dr. G. R. Welch for their guidance and support throughout the course of this research.

Thanks also go to my colleagues of the sub-femtosecond lab: A. Burzo, A. Churgreev, D. Pestov, L. Wang, X. Wang, and M. Zhi, for their help during my experiments. I would like to thank F. Zhu and Dr. A. Kolomenskii for the delightful cooperation. Some of the experiments done with F. Zhu are included in this dissertation. I also want to extend my gratitude to the department faculty and staff for making my time at Texas A&M University a great experience, especially S. Smith for her help on my degree work.

I feel delightful that I can spend wonderful time with my friends in these years, and I am in debt to them too: Y. Chang, C. Chen, M. Watabe and many others in Texas; M. Yuan, T. Yan and many others in China. There are also many friends in A&M I need to thank for helping me with my English, including my English teacher Mrs. Pulak.

Finally, thanks to my mother, father, sister and our big family for their encouragement and love.

TABLE OF CONTENTS

LIST OF FIGURES

FIGURE Page

FIGURE Page

FIGURE Page

FIGURE Page

FIGURE Page

1. INTRODUCTION

In 1878, spurred on by Leland Stanford, a former Governor of California and business man, to execute experiments to prove Stanford's claim that horse's hooves leave the ground at the same time during a trot, Eadweard J. Muybridge, an English photographer, successfully photographed a horse in fast motion using a series of twenty-four cameras. This is believed to be the birth of modern motion picture or movie which affects people's lives deeply. At the same time, this successful experiment also shows the basic idea to perceive the dynamics of nature. However this ability is ultimately limited by the temporal resolution of the instruments available.

Mechanical shutters allow for resolution in the millisecond range, whereas stroboscopic illumination allows us to probe the microsecond range. Modern electronic sampling oscilloscopes eventually brought the limit down into the picoseconds range. The advances in ultrafast optics have permitted the generation of light wave packets comprising only a single oscillation cycle of the electric and magnetic fields, and had the temporal resolution of measurements into the sub-femtosecond (1 femtosecond = 10^{-15} s) regime, allowing for the real time observation of electron dynamics in molecular and even atomic scale (1 attosecond = 10^{-18} s) [1],[2],[3].

Femtosecond lasers show not only great advantage in temporal resolution but also the high intensity they can achieve. With the same amount of energy being confined in short time duration, the peak power increases a lot. This high peak power leads to efficient nonlinear optics processes, such as Raman effect, two photon fluorescence etc., without damaging the sample. This high intensity but low energy makes femtosecond lasers suitable for nonlinear Raman spectroscopy of biology samples, especially living samples. Raman spectroscopy is one of the most powerful techniques of nonlinear spectroscopy, which has found numerous applications in condensed- and gas phase analysis, plasma diagnostics, investigation of molecular relaxation processes,

---

This dissertation follows the style of *Journal of the Optical Society of America*.

temperature and concentration measurements, condensed-phase studies, and femtochemistry, far from being limited to biological studies just mentioned here. Nowadays various kinds of Raman spectroscopy techniques have become a routine tool of modern optical experiments, giving rise to many successful engineering applications in modern physics, chemistry, and biology. “Similar to frequency-tunable sources of coherent radiation, which revolutionized nonlinear optics in its early days, allowing many delicate spectroscopic experiments, including nonlinear spectroscopic studies, to be performed, the impressive progress of femtosecond lasers in the 1990s has resulted in the breakthrough of the nonlinear Raman spectroscopy to new unexplored areas, giving rise to several elegant new ideas and approaches, permitting more-complicated systems and problems to be attacked, and leading to the measurements of fundamental importance.”[4],[5]

The femtosecond lasers with high repetition rates are also applied in high-capacity telecommunication systems, photonic switching devices, optical interconnections and for clock distribution. Recently, the broadband frequency combs have been used for high precision optical frequency metrology and medical diagnostics. The extreme concentration of energy in femtosecond pulses is also useful for material processing because much finer structures can be created in the absence of thermal interaction caused by longer pulses [6]. Moreover, with the using for reference of chirped Radar techniques to laser system, now the so called chirped pulse amplification technique can help to generate several hundred terawatts (TW, 10^{12} W) or even petawatts (PW, 10^{15} W) laser pulses [7]. These amplified ultra-high intensity laser systems are applicable in the research of relativity, nuclear physics and even cosmology in an optical lab. In 2011 the national Ignition Facility at Lawrence Livermore national Laboratory is expected to produce up to 1.8 MJ (750 TW) laser pulses, which will spur the study of inertial fusion and fusion/fission as clean, environmentally sustainable forms of energy [8].

At the same time, most of the femtosecond systems built nowadays are based on the Ti:sapphire crystal and the wavelength can only be tuned in the spectral range around

800 nm because the limitation of the gain spectrum. Few applications need only a single wavelength in this spectral region, but pulses tunable from the UV to the IR are highly desirable. The easiest way to obtain broadband tunability is to focus a high-energy ($E > 1\mu J$) pulse in a transparent material such as glass, water or sapphire. When the intensity reaches 10^{13}W/cm^2, the beam undergoes self-focusing and self-phase-modulation, and breaks up into small filaments, while the spectrum of each filament increases until the radiation becomes perfectly white. A continuous spectrum ranging from 200 nm to 1500 nm can then be produced. However the spectral density decreases rapidly when the wavelength is tuned away from the fundamental wavelength (800 nm). Moreover, the initial pulse energy of the input pulse is spread over the whole bandwidth, leading to small intensities in wavelength ranges far from the fundamental wavelength. Although supercontinuum generation is widely used and very versatile for probe pulses, it cannot in general provide a high enough energy per pulse in a reasonable bandwidth to be used to pump or trigger the phenomenon under study. Or, in order to obtain higher energies while keeping or even extending the tuning range, one must rely on parametric interactions in nonlinear crystals, which will also result in a complicated system and require more energy for this operation [9]. The system total efficiency is low: the standard pump laser is about 4 μJ and the output visible pulse is about 0.15 μJ [10]. Therefore a simple and efficient tunable femtosecond laser system is very appreciated in the ultrafast community.

The femtosecond laser pulse is strongly related with the optical soliton that the envelope of optical pulse does not change with the propagation in dispersion media. Optical solitons are now wildly applied in the telecommunications and the ultrashort lasers. When there is perturbation being acted on a soliton (e.g. by a localized loss in the fiber or modified parameters in the laser cavity), a soliton will reshape its form and shed the excess energy into dispersive waves (non-solitonic wave). From a practical viewpoint, the interaction between a soliton and a dispersive wave can be detrimental to applications not only by dissipating the energy, but also by affecting the performance of soliton-based telecommunication system, or by limiting the pulse duration in a soliton

laser. However, all the new frequencies generated in nonlinear process can be viewed as losses of original pump light. Then for the same reason all the nonlinear losses could be new frequency conversion methods as well. We will discuss the possibility to make use of the dispersive wave to generated tunable light. Meanwhile, with the ultrashort pulse duration kept in mind, we may also try to generate ultrashort laser pulses by this method.

In the following section, I will first give brief introductions to the femtosecond optics and necessary nonlinear optics, which are needed to discuss soliton laser for this dissertation. Then I will show the theoretical and experimental results of femtosecond dispersive wave generation in Ti:sapphire laser. This is the first attempt for people try to make use of dispersive waves. Next, I show how this idea is extended into femtosecond pulse generation in novel fibers, which gives more than octave spectral bandwidth tunability. To our knowledge, this is the largest reported tuning range for efficient nonlinear optical frequency conversion obtained with such a simple and low energy femtosecond laser. At the same time, our new experimental results point out that the mechanism for the supercontinuum generation in such novel fibers needs deeper studies. Later, I will present the results of applying such a simple laser system into coherent Raman micro-spectroscopy. At last, after summarizing the work, I will give some latest experimental results that indicate many new developments can be made based on this dissertation.

2. BASICS OF FEMTOSECOND OPTICS

The interest in ultrashort optical pulses begins with the invention of the laser and has been a continuous progress toward shorter and shorter time scales. Actually the earliest solid-state lasers were naturally pulsed, and the development of continuous wave lasers required significant additional effort [11]. The development of first from nanosecond pulses to picosecond pulses then to femtosecond pulses is busted by the emergence of many important applications mentioned in the introduction section including communication at ultrahigh data rates and probing of ultrafast physical, chemical, and biological phenomena, which require either ultrashort temporal duration or ultrahigh optical intensity [12].

An optical pulse is light with limited time duration, and can be described as $A(t) = E(t)e^{i\omega_0 t}$ in the time domain. In the spectrum domain, it is described as $A(\upsilon) = \int A(t)e^{-i2\pi\upsilon t}dt$. It is clearly shown here that they are a pair of Fourier transform. Because of the Fourier transform relation between $A(t)$ and $A(\upsilon)$, the spectral width is inversely proportional to the temporal width. The coefficient of the proportionality depends on both the pulse shape and the definition of width, which again is determined by the Fourier transform relation. If a femtosecond electrical pulse were to be generated, it would cover a spectral band of hundreds of THz, which equals the entire frequency range extending from 0 Hz to the edge of the visible band ($0.3\mu m$). Additionally, by virtue of the uncertainty principle $\Delta E \cdot \Delta t \geq h/2$, such a pulse would have an energy uncertainty exceeding $1.5\ eV$, *i.e.*, roughly the magnitude of the bandgap energy in typical semiconductors, which would make conventional electronics unreliable [12].

In a free-running laser, both longitudinal and transverse modes oscillate simultaneously without fixed mode-to-mode amplitude or phase relations. The resulted laser output is a time-averaged statistical mean value. Let us now consider a laser oscillating in a large number, N, of longitudinal modes with modes difference $\Delta\upsilon$.

Under ordinary circumstances, phases of these modes have random values, and, for continuous wave oscillation beam, intensity shows random temporal behavior. The output beam consists of a random sequence of light pulses. Despite this randomness, since these pulses arise from the sum of $A(\upsilon)$ frequency components evenly spaced in frequency domain, the pulse waveform has the following features which are characteristics of a Fourier series: 1) The waveform is periodic with a period $\tau_p = 1/\Delta\upsilon$. 2) Each light pulse of the random waveform has a duration $\Delta\tau_p$ roughly equal to $1/\Delta\upsilon_L$, where $\Delta\upsilon_L \simeq N\Delta\upsilon$ is the total oscillating bandwidth. Thus, for lasers with relatively large gain bandwidths, such as solid-state, dye, or semiconductor lasers, $\Delta\upsilon_L$ may be comparable large; hence short noise pulses with durations of picoseconds or less can be produced. However, in most cases it is the average value is monitored. Because the response time of a conventional photodetector is usually much longer than a few picoseconds, we cannot resolve this complex temporal behavior in the detected output of a random-phase, multimode laser. The output power is the sum of powers in the modes, hence is proportional to NA^2. This random phase will lead to noise-like signals that even with extremely large gain bandwidth, extremely short optical "pulses" or spikes can be generated, but there is no way to pick up or make use of such extremely short "pulse". Then the other key to have ultrashort pulses generated other than the broad bandwidth in spectrum domain, is a fixed phase relation [13],[14].

Suppose now that the oscillating modes, while still having equal or comparable amplitudes are somehow made to oscillate with some well-defined relation between their phases. Such a laser is referred to as mode locked, and the process by which modes are made to adopt a definite phase relation is referred as mode locking. We consider a simple case of $2n+1$ longitudinal modes oscillating with the same amplitude E_0, and assume that the phases φ_l of the modes in the output beam to be locked according to the relation $\varphi_l - \varphi_{l-1} = \varphi$. The total filed $E(t)$ of the wave at any given point in the output beam can be written as [14]:

$$E(t)=\sum_{-n}^{n}E_0 e^{i((\omega_0+l\Delta\omega)t+l\varphi)} \\ =E_0\cos\omega_0 t\left\{1+2\cos(\Delta\omega t+\varphi)+2\cos\left[2(\Delta\omega t+\varphi)\right]+\cdots+2\cos\left[n(\Delta\omega t+\varphi)\right]\right\}, \quad (2.1)$$

and making use of the relation of:

$$\cos\beta+\cos 2\beta+\cdots+\cos N\beta=\frac{\sin\left(\frac{1}{2}N\beta\right)\cos\left(\frac{1}{2}(N+1)\beta\right)}{\sin\left(\frac{1}{2}\beta\right)}. \quad (2.2)$$

The field in time domain will be expressed as:

$$A(t)=E_0\frac{\sin[(2n+1)\Delta\omega t/2]}{\sin(\Delta\omega t/2)}. \quad (2.3)$$

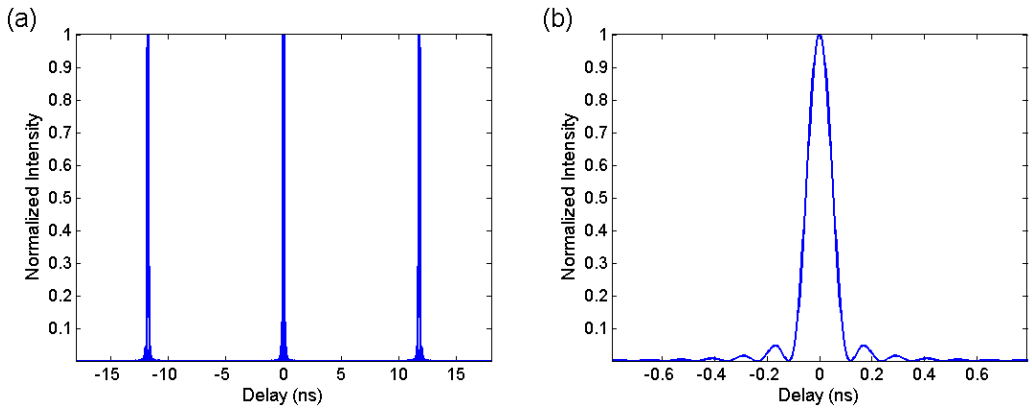

Fig. 2-1. The mode-locked pulses behavior in time domain: (a) the pulse trains with temporal seperations corresponding to the cavity round trip time (longitudinal mode separation); (b) the zoom in picture of a single pulse. Here, because we use a square function shape of the spectrum in the spectral domain, the pulse shape is its Fourier transformation in time domain.

Oscillating modes are seen to interfere so as to produce a train of evenly spaced light pulses. Pulse maxima occur when the denominator in Eq. (2.3) vanishes, and

$A = (2n+1)E_0$. The next pulse occurs when the denominator in Eq. (2.3) vanishes again, with the time delay:

$$\tau_p = \frac{2\pi}{\Delta\omega} = \frac{1}{\Delta\upsilon}, \tag{2.4}$$

where the $\Delta\upsilon$ is the frequency separation between two consecutive modes as mentioned earlier. Fig. 2-1 (a) shows clearly the behavior of mode locked pulse trains, and Fig. 2-1 (b) shows a closer look of the single pulse. For more realistic case, the spectral envelope is generally expected to have a bell shape, so a numerical factor that depends on the particular shape of the spectral intensity distribution needs to be applied on Eq. (2.4). Even so it won't change the main characteristics of mode locked laser pulse, and I show such an extremely short Gaussian pulse in Fig. 2-2. We learn from what discussed above that: under mode locked condition, the output beam consists of a train of mode locked pulses; the duration of each pulse is about equal to the inverse of the oscillation bandwidth; for the same number of oscillating modes and for the same field amplitudes, the ratio between the peak pulse power in the mode locked case and the average power in the non mode locked case is equal to the number, (2n+1), of oscillating modes. So that mode locking is thus useful not only for producing pulses of very short duration but also for producing high peak powers [13],[14]. Here, we have discussed about the mode-locking of longitudinal modes, but it does not mean that it is not doable for transverse modes. The transverse mode-locking was achieved too [15],[16],[17], however it is not suitable for ultrashort pulse generation due to the high loss the high order transverse modes suffering within the laser cavity [18],[19],[20].

Since we are talking about ultrashort optical pulses, and it is often useful to have a measure of the width of the pulse function. The width of a function of time $A(t)$ is its time duration and the width of its Fourier transform $A(\upsilon)$ is its spectral width (or bandwidth). However there is no unique definition for the width, a plethora of definitions are in use. All definitions, however, share the same property that the spectral width is inversely proportional to the temporal width, in accordance with the scaling

property of the Fourier transform. The following definitions are used at different places in the ultrafast optics community: root-mean-square (rms), power-equivalent width and the 1/e-, Half-Maximum, and 3-dB Widths [12],[13],[14]. The mostly encountered measure is the full-width at half-maximum (FWHM) and we talk a little bit more about its physical properties here just for the enough self-consistency for this dissertation.

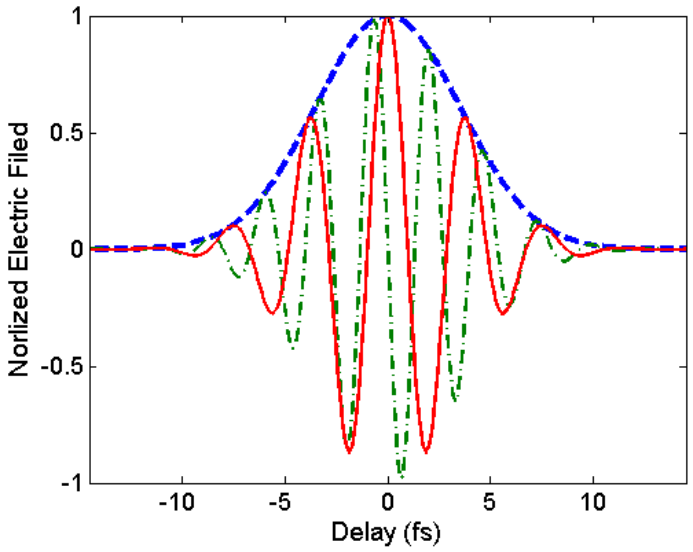

Fig. 2-2. A sample electronic field of the Gaussian pulse ($\Delta\tau_p$= 10 fs, λ= 800 nm): the blue dashed line is the Gaussian envelope, and red solid line and green dashed-dotted line is so called cosine and sine pulse respectively, because they show different phase compared with the peak of the envelope.

Again, in most cases the measured physical quantity is the intensity but not the field itself so our definitions are also related with the intensity not the real time filed itself, even though there is chance to picture the optical field now [21]. We obtain the special pulse function in time domain in previous discussion, see Eq. (2.3), because we assumed the certain spectral shape. In general, it is always needed to assume a pulse shape or spectrum shape before discussing the pulse duration. Meanwhile benefited from the good Fourier transformation characteristic and other important physical meanings, Gaussian pulse (or spectrum shape) is the most used, and we will give the example for this reason. We can therefore write the amplitude E_l of the l-th mode as:

$$E_l^2 = E_0^2 e^{-\left(2l\Delta\omega/\Delta\omega_L\right)^2 \ln 2}. \tag{2.5}$$

After we do the Fourier transformation, and will get:

$$A^2(t) \propto e^{-\left(2t/\Delta\tau_p\right)^2 \ln 2}, \tag{2.6}$$

where $\Delta\tau_p$ is the width (FWHM) of the pulse intensity and is give by:

$$\Delta\tau_p = \frac{2\ln 2}{\pi\Delta\upsilon_L} = \frac{0.441}{\Delta\upsilon_L}. \tag{2.7}$$

When the mode-locking condition holds, the field amplitude is given by the Fourier transform of the magnitude of the spectral amplitude. In such a case, the pulse width $\Delta\tau_p$ is related to the width of the laser spectrum $\Delta\upsilon_L$ by the relation $\Delta\tau_p = \beta_{TL}/\Delta\upsilon_L$, where β_{TL} is a numerical factor that depends on the particular shape of the spectral intensity distribution, *i.e.* the number of 0.441 in Eq. (2.7). A pulse of this sort is said to be transform-limited [14]. For the other pulse shapes, detailed information can be found in many references, *e.g.* Ref. [12].

Then, in practical how can we measure such short pulses? All the experiments I carry out in this dissertation are using the intensity autocorrelation method [22], but nowadays many advanced methods are developed, like frequency resolved optical gating (FROG) [23], spectral phase interferometry for direct electric field reconstruction (SPIDER) [24], and others (DOSPM [25], ENSTA [26], XPM [27], MIFROG [28], IAC Spectrum [29]) as well. However the basic idea is similar. The intensity autocorrelation is an attempt to measure the pulse's intensity vs. time. It's what results when a pulse is used to measure itself in the time domain, since it might be the fastest tool people can obtain. It involves splitting the pulse into two, variably delaying one with respect to the other, and spatially overlapping the two pulses in some instantaneously responding

nonlinear-optical medium, such as a second harmonic generation (SHG) crystal will produce light at twice the frequency of input light with a field that is given by

$$A_{signal}^{SHG} \propto I(t)I(t-\tau)\,. \tag{2.8}$$

Again, due to the slow reaction of the detector, only the average value can be obtained, then

$$A^{(2)}(\tau) = \int I(t)I(t-\tau)dt\,. \tag{2.9}$$

Like what we see above, this measurement result is pulse shape dependent. For the consistency again, we only give a general example of Gaussian pulse which is useful for the discussions in the later part of this dissertation, and more examples can be found in many reference as well [12],[23]. Suppose two Gaussian pulses overlap in time, and we can write (2.9) as:

$$\begin{aligned}
A^{(2)}(\tau) &= \int_{-\infty}^{\infty} f(t)g(t-\tau)dt \\
&\propto \int_{-\infty}^{\infty} e^{-\frac{t^2}{\Delta\tau_{p1}^2}} e^{-\frac{(t-\tau)^2}{\Delta\tau_{p2}^2}} dt = \int_{-\infty}^{\infty} e^{-\left(\frac{t^2}{\Delta\tau_{p1}^2}+\frac{(t-\tau)^2}{\Delta\tau_{p2}^2}\right)} dt \\
&= \int_{-\infty}^{\infty} e^{-\left(\frac{(\Delta\tau_{p1}^2+\Delta\tau_{p2}^2)t^2-2\Delta\tau_{p1}^2 t\tau+\Delta\tau_{p1}^2\tau^2}{\Delta\tau_{p1}^2\Delta\tau_{p2}^2}\right)} dt \\
&= \int_{-\infty}^{\infty} e^{-\left(\frac{(\Delta\tau_{p1}^2+\Delta\tau_{p2}^2)t^2-2\Delta\tau_{p1}^2 t\tau+(\Delta\tau_{p1}^4\tau^2)/(\Delta\tau_{p1}^2+\Delta\tau_{p2}^2)+\Delta\tau_{p1}^2\tau^2-(\Delta\tau_{p1}^4\tau^2)/(\Delta\tau_{p1}^2+\Delta\tau_{p2}^2)}{\Delta\tau_{p1}^2\Delta\tau_{p2}^2}\right)} dt \\
&= e^{-\frac{\tau^2}{\Delta\tau_{p1}^2+\Delta\tau_{p2}^2}} \int_{-\infty}^{\infty} e^{-\left(\frac{(\Delta\tau_{p1}^2+\Delta\tau_{p2}^2)t^2-2\Delta\tau_{p1}^2 t\tau+(\Delta\tau_{p1}^4\tau^2)/(\Delta\tau_{p1}^2+\Delta\tau_{p2}^2)}{\Delta\tau_{p1}^2\Delta\tau_{p2}^2}\right)} dt \\
&= e^{-\frac{\tau^2}{\Delta\tau_{p1}^2+\Delta\tau_{p2}^2}} \int_{-\infty}^{\infty} e^{-\left(\frac{\left(\sqrt{\Delta\tau_{p1}^2+\Delta\tau_{p2}^2}\,t-(\Delta\tau_{p1}^2\tau)/(\sqrt{\Delta\tau_{p1}^2+\Delta\tau_{p2}^2})\right)^2}{\Delta\tau_{p1}^2\Delta\tau_{p2}^2}\right)} dt \\
&\propto e^{-\frac{\tau^2}{\Delta\tau_{p1}^2+\Delta\tau_{p2}^2}} = e^{-\frac{\tau^2}{\Delta\tau_{correlation}^2}}\,.
\end{aligned} \tag{2.10}$$

We see that the correlation function keeps the Gaussian shape but with a parameter $\Delta\tau_{correlation}^2 = \Delta\tau_{p1}^2 + \Delta\tau_{p2}^2$. For the same pulse (autocorrelation situation), it is easy to see that $\Delta\tau_{correlation}^2 = 2\Delta\tau_p^2$, then $\Delta\tau_{correlation} = \sqrt{2}\Delta\tau_p$.

As just mentioned above, when ultra-broad-band gain media (bandwidth as large as 100 THz) are involved, dispersions (both the cavity dispersion and optics dispersion outside the cavity) will play an important role in establishing the shortest mode-locked pulse achievable and maintaining the pulse duration and intensity during the interaction with matters.

When light is propagating in materials, it is naturally suffering the dispersion and absorption which are intimately related. In most cases discussed in this dissertation, we neglect the absorption by material. However, dispersions are extremely important because we are dealing with ultrashort pulses, or in other words because of the extremely large bandwidth.

Consider first a plane, linearly polarized, monochromatic light at frequency ω, propagating along the z-direction in a transparent medium. The eclectic field $E(t,z)$ can be written as $E = A_0 e^{i(\omega t - \beta z)}$, where A_0 is the amplitude constant, ω is the angular frequency and β is the propagation constant which is frequency dependent. This shows that the phase front moves at a velocity

$$v_{ph} = \frac{dz}{dt} = \frac{\omega}{\beta}, \tag{2.11}$$

referred to as the phase velocity of light.

Consider a pulsed plane wave traveling in the z-direction through a lossless dispersive medium with refractive index $n(\omega)$. Assume that the initial complex wavefunction at $z = 0$ is $E = A(t)e^{i\omega_0 t}$, where ω_0 is the central angular frequency and $A(t)$ is the complex envelope of the wave. If the dispersion is weak, *i.e.*, if n varies slowly within the spectral bandwidth of the wave, then the complex wavefunction at a

distance z is approximately $E(z,t) = A(t - z/v_g)e^{i(\omega_0 t - \beta_0 z)}$. The parameter v_g, called the group velocity, is given by

$$v_g = \left(\frac{d\omega}{d\beta}\right)_{\beta=\beta_0} . \tag{2.12}$$

The proof of (2.12) relies on a Fourier decomposition of the envelope $A(t)$ into its constituent harmonic functions. Here I only give the results and more information about the proof is not crucial to this dissertation, which can be found in Ref. [12],[14] as well. Since the group velocity v_g itself is often frequency dependent, different frequency components of the pulse undergo different delays $\tau = z/v_g$. As a result, the pulse spreads in time. This phenomenon is known as group velocity dispersion (GVD). It is just custom reason that the term GVD most mentioned in the ultra-fast optics literatures. On the other hand, the group delay dispersion (GDD) is more important and sometimes holds the true physics meaning, especially in the ultrashort laser system where there are more than one optical elements involved and the optical path for different wavelength may vary. Then for convenient and practical reason, we focus on the system total delay in stead of individuals. If the relation between system total phase ϕ and frequency ω in the frequency range can be approximated by a Taylor expansion:

$$\phi = \phi_0 + \left(\frac{d\phi}{d\omega}\right)_{\omega_0}(\omega-\omega_0) + \frac{1}{2}\left(\frac{d^2\phi}{d\omega^2}\right)_{\omega_0}(\omega-\omega_0)^2 + \frac{1}{3!}\left(\frac{d^3\phi}{d\omega^3}\right)_{\omega_0}(\omega-\omega_0)^3 + \cdots \tag{2.13}$$

In the same way, the dispersion relation between propagation constant and frequency is

$$\beta = \beta_0 + \left(\frac{d\beta}{d\omega}\right)_{\omega_0}(\omega-\omega_0) + \frac{1}{2}\left(\frac{d^2\beta}{d\omega^2}\right)_{\omega_0}(\omega-\omega_0)^2 + \frac{1}{3!}\left(\frac{d^3\beta}{d\omega^3}\right)_{\omega_0}(\omega-\omega_0)^3 + \cdots \tag{2.14}$$

As we all know that the requirement for such expansion is that the quantity $|\omega-\omega_0|$ is small. However, it is still valid for broad bandwidth femtosecond pulse in many cases [30]. We are already familiar with the group velocity $v_g=\left(1\Big/\frac{d\beta}{d\omega}\right)_{\omega_0}$ and the group delay $\tau_g=\left(\frac{d\phi}{d\omega}\right)_{\omega_0}$, the GDD $\left(\frac{d^2\phi}{d\omega^2}\right)_{\omega_0}$, the GVD $\left(\frac{d^2\beta}{d\omega^2}\right)_{\omega_0}$. The higher order terms correspond to the specific order coefficients of the GDD and GVD, for example some terms we will meet later: the third-order dispersion (TOD or 3OD) $\phi'''=\beta'''l$ (l is the propagation length in the dispersive media) and forth-order dispersion (FOD or 4OD). We see the dispersion terms are proportional to the powers of bandwidth, and they will play more and more important roles with larger bandwidth. Meanwhile the higher order terms will play a pulse-limiting role for shorter pulse, and they are important both in and out of the cavity when short femtosecond pulses are propagating through it.

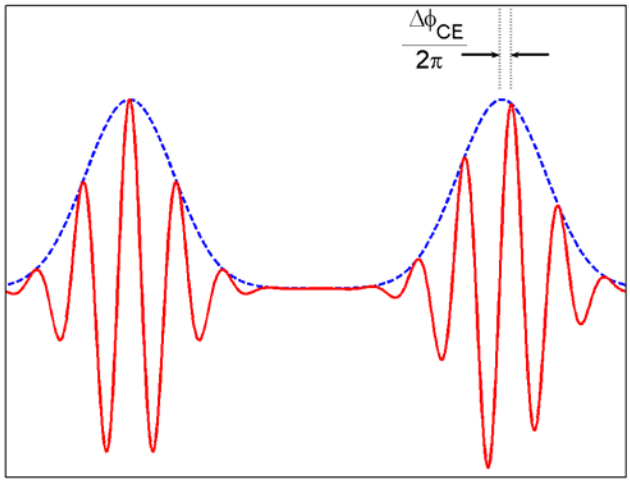

Fig. 2-3. The carrier-envelope phase changes from one pulse to another in the pulse train, because of the difference between phase velocity and group velocity.

As it is shown in Fig. 2-2, if there is the phase difference between of the carrier and envelope, then the real optical filed shows differently in time domain, especially for a very short pulse. The phase difference of the optical carrier and the envelope peak is

called carrier-envelope phase (sometime it is called absolute phase too), shown in Fig. 2-3. This phase is well defined only for pulses that are sufficiently short comparable to the time period of a single optical cycle of the carrier.

As we have assume that the *l*-th mode frequency is $\omega_0 + l\Delta\omega$, we may think that in order to be allowed to oscillator in the cavity the $\omega_0 + l\Delta\omega = m\Delta\omega + 2\pi\delta$, m is an integer, and δ is called offset frequency. Then the carrier-envelope phase will be

$$\Delta\phi_{CE} = -(2\pi)^2 \delta / \Delta\omega . \tag{2.15}$$

For a mode locked laser, we can assume the total GVD is zero otherwise the pulse will spread. In that case,

$$\frac{d\beta}{d\omega} = \frac{1}{v_g} = \text{constant} , \tag{2.16}$$

and we also know $\beta(\omega)$ is function of frequency, so

$$\beta = \beta_{\text{constant}} + \frac{1}{v_g}\omega . \tag{2.17}$$

Since $n = c\beta/\omega$, it yields:

$$n = c\left(\frac{1}{v_g} + \frac{\beta_{\text{constant}}}{\omega}\right). \tag{2.18}$$

Then

$$\begin{aligned} \omega_m &= m\frac{2\pi c}{nL} = m\frac{2\pi c\omega}{c\beta L} = m\frac{2\pi\omega}{\beta L} = m\frac{2\pi}{\beta L}\left(\beta v_g - \beta_{\text{constant}} v_g\right) \\ &= m\frac{2\pi}{L}v_g - \beta_{\text{constant}} v_g \end{aligned} . \tag{2.19}$$

We know that $2\pi v_g / L = \Delta\omega$, and then it shows clearly that the oscillating modes frequencies are not integer times of $\Delta\upsilon$ ($\delta \neq 0$), but there is actually an offset frequency when the dispersion in *n* is included. And this offset frequency is

$$\delta = \frac{\omega_c v_g}{2\pi}\left(\frac{1}{v_g} - \frac{1}{v_{ph}}\right). \tag{2.20}$$

This makes the connection between the offset frequency and the difference between group and phase velocities inside the laser cavity [31]. More details can be found in Ref. [32].

For most common optical media, they show positive GDD or GVD. So, the compensation of the GDD requires a suitable element providing a negative GDD, *e.g.*, showing anomalous dispersion. Naturally, the anomalous GVD is accomplished with strong absorption, so that it is more practical to introduce negative GDD instead of GVD. However, as we mentioned earlier, these two terms are sometimes not strictly distinguished by the society.

The general scheme of dispersion compensation (or pulse compression) is the following. The input pulse is first injected into a phase modulator, which broadens the pulse spectrum imposing a frequency sweep (in time). The spectrally broadened and chirped pulse is sent in a dispersive delay line, which rephases all the new frequency components generated by the phase modulation. Ideally, the dispersive delay line would introduce the opposite chirp on the pulse, thus resulting in the compression of the pulse to its minimum width, $\sim \Delta\tau_p = \beta_{TL} / \Delta\upsilon_L$. This general scheme for compression of optical pulses was proposed independently by Gires and Tournois in 1964 [33] and Giordmaine *et al*. in 1968 [34]. In this dissertation, I have only either ultra-broad bandwidth obtained by Kerr mode-locking or supercontinuum generation in microstructure fibers to be introduced later. Then we need only concentrate on the method to achieve the negative GDD or the dispersion compensation saying in a more general way. More general methods can be found in well organized literatures, for

instance Ref. [35]. In 1968, Treacy demonstrated, for the first time, the use of a pair of diffraction gratings to achieve negative GDD [36]. In 1984, Fork *et al.* obtained a negative GDD by using pairs of Brewster-angled prisms [37], which have been widely used for dispersion control inside laser cavities since they introduce much less loss than others. In both optical systems, the origin of the adjustable dispersion is the angular dispersion that arises from diffraction and refraction, respectively. The dispersion introduced by these systems can be easily calculated by calculating the phase accumulated between the input and output reference planes [35]. More recently, advances in the design of multilayer coatings [38] led to the demonstration of chirped mirrors providing ultra-broadband dispersion control with low losses and the capability of handling high laser intensity [35]. The prism pair has two parts of dispersion: the geometry dispersion and the material dispersion. In most cases, the separation between the two prisms is fixed so that people do not have freedom to change the geometry dispersion. However people are always free to change the material dispersion by adjusting the amount the prism the light goes through. It is because the prism is positioned at the laser beam falling on the minimum deviation angle, then the laser beam won't be shifted by moving the prism along the center line. In this way people are able to control the amount of total dispersion introduced into the optical pulse, and obtain the desired pulse duration easily. The prism pair method has benefit in the low loss and the easy to control, and it is the only one being used in all experiments discussed in this dissertation.

With broad gain bandwidth material, mode locking and dispersion compensation all working together, people can obtain extremely short laser pulses. There are many mode locking methods and gain material, but the laser most actively explored for ultrashort pulse generation is Kerr lens mode locked Ti:sapphire laser. This laser has the largest gain bandwidth and is therefore capable of producing the shortest pulses; it also provides the widest wavelength tunability. We will touch this point in later sections. Typically, the Ti:sapphire crystal is pumped by a diode-pumped, frequency-doubled Nd:YAG laser in order to create an all-solid-state source [39].

3. BASICS OF NONLINEAR OPTICS

"Physics would be dull and life most unfulfilling if all physical phenomena around us were linear. Fortunately, we are living in a nonlinear world. While linearization beautifies physics, nonlinearity provides excitement in physics. Nonlinear effects in electricity and magnetism have been known since Maxwell's time. Saturation of magnetization in a ferromagnet, electrical gas discharge, rectification of radio waves, and electrical characteristics of p-n junctions are just a few of the familiar examples. In the optical region, however, nonlinear optics became a subject of great common interest only after the laser was invented. It has since contributed a great deal to the rejuvenation of the old science of optics." [40]

It is generally believed that the SHG experiment of Franken *et al.* [41] marked the birth of the field of nonlinear optics, even though some nonlinear optical phenomena had been observed long before that, for instance Raman [42] and optical pumping process [43]. In Franken's experiment, they propagated a ruby laser beam at 694.2 nm through a quartz crystal and observed ultraviolet radiation from the crystal at 347.1 nm. The idea was simple. Harmonic generation of electromagnetic waves at low frequencies had been known for a long time. Harmonic generation of optical waves follows the same principle and should also be observable [40],[44]. An ordinary light source is far too weak for such an experiment, so that it was achieved only after the first laser came true in 1960 [11]. Nonlinear optical phenomena are "nonlinear" in the sense that they occur when the response of a material system to an applied optical field depends in a nonlinear manner upon the strength of the optical field. For example, the SHG just mentioned occurs as a result of the part of the atomic response that depends quadratically on the strength of the applied optical field. Consequently, the intensity of the light generated at the SHG tends to increase as the square of the intensity of the applied laser light [44].

Since light is electromagnetic wave, the behavior of light will be governed by Maxwell's equations (For historical reason most nonlinear optics literatures are written in Gaussian units instead of SI Unit, for examples [45],[46],[47]. Here I would follow

them, but nowadays more and more literatures are switched to SI unit including the new edition of Ref. [44].):

$$\nabla \cdot \vec{D} = 4\pi\rho\,, \tag{3.1}$$

$$\nabla \cdot \vec{B} = 0\,, \tag{3.2}$$

$$\nabla \times \vec{E} = -\frac{1}{c}\frac{\partial \vec{B}}{\partial t}, \tag{3.3}$$

$$\nabla \times \vec{H} = \frac{1}{c}\frac{\partial \vec{D}}{\partial t} + \frac{4\pi}{c}\vec{J}\,. \tag{3.4}$$

We are primarily interested in the solution of these equations in regions of space that contain no free charges, so that $\rho = 0$, and that contain no free currents, so that $\vec{J} = 0$. We assume that the material is nonmagnetic so that $\vec{B} = \vec{H}$. However, we allow the martial to be nonlinear in the sense that the fields $\vec{D}$ and $\vec{E}$ are related by

$$\vec{D} = \vec{E} + 4\pi\vec{P}\,, \tag{3.5}$$

where in general the polarization vector $\vec{P}$ depends nonlinearly upon the local value of the electric field strength $\vec{E}$. After proceeding the derive of the optical wave equation in the usual manner: taking the curl of the curl-$\vec{E}$ Maxwell equation (3.3), interchange the order of space and time derivatives on the right-hand side of the resulting equations, and using the assumption we made, we will be able to obtain

$$-\nabla^2\vec{E} + \frac{1}{c^2}\frac{\partial^2}{\partial t^2}\vec{E} = -\frac{4\pi}{c^2}\frac{\partial^2\vec{P}}{\partial t^2}\,. \tag{3.6}$$

It is often convenient to split $\vec{P}$ into its linear and nonlinear parts as

$$\vec{P} = \vec{P}^{(1)} + \vec{P}^{NL}, \tag{3.7}$$

and we introduce a frequency-dependent dielectric tensor $\varepsilon^{(1)}$ so that

$$\begin{aligned} \vec{D} &= \vec{D}^{(1)} + 4\pi\vec{P}^{NL} \\ \vec{D}^{(1)} &= \vec{E} + 4\pi\vec{P}^{(1)} = \varepsilon^{(1)} \cdot \vec{E} \end{aligned}. \tag{3.8}$$

Then, (3.6) can be rewritten as

$$-\nabla^2\vec{E} + \frac{\varepsilon^{(1)}}{c^2} \cdot \frac{\partial^2\vec{E}}{\partial t^2} = -\frac{4\pi}{c^2}\frac{\partial^2\vec{P}^{NL}}{\partial t^2}. \tag{3.9}$$

In this proceeding I omit a term of $\nabla(\ln\varepsilon)$, which is negligible in most cases but may show important effects on waveguides with microstructures comparable with wavelength of electromagnetic wave. It will be given more detailed discussion in the later part of the dissertation. The $\vec{P}^{NL}$ term acts as a source term which couples different frequencies electromagnetic waves together, in that way the electromagnetic wave propagation is no longer linear process. Either new frequencies can be generated, like SHG, optical parametric generation (OPG) *etc*, or the propagation characters can be changed or affected by the waves, like self-phase modulation (SPM), cross-phase modulation (XPM), optical conjugate, *etc*.

Because of the nonlinearity, lots interesting phenomena will stand out when the laser intensity is high enough and the material holds good nonlinear susceptibility. This makes the optics more colorful. Optical soliton is one of these nonlinear effects, which plays important role nowadays in optical communications and ultrafast optics as mentioned in the previous section.

Solitons are localized concentrations of field energy, resulting from a balance of dispersive and nonlinear effects. They are ubiquitous in the natural sciences. The very first observation of soliton was made in 1834 by the hydrodynamic engineer John Scott Russell while he was riding his horse along a canal near Edinburgh, when a barge

abruptly stopped he was struck by the sight of what he called “the great solitary wave”, that he followed for a few miles before losing it in the meanders of the canal. He wrote in his report (this part has been cited in many books and papers) [48]:

> I was observing the motion of a boat which was rapidly drawn along a narrow channel by a pair of horses, when the boat suddenly stopped—not so the mass of water in the channel which it had put in motion; it accumulated round the prow of the vessel in a state of violent agitation, then suddenly leaving it behind, rolled forward with great velocity, assuming the form of a large solitary elevation, a rounded, smooth and well-defined heap of water, which continued its course along the channel apparently without change of form or diminution of speed. I followed it on horseback, and overtook it still rolling on at a rate of some eight or nine miles an hour, preserving its original figure some thirty feet long and a foot to a foot and a half in height. Its height gradually diminished, and after a chase of one or two miles I lost it in the windings of the channel. Such, in the month of August 1834, was my first chance interview with that singular and beautiful phenomenon which I have called the Wave of Translation.

Unfortunately, the criticizing made by two great scientists Sir G. B. Airy and G. G. Stokes resulted him in turning his research into other fields. After 161 years, in 1995 the solitary wave was created again in the Union Canal near Edinburgh with first failure in 1985 [48]. Optical soliton was first obtained experimentally in 1980 [49], even though the theoretical researches were much earlier than that [50]. One thing needs to be pointed out is that the optical soliton is different from the hydrodynamic soliton (the nontopological soliton) originally observed by Russell. Optical soliton is a “wave packet” that behaviors like soliton. This kind of soliton is made of a carrier wave modulated by an envelope signal and this is the reason that it is named “envelope soliton” [48]. We have seen in previous section that even though the soliton’s envelope does not change along the propagating, the real electromagnetic field is change along the propagation with time.

The predominant nonlinear optical process for optical soliton is SPM, which is the phase changing of an optical pulse resulted from the nonlinearity of the refractive index of the medium. First, consider the propagation of the optical pulse

$$E(z,t) = A(z,t)e^{i(k_0 z - \omega_0 t)} \tag{3.10}$$

through a medium characterized by a nonlinear refractive index of the sort

$$n(t) = n_0 + n_2 I(t), \tag{3.11}$$

where $I(t) = \left(n_0 c/2\pi\right)\left|A(z,t)\right|^2$. Note that for the present we are assuming that the medium can respond essentially instantaneously to the pulse intensity. We also assume the nonlinear medium is sufficiently short that no reshaping of the optical pulse can occur within the medium; the only effect of the medium is to change the phase of the transmitted pulse by the amount

$$\phi_{Kerr}(t) = -n_2 I(t)\omega_0 L / c. \tag{3.12}$$

If we assume the slowly varying field amplitude $A(z,t)$ in terms of its spectral component as

$$A(z,t) = \int A(z,\omega)e^{-i\omega t}\, d\omega/2\pi, \tag{3.13}$$

and $E(z,\omega)$ and $A(z,\omega)$ are related by

$$E(z,\omega) \simeq A(z,\omega-\omega_0)e^{ik_0 z}. \tag{3.14}$$

In terms of the quantity $A(z,\omega)$ (the slowly varying field amplitude in the frequency domain) the wave equation (3.9) becomes:

$$\frac{\partial^2 A}{\partial z^2} + 2ik_0 \frac{\partial A}{\partial z} + \left[k^2(\omega) - k_0^2 \right] A = -\frac{4\pi\omega^2}{c^2} P^{NL}(z,\omega) e^{-ik_0 z}. \qquad (3.15)$$

Where

$$k^2(\omega) = \varepsilon(\omega)(\omega^2/c^2). \qquad (3.16)$$

We approximate $k(\omega)$ as a power series in the frequency difference $\omega - \omega_0$, then plug in equation (3.16) to get:

$$k^2(\omega) = k_0^2 + 2k_0 k_1(\omega - \omega_0) + 2k_0 D_\omega + 2k_1 D_\omega + k_1^2(\omega - \omega_0)^2 + D_\omega^2, \qquad (3.17)$$

where $D_\omega = \sum_{n=2}^{\infty} \frac{1}{n!} k_n (\omega - \omega_0)^n$. Then we plug into equation (3.15) to obtain the wave equation:

$$\begin{aligned} \frac{\partial^2 A}{\partial z^2} + 2ik_0 \frac{\partial A}{\partial z} + \left[2k_0 k_1(\omega - \omega_0) + 2k_0 D_\omega + 2k_1 D_\omega(\omega - \omega_0) + k_1^2(\omega - \omega_0)^2 \right] A \\ = -\frac{4\pi\omega^2}{c^2} P^{NL}(z,\omega) e^{-ik_0 z} \end{aligned}. \qquad (3.18)$$

Where I have dropped the contributions of D_ω^2 because it is small in most cases, and we will talk about its effects later. We now convert this expression into the wave equation in time domain. To do so, we multiply equation by $\exp\left[-i(\omega - \omega_0)t \right]$ and integrated over all values of $\omega - \omega_0$.

$$\begin{aligned} \left[\frac{\partial^2}{\partial z^2} + 2ik_0 \left(\frac{\partial}{\partial z} + k_1 \frac{\partial}{\partial t} \right) + 2ik_1 D \frac{\partial}{\partial t} + 2k_0 D - k_1 \frac{\partial^2}{\partial t^2} \right] A(r,t) \\ = \frac{4\pi}{c^2} \frac{\partial^2 P^{NL}(r,t)}{\partial t^2} e^{-i(k_0 z - \omega_0 t)} \end{aligned}, \qquad (3.19)$$

where $D = i\sum_{m=2}^{\infty} \frac{k_m}{m!}\left(i\frac{\partial}{\partial t}\right)^m$. With the slow varying envelope approximation $\frac{\partial^2}{\partial z^2} \ll ik_0 \frac{\partial}{\partial z}$, and the transform of the retarded frame by $z' = z$ and $\tau = t - z/v_g = t - k_1 z$, *i.e.*

$$\begin{aligned} \frac{\partial}{\partial z} &= \frac{\partial}{\partial z'} - k_1 \frac{\partial}{\partial \tau} \\ \frac{\partial}{\partial t} &= \frac{\partial}{\partial \tau} \end{aligned}, \tag{3.20}$$

we obtain the new wave equation

$$\left[2ik_0 \frac{\partial}{\partial z'} + 2k_0 D\right] A(r,t) = \frac{4\pi\omega_0^2 P^{NL}(r,t)}{c^2}. \tag{3.21}$$

In many cases, when optical pulse propagates in fiber the lowest nonlinearity is third order, because of the isotropic structure. Then $P^{NL} = 3\chi^{(3)}|A|^2 A$, and we plug into the equation (3.21). We omit higher order dispersion terms again, and the equation will read as:

$$\frac{\partial A}{\partial z'} + \frac{1}{2} ik_2 \frac{\partial^2 A}{\partial \tau^2} = i\frac{6\pi\omega_0}{n_0 c}\chi^{(3)}|A|^2 A. \tag{3.22}$$

Compare with the expansion of k and equation (2.14), they have same expression and physics meaning, as discussed in previous section. In most cases equation (3.22) is written the way below and is called as the nonlinear Schrödinger equation (NSE):

$$\frac{\partial A}{\partial z'} + \frac{1}{2} i\beta_2 \frac{\partial^2 A}{\partial \tau^2} = i\gamma|A|^2 A. \tag{3.23}$$

From the NSE (3.23), we see that it is possible for the effects of GVD to compensate (or balance) the effects of SPM, and optical pulses can propagate through a dispersive, nonlinear optical medium with an invariant shape. Such pulses are known as temporal optical solitions. A fundamental soliton of the simplified NES

$$i\frac{\partial u}{\partial \xi}+\frac{1}{2}\frac{\partial^2 u}{\partial \tau^2}+|u|^2 u=0, \tag{3.24}$$

can be described as $u_{sol}^0(z,t)=A\sec h(At)\exp(ik_{sol}z)$, where $k_{sol}=\frac{A^2}{2}$, the soliton solution. At the same time, linear plane waves are also solutions of this equation. Now let's involve the parts of high order dispersion in equation (3.24)

$$i\frac{\partial u}{\partial \xi}+\frac{1}{2}\frac{\partial^2 u}{\partial \tau^2}-i\zeta\frac{\partial^3 u}{\partial \tau^3}+\eta\frac{\partial^4 u}{\partial \tau^4}+|u|^2 u-\gamma u\frac{\partial}{\partial \tau}\left(|u|^2\right)=0. \tag{3.25}$$

If solitons are formed under such conditions, they will suffer the perturbation of high order dispersions. Solitons will reshape their forms, and energies may be transferred to some phase matched dispersive (nonsolitonic) waves [51],[52]. The linear dispersion relation corresponding to the equation (3.25) with omitting the TOD by substituting into $e^{i(k_{lin}z+\omega t)}$, is

$$k_{lin}(\omega)=-\frac{1}{2}\omega^2+\eta\omega^4=\frac{A^2}{2}. \tag{3.26}$$

Here, I omit the TOD term only because all the experiments I carried in this dissertation are related with a strong FOD term. Actually, in most cases it is the TOD term dominates the perturbation. To the lowest order in η, the resonant frequency is

$$\omega_0=\frac{1}{\sqrt{2\eta}}\left[1+\left(A\sqrt{\eta}\right)^2+O\left(\left(A\sqrt{\eta}\right)^4\right)\right]. \tag{3.27}$$

We see in case of only 4OD, there are two spectrally symmetric frequencies $+\omega_0$ and $-\omega_0$ sharing same wave vector with soliton. During the study for the conventional fibers, researches found that the perturbation by high order dispersion was small so that energy transferred from soliton to dispersive wave should be negligible [52]. Later in this dissertation, we will show that in some circumstances this phenomenon can be strong. In the discussion above, we obtain the NSE in a simple way, but a stricter derivation can be found in Ref. [48] and [53].

Until now, I only give one example of the nonlinear process -SPM, but the nonlinear optics is much richer than that. I cannot give a full picture of nonlinear optics here, but I want to briefly talk about the groups of the phenomena. SPM is an example of what called as parametric process. “The origin of this terminology is obscure, but the word parametric has come to denote a process in which the initial and final quantum-mechanical states of the system are identical. Consequently, in a parametric process population can be removed from the ground state only for those brief intervals of time when it resides in a virtual level. According to the uncertainty principle, population can reside in a virtual level for a time interval of the order of $T_1/\delta E$, where δE is the energy difference between the virtual level and the nearest real level. Conversely, processes that do involve the transfer of population from one real level to another are known as non-parametric processes. One difference between parametric and nonparametric processes is that parametric processes can always be described by a real susceptibility; conversely, nonparametric processes are described by a complex susceptibility. Another difference is that photon energy is always conserved in a parametric process; photon energy need not be conserved in a nonparametric process, because energy can be transferred to or from the material medium. As a simple example of the distinction between parametric and non-parametric processes, we consider the case of the usual (linear) index of refraction. The real part of the refractive index is a consequence of parametric processes, whereas its imaginary part is a consequence of nonparametric processes, since the imaginary part of the refractive index describes the

absorption of radiation, which results from the transfer of population from the atomic ground state to an excited state." [44]

Many nonlinear processes are parametric processes, like we mentioned SHG, SPM, sum- and difference- frequency generation, OPG (including up conversion and down conversion), and so on (The term "parametric" is following the Ref. [44]. One notable physicist, Leonid V. Keldysh points out it might not be the best one to be used here, but the physics processes are clearly explained as above). At the same time, processes like saturable absorption, two-photon absorption and stimulated Raman scattering are good examples of non-parametric ones. However, this kind of separation is just a classification in terminology. In the real physics processes, both kinds of processes are involved and may interact with each other as well. The coherent anti-Stokes Raman scattering (CARS) is a good example of this. In most cases, this temporal difference between the tow processes may not that notable. However with the help of femtosecond laser, its difference starts showing out. Later in this dissertation, we will discuss more how to separate the nonparametric Raman signal from parametric background in order to enhance the signal to noise ratio with a simple method.

4. DISPERSIVE WAVE GENERATION IN TI:SAPPHIRE LASER

As we mentioned in section 2 that the laser most actively explored for ultrashort pulse generation is Ti:sapphire ($Ti:A1_2O_3$) mode locked laser. This laser has the largest gain bandwidth and is therefore capable of producing the shortest pulses; it also provides the widest wavelength tuning range (broad vibronic fluorescence band which allows tunable laser output between 670 and 1070 nm). Typically, the Ti:sapphire crystal was pumped by a continuous wave argon laser, but the argon laser is now replaced with a diode-pumped, frequency-doubled Nd:YAG or $Nd:YOV_4$ laser in order to create an all-solid-state source [39],[54],[55],[56],[57].

There are many methods to achieve mode locking [13],[14],[58]. For Ti:sapphire, it is mainly achieved by the method of Kerr-lens mode locking. Consider a medium exhibiting optical Kerr effect so that its refractive index can be changed with time due to the light pulse intensity changing with time. This will result what called SPM shown in previous section. Note that, around the peak of the pulse the frequency chirp induced by SPM increases linearly with time. Suppose now that the medium has also negative GDD. In this case, during propagation in this medium the pulse tends to acquire an instantaneously frequency chirp that decreases linearly with time. The two effects thus tend to cancel each other, so we expect that, under appropriate conditions, the effects of SPM exactly cancel that due to dispersion, for the whole pulse, which is called soliton as discussed. In this case, very short pulses are generated. A record of 6 fs pulse duration was achieved by Fork *et al.* using pulse compression external to the cavity [59].

Besides all the applications we mentioned in the introduction for a single pulse, the synchronized femtosecond multiple-wavelength pulses are widely used in various pump-probe experiments, and are particularly important for the femtosecond adaptive spectroscopic technique for rapid identification of biological and chemical agents [5]. This technique relies on using multiple (shaped) laser pulses with adjustable delays to prepare a significantly large quantum coherence, which can dramatically increase the nonlinear response in atomic, molecular or solid state media without overwhelming

absorption [60],[61]. These multiple-wavelength femtosecond pulses are often obtained by using a femtosecond laser amplifier to pump optical parametric amplifiers (OPAs) to produce multiple synchronized tunable outputs.

Meanwhile, one of such pump-probe technology, the CARS spectroscopy is found to be a strong tool to obtain real-time microscopic imaging with high chemical contrast, which we will discuss more in the later section. The good resolution of the image relies on the tight focusing of laser light, and often operates with bare laser oscillators (no amplifiers) with high repetition rate and lower pulse energy which may help avoiding “parasitic” nonlinear processes (which are more pronounced for short pulses with higher peak intensity). While single ultrashort pulse can produce impulsive Raman excitation [62], instead of using a pair of narrower-linewidth pulses with a tunable frequency difference allows selective excitation of selected Raman bands. Synchronized dual-wavelength femtosecond lasers are also used to study scattering mechanisms of highly energetic carriers in semiconductors [63], selective excitation in semiconductor quantum wells [64], and time resolved transietnts in chemical reactions [65]. In addition, synchronous multiple-wavelength lasing may be used for frequency mixing and tunable far-infrared generation [66]. Therefore obtaining multiple-wavelengths pulses directly from a femtosecond oscillator is of significant practical importance. In this section we briefly review the previous work on generating the multi-wavelength femtosecond pulses, and then present a simple technique for generating synchronized dual-wavelength (or multi-wavelength) pulses in a mode-locked Ti:sapphire laser based on the solitonic behavior of femtosecond pulse.

In the past, laser scientists have studied both continuous-wave and pulsed multiple-wavelength laser operation in neodymium-doped crystals [67], and in injection-seeded Ti:sapphire crystals [68]. In addition, multi-wavelength operation of the mode-locked Ti:sapphire laser has attracted great interest, because of the broad bandwidth and short pulse duration it can generate [66],[69],[70],[71],[72]. In these previous reports, dual-wavelength generation was obtained by manipulating either the gain spectrum or the laser cavity dispersion. For example, de Barros *et al.* employed a double slit (or a

normal slit with a 150 um thick fiber in the middle) in order to shape the spectrum at the symmetry plane of the dispersion-compensating prism configuration inside the laser cavity [66]. With the same idea by putting a wire into the laser beam within the laser cavity, we also obtain dual-wavelength mode locking. However, in our experiments, by this method it is hard to start the mode locking and not easy to tune the wavelengths either.

Dual-wavelength generation was also obtained by Zhang *et al.* by slightly misaligning the dispersive prism, which caused what the authors named self-spectrum splitting [69]. Synchronized picosecond pulses at two distinct frequencies in the violet spectral region have been obtained by frequency-doubling of femtosecond pulses in a dual-period quasi-phase-matching crystal [70]. Furthermore, Leitenstorfer *et al.* made use of two laser cavities sharing the same Ti:sapphire crystal as the gain medium, and achieved widely tunable two-color lasing with relative pulse jitter less than 2 fs [71]. Zhu *et al.* made use the same idea to generate a femtosecond pulse synchronized with a picosecond pulse [72]. All the work employing coupled-cavity systems requires precise adjustment of the two cavity lengths such that the two repetition rates are matched to allow pulse synchronization. In the work of Zhu *et al.*, the mismatch of the laser cavity length was controlled within $0.2\mu m$ [72]. Another potential disadvantage of a dual-cavity system is that it may produce two separate output beams [71], and recombining these beams may add complexity and cause energy loss. Below we will see how to obtain this dual-wavelength operation in a different way.

As discussed, the mode locked laser pulse inside the laser cavity (or propagating in fiber) can be viewed as soliton, and the soliton pulse inside the Ti:sapphire laser cavity can be described with the simple nonlinear Schrödinger equation (NSE):

$$\frac{\partial}{\partial z}\upsilon(z,t) = -i\frac{1}{2}\beta''(z)\frac{\partial^2}{\partial t^2}\upsilon(z,t) + i\kappa(z)\left|\upsilon(z,t)\right|^2\upsilon(z,t), \qquad (4.1)$$

where $\upsilon(z,t)$ is the complex amplitude of the pulse envelope, $\beta''(z)$ is GVD, $\kappa(z)=\frac{\omega_0}{c}\frac{n_2}{A_{eff}}$ is positive in Ti:sapphire crystal and 0 elsewhere, A_{eff} is the effective mode area, and n_2 is the Kerr coefficient. For fibers and Ti:sapphire lasers, the change in the sign of the dispersion causes "dispersion managed solitons" to temporally broaden and recompress or "breathe" as they propagate [73],[74].

As we talked in section 2, to achieve short a femtosecond pulse, a broad bandwidth spectrum is needed. For such a large bandwidth, dispersion plays an important role. For a Ti:sapphire oscillator with a four-prism sequence, GDD is compensated to zero, and to achieve the smallest value for TOD optical materials with a small ratio of TOD with GDD are selected. In general the cavity starts with the smallest value of positive second order dispersion (SOD) to ensure the smallest values of both SOD and TOD from the four-prism sequence [14]. This is the reason that the fused silica is the most common material for the prism inside the laser cavity, and also in all experiments discussed in this dissertation.

In the Eq. (4.1) we only take into account the GDD term. As the laser pulse spectrum is getting broader, the higher order dispersions need to be taken into account. We can add an extra operator of high order dispersions $D=i\sum_{m=3}^{\infty}\frac{\beta_m}{m!}\left(i\frac{\partial}{\partial t}\right)^m$ into the equation, where β_m is the m-th order of dispersion coefficient. Because of the perturbation by the high orders dispersions, there are new frequencies which may be generated. We assume that the pulses generated are no longer soliton only, but dispersive waves as well, and the Eq. (4.1) will be written as:

$$\begin{aligned}\frac{\partial}{\partial z}\left(\upsilon_s(z,t)+\upsilon_d(z,t)\right)=&-i\frac{1}{2}\beta''(z)\frac{\partial^2}{\partial t^2}\left(\upsilon_s(z,t)+\upsilon_d(z,t)\right)\\&+i\kappa(z)\left|\left(\upsilon_s(z,t)+\upsilon_d(z,t)\right)\right|^2\left(\upsilon_s(z,t)+\upsilon_d(z,t)\right),\\&+i\sum_{m=3}^{\infty}\frac{\beta_m}{m!}\left(i\frac{\partial}{\partial t}\right)^m\left(\upsilon_s(z,t)+\upsilon_d(z,t)\right)\end{aligned}\qquad(4.2)$$

$\left(\upsilon_s(z,t)+\upsilon_d(z,t)\right)$ corresponds to the total field with pure soliton and dispersive wave. It is reasonable to assume that the temporal amplitude, bandwidth and energy of the dispersion fields are smaller than that of soliton, and the ratio of $\left|\frac{\upsilon_d^2(z,t)}{\upsilon_s^2(z,t)}\right|$ is small, which in our experiment is smaller than 0.1 at the center of Ti:sapphire crystal. The dispersion at this point is supposed to be minimized [74]. For simplicity, we omit the $O(\upsilon_d^2)$ terms, which correspond to the SPM of dispersive waves and the XPM of soliton by dispersive waves, and the Eq. (4.2) is simplified as:

$$\frac{\partial}{\partial z}\upsilon_d = -i\frac{1}{2}\beta''\frac{\partial^2}{\partial t^2}\upsilon_d + i\kappa\left(2\left|\upsilon_s\right|^2\upsilon_d + \upsilon_s^2\upsilon_d^*\right) + i\sum_{m=3}^{\infty}\frac{\beta_m}{m!}\left(i\frac{\partial}{\partial t}\right)^m\upsilon_d . \qquad (4.3)$$

Here, we have already taken into account the equation of (4.1), with high order terms included, and the term of $i\kappa\left(2\left|\upsilon_s\right|^2\upsilon_d + \upsilon_s^2\upsilon_d^*\right)$ can be understood as XPM of dispersive wave by soliton (the asterisk denotes complex conjugation). Normally, the high-order dispersions are small and only phase matched or resonant dispersive waves (RDWs) can have energy transferred from soliton to dispersive waves efficiently. In the case of 3OD, there is only one unstable frequency, but in the case of only 4OD, there are two symmetric unstable frequencies lying beside the soliton as we have shown in section 3 [52],[75],[76]. With the help of the phase matching condition, we can simply write $\upsilon_s\upsilon_d^* = \upsilon_s^*\upsilon_d$, and Eq. (4.3) can be written as:

$$\frac{\partial}{\partial z}\upsilon_d = -i\frac{1}{2}\beta''\frac{\partial^2}{\partial t^2}\upsilon_d + 3i\kappa\left|\upsilon_s\right|^2\upsilon_d + i\sum_{m=3}^{\infty}\frac{\beta_m}{m!}\left(i\frac{\partial}{\partial t}\right)^m\upsilon_d . \qquad (4.4)$$

What we see Eq. (4.4) is similar to Eq. (4.1) but the SPM term is taken place by an XPM term and with high-order dispersions included. If we omit the high order dispersions again because the bandwidth of the RDW is much smaller than that of the main soliton, we will get,

$$\frac{\partial}{\partial z}\upsilon_d = -i\frac{1}{2}\beta''\frac{\partial^2}{\partial t^2}\upsilon_d + 3i\kappa\left|\upsilon_s\right|^2\upsilon_d\,, \tag{4.5}$$

and there will be a soliton-like solution under the similar requirement for Eq. (4.1) [48],[77], but an XPM term is in place of the SPM term with 3 times the mount of power, so that it is required with more negative dispersion to compensate for this situation. Then new wavelength soliton-like pulses can be generated if the equation of (4.5) is satisfied. It is shown in the NSE that the soliton needs dig the "well"-the nonlinearity- by itself in order to balance the dispersion. However in this case, the main soliton needs to dig the "well" for the other soliton like pulses to balance the dispersion. Furthermore, if we can compensate up to 4OD, there are going to be two different wavelength soliton-like pulses generated by the main soliton.

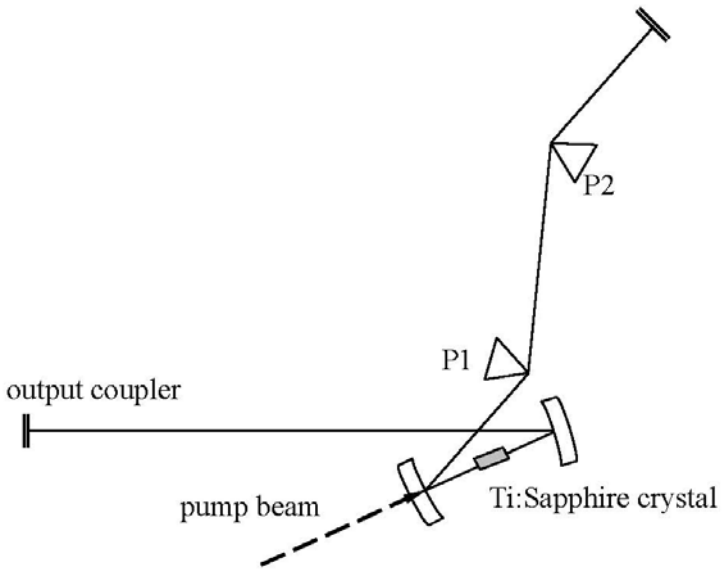

Fig. 4-1. Simplified schematics of the Ti:sapphire laser oscillator. P1 and P2 are the dispersion-compensation prisms.

We use a folded cavity mode-locked Ti:sapphire laser oscillator (Kapteyn-Murnane Labs, TS laser kit), which is show as Fig. 4-1. The laser cavity contains one pair of Brewster-angle fused silica prisms that serve to compensate the intracavity dispersion. The Ti:sapphire crystal is cut at Brewster angle and is 3 mm thick, with the

figure of merit (FOM) >300. All mirrors are coated for high reflection in the wavelength range from 700 nm to 880 nm, and the output coupler transmission is 12%. The Ti:sapphire oscillator is pumped by a solid-state CW laser (Coherent, Verdi V5), working at a 3.8 W output power with a 532 nm wavelength. The oscillator output spectrum is recorded by a fiber-coupled spectrometer (Ocean Optics, HR4000CG-UV-NIR).

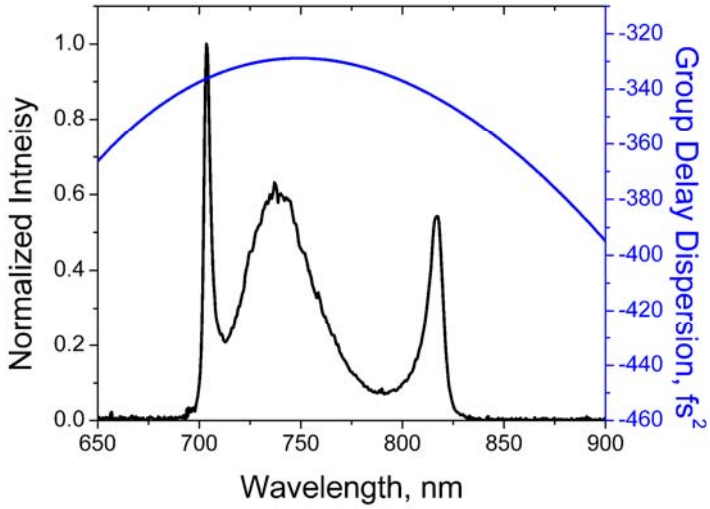

Fig. 4-2. Spectrum (black solid line) of main soliton with two dispersive waves sitting on both sides. Calculated group delay dispersion (blue dashed line) included at different wavelengths.

By carefully adjusting the dispersion of the cavity, we achieve the simultaneous oscillating of the three “solitons”, the main one and two other high order dispersion resulted solitons sitting on both sides of the main soliton, shown in Fig. 4-2. We also calculate the intracavity GDD, and show it in Fig. 4-2 to compare with the solitons spectra. The pulse duration is measured with an autocorrelator (APE, Pulse Check), showing that the main soliton has pulse duration 60 fs, which is stretched by positive dispersion of the output coupler. And the two dispersive waves are also femtosecond pulses, with pulse duration of about 118 fs and 125 fs at the blue side and the red side of the main soliton respectively. As discussed in section 2 that we need assume a pulse

shape before talking about the actual pulse duration. Here and after, all spectral shapes and pulse shapes are assumed as Gaussian function without further notifications. The GDD curve from Fig. 4-2 confirms the requirement of equation (4.5) that the dispersive waves resulted solitons will need more negative dispersions to balance with XPM by the main soliton. This may also tell us the quantity of SPM with the main soliton.

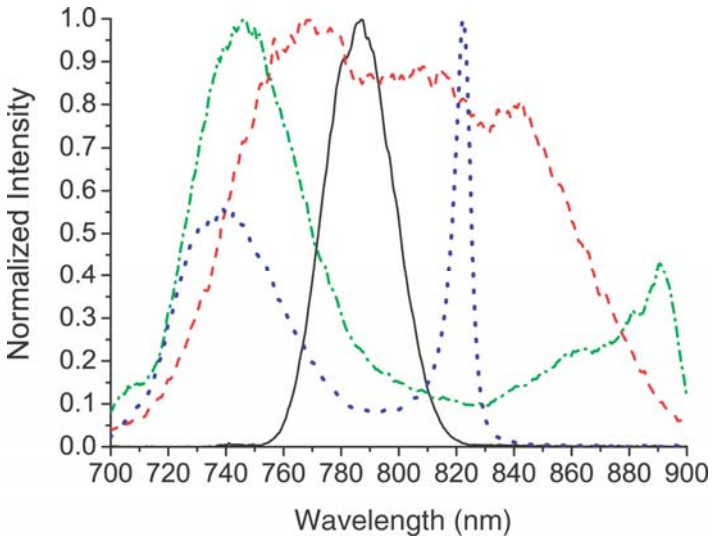

Fig. 4-3. Output spectrum of the Ti:Sapphire laser at various positions of the dispersion-compensation prism (prism P1 in Fig. 4-1). The solid line corresponds to the minimum prism insertion (d=0) that produces laser oscillation. Dashed, dashed-dotted, and dotted lines correspond to d=1.30 mm, 1.37 mm, and 1.49 mm, respectively. For certain prism positions the spectrum splits into two distinct peaks (adapted from Ref. [75]).

In the laser cavity, we use a pair of prisms to compensate intra-cavity dispersions. To have the blue side soliton oscillating, we need to insert the prism close to the end mirror, P2 in Fig. 4-1, a lot into the laser beam. This will introduce too much positive dispersion (by material) in our system, which limits the tunability of this multi-soliton operation. For this reason, we will keep the prism P2 just into the laser mode that the main soliton will oscillate, but any wavelength shorter than the main soliton won't be able to pass the prism P2 due to the larger deviation angle at shorter wavelengths after the prism P1 [47]. For this reason, we will have only two solitons oscillating in the cavity, the main soliton and the red side dispersive wave soliton, with the frequency

difference between them tunable via changing cavity dispersion because of the changing of the phase matching condition. To emphasize the tuning of our system, we focus on this range of our system. But it does not mean that it can only work under this condition. There are two possibilities that may help to solve this issue: one can use chirped mirrors instead of prisms pair to compensate the intra-cavity dispersions or extend the distance between two prisms to introduce larger negative dispersions into the system, which may be helpful for our system.

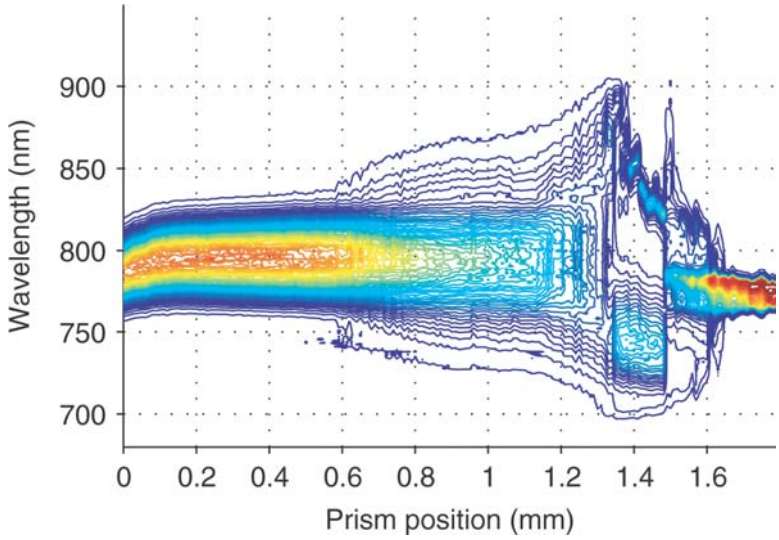

Fig. 4-4. Contour plot of the laser intensity as a function of the output wavelength and prism P1 position, showing the general spectral behavior pattern described in the text (adapted from Ref. [75]).

Here, we show a full picture of the laser behaviors starting with the two intracavity dispersion-compensation prisms adjusted for giving largest negative dispersion. At this condition the tip of prism P1 in Fig. 4-1 is inserted into the laser mode just far enough to allow laser oscillate, and the generated bandwidth is relatively narrow (shown by the solid line in Fig. 4-3). We then start inserting the prism P1 further into the laser mode, and observe gradual broadening of the output spectrum. The dashed line in Fig. 4-3 shows a substantially broadened spectrum with the prism P1 inserted by d = 1.30 mm as measured from the initial position. As we continue moving the prism P1 into the laser mode, we observe splitting of the spectral distribution into two distinct peaks, separated by as much as 150 nm (dashed-dotted line for d = 1.37 mm). From this

point on, if we continue inserting the prism P1 into the beam, the spectral peak separation decreases. As an example, the dotted line in Fig. 4-3 shows two peaks separated by about 85 nm for d = 1.49 mm. Further insertion of prism P1 into the laser mode leads to further reduction of the spectral peak separation, and eventually to a spectral collapse into a single peak, which corresponds to the mode locking in positive dispersion range. The general behavior pattern described in this paragraph is clearly seen in Fig. 4-4, where we show a contour plot of the laser intensity as a function of the output wavelength and prism P1 position.

When we talk about the dispersion it is the real optical path matters instead of the position of the prism. However the optical path is very easy to calculate from the depth, as shown in Fig. 4-5.

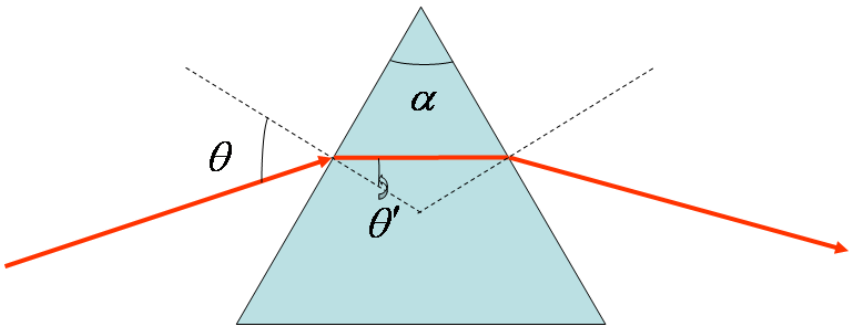

Fig. 4-5. Scheme of the relationships between input angle and the angle of the prism.

In most cases, to minimize the interface reflection many the optical elements are cut into the Brewster angle as we talked about in the introduction [37]. Especially in a laser cavity, that will help to reduce loss when laser bounces within the cavity. This is also the reason that most laser outputs are p-polarized. However, in the case of ultrafast laser, the prism also needs to be set to work at the minimum deviation angle so that the laser mode is not devastated by the dispersion of the prism. The prisms working in femtosecond lasers cavity are cut to have the Brewster angle and minimum deviation angle coincide. Then, the apex angle of the prism is fixed for same material. Let us take a little bit time to see their relation. For Brewster angle $\theta_B = \tan^{-1} n$, n is the material

refraction index. When working at the minimum deviation angle, they have the relation that $\alpha = \pi - 2(\pi/2 - \theta') = 2\theta'$. We know that $\sin\theta = n \cdot \sin\theta'$, so

$$\begin{aligned} \alpha &= 2\theta' = 2\sin^{-1}(\sin\theta/n) \\ &= 2\sin^{-1}(\sin\theta/\tan\theta) = 2\sin^{-1}(\cos\theta) \\ &= 2\sin^{-1}(\cos\theta) = 2\sin^{-1}\left(1/\sqrt{1+\tan^2\theta}\right), \\ &= 2\sin^{-1}\left(1/\sqrt{1+n^2}\right) \end{aligned} \tag{4.6}$$

the apex angle is determined by the refraction index and equals to $2\sin^{-1}\left(1/\sqrt{1+n^2}\right)$. For common material like fused silica $n = 1.456$, $\alpha = 68.96^\circ$; glass BAK1 $n = 1.56$, $\alpha = 65.32^\circ$. With the knowledge of the depth of the prism in laser mode, we can easily find the extended optical path is $l = 2d \cdot \left[n \cdot \tan(\alpha/2) - \sec\left(\alpha/2 + \pi/2 - \tan^{-1} n\right)\right]$. We also need double it when counting the round trip. In the discussion above we make use of the symmetric property of the minimum deviation angle. It is same and easy as well to obtain the relation from the equation of the minimum deviation angle directly.

Christov *et al.* have performed extensive theoretical studies of mode-locked operation of a laser with excessive cavity dispersion, which can lead to production of the double-peaked spectrum [78]. Their model included multiple effects of linear and nonlinear pulse propagation inside a traditional mode-locked laser cavity. They have concluded that "when one of the prism is moved for insertion of $340\mu m$ more glass" (compared to the prism position at which a perfect dispersion compensation is expected), then, "because of the extra positive GVD a broader spectral region has nearly the same transit time in the cavity." [78] This is expected to lead to production of a broader laser bandwidth, and ultimately, when even more glass is inserted, to lead to bandwidth splitting. The experiments by Zhou *et al.* displayed good agreement with the simulations, for relatively small prism insertion, and only showed a shallow dip between two broad peaks and not a clear two-wavelength operation [74]. We estimate that their maximum prism insertion corresponds to that of less than 1.350 mm in our experiments.

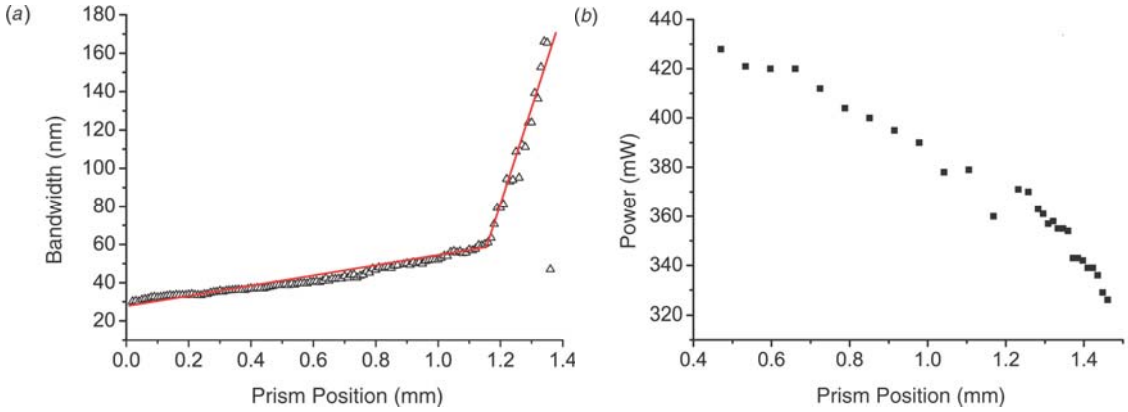

Fig. 4-6. Total bandwidth of the generated spectrum (a) and laser output power (b) vs. prism P1 position. Straight lines of very different slopes provide good fit for the two regions in part (a) (adapted from Ref. [75]).

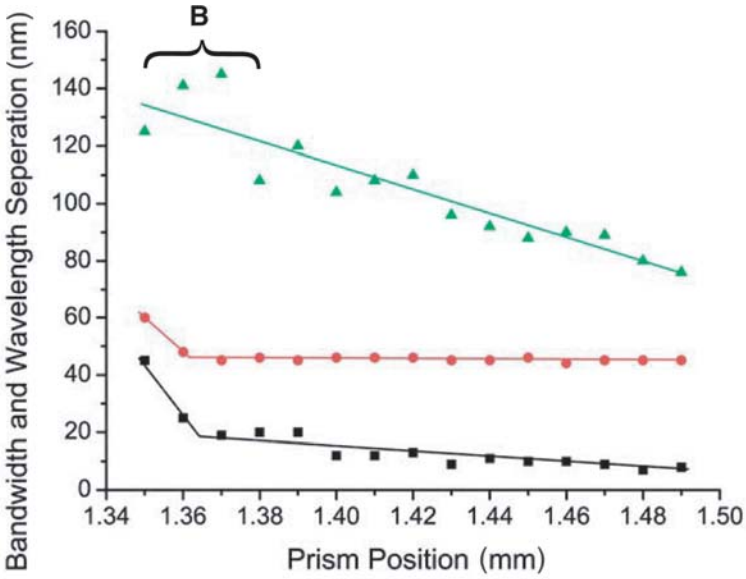

Fig. 4-7. FWHM bandwidth (squares and circles) and wavelength separation (triangles) of the two spectral peaks vs. displacement of the dispersion-compensation prism (prism P1 in Fig. 4-1). Squares correspond to the longer-wavelength part of the spectrum, whose peak wavelength changes with prism P1 position the most. The region noted by the letter B corresponds to the mode beating condition that is discussed later in the text (adapted from Ref. [75]).

We now continue with a more detailed investigation of the effect of additional

dispersion on the operation of the mode-locked laser. Fig. 4-6 (a) shows the increase of the total spectral bandwidth of the mode locked laser as prism P1 is moved from the position of minimum insertion that allows mode-locking (d = 0), into the cavity beam. The measured FWHM bandwidth increases almost linearly as the prism moves in (while the spectrum maintains a nearly Gaussian profile) up to the position of d=1.17 mm. From that point on, the spectrum becomes substantially distorted; as prism P1 is moved in, the spectrum acquires a flat-top, and then a double-bump shape; such shapes are commonly seen when mode-locked oscillators are made to produce pulses shorter than 15 fs. Between prism positions of 1.17 mm and 1.35 mm the total spectral bandwidth growth rapidly (and again almost linearly), and reaches values over 150 nm. The bandwidth increase is accompanied by a modest reduction of the total generated laser power, as shown in Fig. 4-6 (b).

As prism P1 is further inserted into the cavity mode, the RDW starts to build up which evolve as shown in Fig. 4-3. As qualitatively seen from Fig. 4-4, both of the spectral peaks shift in frequency (the RDW peak shifts more rapidly). In most conditions, the center wavelength of the soliton is more stable, and only change in the range of 740 nm to 750 nm, while the RDW shifts from 890 nm to 810 nm. The peak widths change with the prism position as well (squares and circles in Fig. 4-7, with the lines given simply to guide the eye), because the change of the phase matching condition. The wavelength difference of the two spectral peaks varies from 140 nm to 80 nm as shown by triangles in Fig. 4-7. This tuning range corresponds to frequency difference varying from 2187 cm^{-1} to 1272 cm^{-1}, which covers for example the “fingerprint region” of the Raman spectrum for many molecules. It is also because the phase matching condition that the energy can only be transferred to certain range, the two spectral peaks have unequal widths. We have attempted to adjust the two peaks by positioning a slit inside the cavity (close to the prism P2) and blocking parts of the spectrum. We find that we can substantially reduce the bandwidth of the soliton bandwidth, but can not make the RDW broader as expected. Zhang *et al.* pointed out that during their experiment the splitting of the spectrum was sensitive to vibrations, and that tapping on one of the

cavity components may result in merging of the two spectral peaks [69]. On the contrary, in our experiments the mode-locking is quite stable for all the tuning range since the cavity physical parameters will be kept same. Even after restarting the laser, the mode-locking is achieved easily and very reproducibly at all conditions, including the double spectral peak operation which starts automatically if prism P1 is set at the appropriate position. This is also true for the mode locking in positive GDD region, although it requires better alignment of the laser cavity. It is because all these condition are results of real physics parameters of laser cavity, so it is stable and fixed.

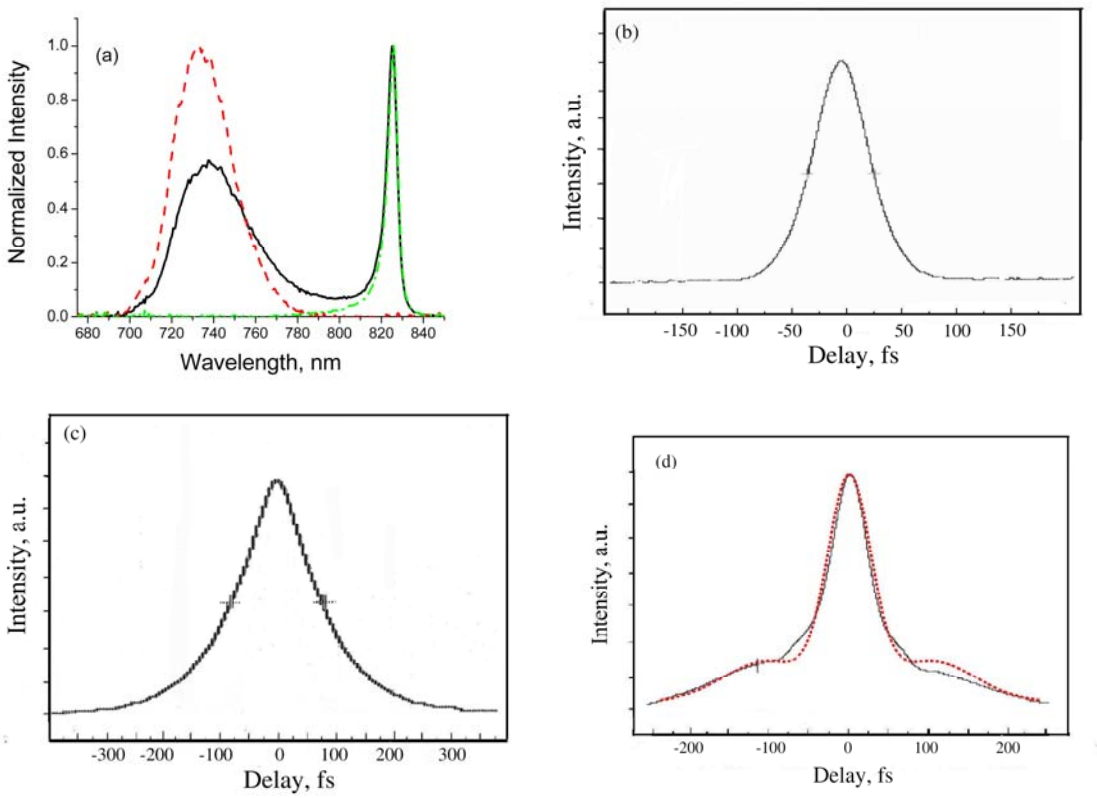

Fig. 4-8. The spectrum of main soliton (dashed line), dispersive wave (dashed-dotted line) and total spectrum (solid line) (a); Autocorrelation of main soliton with pulse duration 49.7 fs for Gaussian pulse (b); Autocorrelation of dispersive wave soliton with pulse duration 124 fs for Gaussian pulse (c); Autocorrelation of both solitons (solid line) and fitted line (dashed line) with a 49.7 fs pulse and a 125 fs pulse with 118 fs delay (d).

Under the configuration with only one RDW generated, a sample spectrum is shown with solid line in Fig. 4-8 (a). It is straightforward to check the pulse durations of the pulses. We block either part of the spectrum outside the cavity and measure the pulse durations with the autocorrelator. As the spectrum of the main soliton shown in Fig. 4-8 (a) with the dashed line, we measure the pulse duration to be 49.7 fs for Gaussian pulse, and the autocorrelation is shown in Fig. 4-8 (b), which is longer than the transform limited value 23.7 fs, calculated from the spectrum. It is because the dispersion of output coupler. With the spectrum of dispersive wave soliton shown in Fig. 4-8 (a) with the dashed dotted line, we measured the pulse duration to be 124 fs for Gaussian pulse, with the autocorrelation shown in Fig. 4-8 (c), which is close to the transform limited value of 125 fs calculated from the spectrum because the dispersion has lesser effect on narrower bandwidth. We also measure the autocorrelation of the solitons together, with the autocorrelation figure shown Fig. 4-8 (d), and fitted by two Gaussian pulses with pulse duration 49.7 fs and 124 fs respectively and 118 fs delay. The fitted line shows quite good agreement with the measurement, instead of that the measurement curve is a little bit asymmetric.

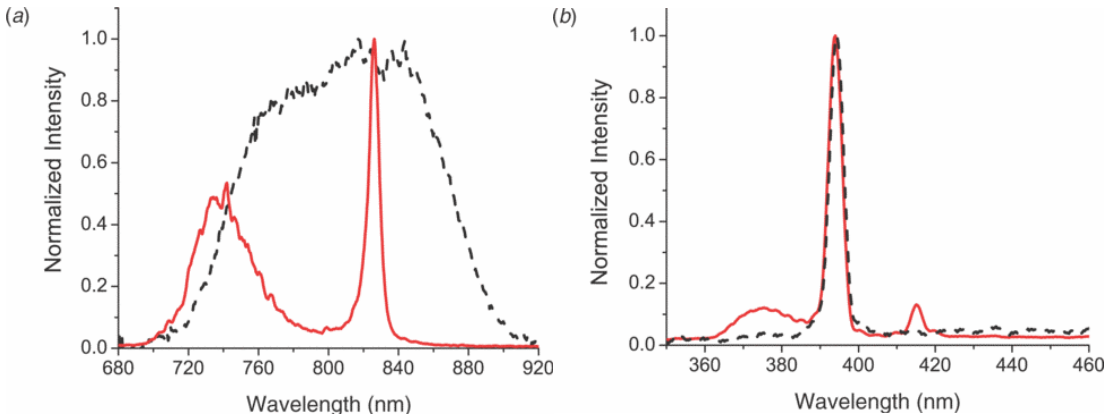

Fig. 4-9. Spectral intensity of the dual-wavelength laser output (a) and its up-conversion by SHG and SFG in an LBO crystal (b) (adapted from Ref. [75]).

Obviously, even though the two pulses are synchronized inside the laser cavity, they can accumulate a relative pulse delay as they propagate through dispersive components on their way out. For example, in addition to our result above Zhang *et al.*

[69] have measured a pulse delay of about 46 fs. Such pulse delays accumulated through dispersive components of a setup can be easily compensated (or pre-compensated) by standard negative-dispersion devices.

To make the difference between the single soliton operation and multi-pulse operation clearer, we compare their SHG signals here. With our Ti:sapphire laser operated in the dual-wavelength regime (spectrum shown in Fig.4-9 (a), with the two peaks centered at 740 nm and 826 nm), we directly couple the laser output into a 1 mm long LBO crystal (CASTECH) by using a 100 mm focal length lens, and obtain second order nonlinear generation, with spectrum shown in Fig. 4-9 (b). In addition to SHG at around 370 nm and 414 nm wavelengths, we obtain SFG at 394 nm, which also confirm that they are overlapped in time. By using an additional (external) dispersion compensating prism pair, we are able to achieve moderate additional enhancement of the SFG peak compared to the SHG peaks. When we use a broadband single soliton operation (obtained at a smaller prism P1 insertion), we only get SHG at around 395 nm; this is because our LBO crystal is cut at the angle ($\theta = 90^\circ \ \varphi = 33.7^\circ$) [79] optimized for phase matching at that wavelength. Phase matching is the likely cause of the enhancement of the SFG peak as compared to the SHG peaks that we observe in Fig. 4-9 (b). One thing I want to make it clear is that even I say SHG of femtosecond pulse here, but strictly speaking it is SFG. A simple argument is that if it is only the double of fundamental frequency then the frequency separation will double too. If this is true, the repetition rate of the pulses will double as well. Actually, the SHG for femtosecond pulses is the SFG between all the frequency combs. However, the offset frequency of the SHG will be doubled, and this is how people measure the offset frequency by comparing this doubled offset frequency with original one.

We show in the previous part of this section that the RDWs can be short pulses as long as the main soliton digs the “well” for RDWs to balance the linear dispersion. Further, as pointed in the introduction of femtosecond optics that to generated ultrashort pulse not only certain spectral bandwidth is needed but also the mode locking is required. In this sense, the femtosecond RDWs are mode locked pulses too. Because the phase

matching between the main soliton and RDWs they should have exact same repetition rate, however it is still uncertain that if they can keep same carrier envelope phase. Then, we measure the laser repetition rate, by using a fast photodetector and a spectrum analyzer. Under a normal operation of a mode locked laser, we expect to see a single peak in the 100 MHz range of the spectrum, corresponding to the laser repetition rate. If we effectively have two independent lasers operating at the same repetition rate but with different offset frequencies, in addition to the main spectral peak at the repetition frequency, we expect to see sidebands that correspond to laser mode beating between the two lasers. Workers in the field of femtosecond optical frequency combs have demonstrated that such beating can be used to monitor and control mode-locking of two or more frequency combs [80].

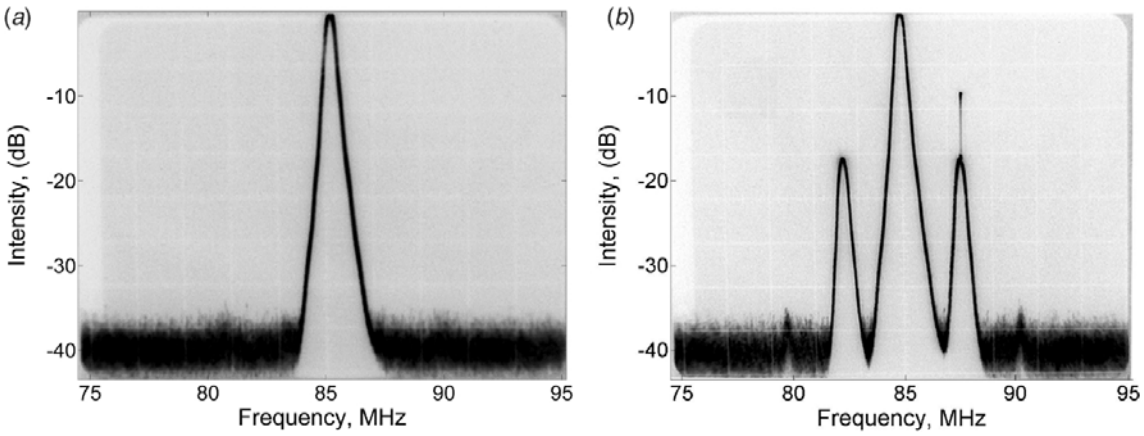

Fig. 4-10. Repetition rate signal obtained by using a fast photodetector and a spectrum analyzer: Under conditions of small and large intracavity dispersion (a), and with intermediate intracavity dispersion (b), which corresponds to the region marked by a bracket with a letter B in Fig. 4-7 (adapted from Ref. [75]).

We vary the intracavity dispersion (inserting prism P1), and monitor our laser repetition frequency by detecting the (fundamental) laser output with a photodiode (THORLABS, DET210) and using a spectrum analyzer (ATTEN, AT5011). Under most conditions, we observe a single stable peak at the 85.1 MHz laser repetition rate [Fig. 4-10 (a)]. However, in a narrow range of parameters (noted by a bracket with a letter B in Fig. 4-7) we observe a pair of stable sidebands separated by a few-MHz frequency shift.

Fig. 4-10 (b) shows beating sidebands offset by 2.6 MHz from the main 85.1 MHz peak; this picture corresponds to the spectrum shown Fig. 4-3 (dashed-dotted line, obtained at d = 1.37 mm). We conclude that under this limited range of conditions we have two independent interleaving frequency combs offset by this frequency shift. It is interesting to note that the beating frequency is stable, which must mean that the carrier-envelope phase difference between the two laser pulses (synthesized by the two combs) changes at this fixed rate [31]. As we increase the intracavity dispersion (by inserting the prism P1 further into the cavity mode), the beating sidebands quickly disappear, even though there is substantial (easily measurable) intensity in the spectral region between the two laser peaks. The measurement result shown in Fig. 4-10 (a) corresponds to the spectrum shown in Fig. 4-3 (dotted line, obtained at d = 1.49 mm), which is also similar to the spectrum in Fig. 4-9 (a). Now we take a better look of this beating signal. As we pointed out that the offset frequency comes from the difference between group velocity and phase velocity. Then in our case, we have two femtosecond pulses share the same group velocity, then this beating signal actually indicates the different phase velocity between these two far detuned wavelengths:

$$\delta_1 = \frac{\omega_{c1} v_g}{2\pi}\left(\frac{1}{v_g} - \frac{1}{v_{ph1}}\right) \tag{4.7}$$

$$\delta_2 = \frac{\omega_{c2} v_g}{2\pi}\left(\frac{1}{v_g} - \frac{1}{v_{ph2}}\right) \tag{4.8}$$

If $v_g = 0.999999c$, $v_{ph} = c$, c is speed of light, then $\delta = \frac{\omega}{2\pi}\frac{0.000001}{0.999999} = 43.9\text{MHz}$. Well, with two femtosecond pulse synchronized, and the small beating frequency indicates that now the phase velocity matters in this 2 MHz difference. Since $\Delta\phi_{CE} = \delta\phi - \text{N}\cdot 2\pi$, this does not mean that v_{ph} difference is 20 times smaller than the example given above.

As mentioned above, the main cause of this operation is the cavity dispersion, so

this mechanism is general, and not limited to Ti:sapphire laser. It will work at other soliton like lasers. For the RDW generation, it does not involve complicated coupled cavities or two-slit systems. It is easy to obtain the synchronized dual-wavelength femtosecond pulses in a single mode-locked Ti:sapphire laser cavity. Furthermore, we have obtained simultaneous tri-wavelength generation in the violet range of the spectrum, by converting these dual-wavelength femtosecond pulses via second-order nonlinear optical processes in an LBO crystal, without the need for any external pulse delay compensation. This simple multiple-wavelength system, with easily tunable spectrum, may become useful for femtosecond CARS spectroscopy in a microscope configuration, frequency-difference generation, and other types of multi-color excitation experiments [81]. Our experiments confirme that the RDW are femtosecond soliton with satisfying of equation (4.5). The frequency difference, can be tuned in a certain range. We showed that the two pulses' wavelength difference could be tuned in range $2187\ \mathrm{cm}^{-1}$ to $1272\mathrm{cm}^{-1}$. By similar calculation of the dispersions of our system, it shows that the tuning range could be extended by increasing the distance of prism pair which will cause the increase of the cavity length and reduce the repetition rate of the oscillator [14]. In our system, we had the fused silica prisms. It will be interesting to check if it could be applied in Ti:sapphire systems with other material prism pairs. We used the same parameters we had for our system to simulate for BK7 and CaF_2 glass. It is interesting to see that with BK7 glass, it needs less length of the cavity but the tuning range will be much smaller than fused silica. With the same situation for CaF_2 glass, to achieve this two solitons operation, it will require twice the length of laser cavity for fused silica and the tuning range is the same order as fused silica. For this reason, fused silica is a reasonable good material for the prisms inside a cavity. As we have shown in experiments that the RDWs have same repetition rate as the soliton, and even keep same carrier envelope phase in most cases. However this not true if these two wavelengths are separated widely, this will impact the applications where phase matters. In the next section about the RDWs applications in fibers, we will show it is an important issue.

5. DISPERSIVE WAVE GENERATION IN PHOTONIC CRYSTAL FIBERS

Photonic crystal fiber (PCF) is a new class of optical fiber based on the properties of photonic crystals. In general, such fibers have a cross-section with microstructures.

A crystal is a periodic arrangement of atoms or molecules. The pattern with which the atoms or molecules are repeated in space is the crystal lattice. The crystal presents a periodic potential to an electron propagating through it, and both the constituents of the crystal and the geometry of the lattice dictate the conduction properties of the crystal. Importantly, the lattice can also prohibit the propagation of certain waves. There may be gaps in the energy band structure of the crystals, meaning that the electrons are forbidden to propagate with certain energies in certain direction. For example, a semiconductor has a complete band gap between the valence and conduction energy bands [12],[82].

As we all know that optical waves are inherently periodic. They interact with periodic media in a unique way, particularly when the scale of the periodicity is about the same order of the wavelength (like gratings). For example, spectral bands emerge in which light waves cannot propagate through the medium without severe attenuation. Waves with frequencies lying within these forbidden bands, called photonic bandgaps. It is analogous to the electronic properties of crystalline solids such as semiconductors we just mentioned. This is also the origin of the color in butterfly wings, peacock feathers, and holograms such as those found on credit cards. Because of this analogy with the crystal, the photonic periodic structures have come to be called photonic crystals. Nowadays, photonic crystals have found many applications, including special filters, waveguides, and resonators, and many more applications are in the offing [12],[82].

The term of “photonic crystal” was first introduced by Yablonovitch in 1989 [83]. But the idea of one dimensional stop band itself is rather old, having been derived by Lord Rayleigh in an 1887 issue of Philosophical Magazine [84],[85],[86]. In the following paper in 1888, Rayleigh stated: “I have discussed in a recent paper the propagation of waves in an infinite laminated medium (where, however, the properties

are supposed to vary continuously according to a harmonic law), and have shown that, however slight the variation, reflexion is ultimately total, provided the agreement be sufficiently close between the wavelength of the structure and the half-wavelength of the vibration." Thus, by 1887 lord Rayleigh had ready known the actual magnitude of the forbidden stop band for 1D structure. What we call "photonic crystal" now, is more associated with two or three dimensionally periodic structures. And this is much related 3D crystal of X-ray crystallography, which is a Bragg reflection of X-ray by crystals. In 1914, C. G. Darwin (grandson of Charles) derived the "dynamical theory of X-ray diffraction" -in other words- the theory that includes the effect of X-ray standing waves, finite mini-gaps, *etc* [84]. It seems that ordinary crystals have bandgaps for X-ray, but why not ordinary "photonic crystal"? Yabonovitch gave an explanation in a review paper [84]: that refractive-index contrast for X-rays is tinny. "The high index contrast is the main new feature of photonic band structures beyond dynamical X-ray diffraction." So respect for Rayleigh and other historical figures, people use the photonic crystal name only for high-index-contrast 2D or 3D period structures. In this dissertation, I will limit my discussion to 2D structure -PCF.

At this moment, the most successful application of photonic crystals is still PCF, the fiber with wavelength-scale periodic structures and having "stop bands". Appropriately designed, the holey photonic crystal cladding, running along the entire length of the fiber, can prevent the escape of light from a hollow core. Thus, it becomes possible to escape the straitjacket of total internal reflection and trap light in a hollow fiber core surrounded by glass [87],[88].

Standard "step index" optical fibers guide light by total internal reflection (TIR), which operates only if the core has a higher refractive index than the encircling cladding. Under the TIR rays of light in the core, striking the interface with the cladding, are completely reflected. The wave nature of light dictates that guidance occurs only at certain angles, *i.e.*, that only a small number of discrete "modes" can form. On the other hand, if there exhibit ranges of angle and color ("stop bands") where incident light is strongly reflected, then in photonic band gap (PBG) materials, these stop bands broaden

to block propagation in every direction, resulting in the suppression of all optical vibrations within the range of wavelengths spanned by the PBG [87]. As we just mentioned, it was believed that refractive index difference needs to be as large as 2.2:1 to create a photonic band gap in 2D. Later it was realized that in fiber the existence of bandgaps could be true for a structure comprising just air (index 1.00) and fused silica (index 1.45) [89], with the propagation along the third axis—the direction of invariance (the refractive index difference reduced a lot).

Rusell first came to the idea that to trap light in a hollow core by means of 2D photonic crystal of microscopic air capillaries running along the entire length of a glass fiber [88]. There had been previous work on microstructured fibers, *e.g.* Bragg fiber [90], but this was first attempt to produce photonic crystal lattices of air holes in fiber form. Their first plan was to drill holes in a short rod of silica glass and then draw it down to fiber. Well, silica is mechanically very hard material, and impossible to machine with their tools [87]. Later, Rusell's team stacked individual cylindrical elements into a 2D close packed array, and drew them into a honeycomb of $\sim 10 \mu m$ diameter waveguide pixels, each surrounded by black glass to reduce crosstalk. They made use of a technology first used in the third- to first-centuries BC by the Egyptians to make mosaic glass. The technique's success is largely due to the mechanical stability of the structure—the surface tension forces tend to balance out, allowing formation of highly regular lattices of holes during the drawing process. Overall collapse ratios are as large as 50,000 times have been realized and continuous holes as small as 25 nm in diameter have been demonstrated, earning an entry in the Guinness Book of Records in 1999 for the World's Longest Holes [87],[88]. The first silica-air PCF structure was made in late 1995 by stacking 217 silica capillaries, specially machined with hexagonal outer cross sections and a circular inner cross section [88].

Even the most extraordinary property of the PCF is that it can guide mode in the hollow core with the help of the PBG. The solid core PCF also shows great new features, and we will concentrate on one of them in the later part. Because the PCF can hold many modes, those modes encounter different guiding features. Some modes are guided

strongly, but some are not (leaking modes). Thus in PCF, three mechanisms: TIR, PBG and leaking help this kind fiber to achieve special optical propagating properties. It looks rather ironic of TIR being involved into the PCF, but for positive core-cladding index difference PCF, the TIR guided modes will dominate with PBG making special properties. Now people have various kind of PCF — large mode area, dispersion controlled, hollow core, birefringent and multicore, which also have been used for different applications, including the supercontinuum one plays important role of metrology of frequency these days [91].

The complex structure of PCF -in particular, the large refractive-index difference between glass and air- makes its electromagnetic analysis challenging. Maxwell's equations must usually be solved numerically using one of a number of specially developed techniques. Although standard optical fiber analyses and a number of approximate models are occasionally helpful, these are only useful as rough guidelines to the exact behavior unless checked against accurate numerical solutions [88].

$$\begin{aligned}
&\frac{\partial^2 E_x}{\partial y^2}+\frac{\partial^2 E_x}{\partial x^2}-\frac{\partial \ln \varepsilon}{\partial y}\left(\frac{\partial E_x}{\partial y}-\frac{\partial E_y}{\partial x}\right)+\left(\varepsilon k^2-\beta^2\right)E_x=0\\
&\frac{\partial^2 E_y}{\partial x^2}+\frac{\partial^2 E_y}{\partial y^2}-\frac{\partial \ln \varepsilon}{\partial y}\left(\frac{\partial E_x}{\partial y}-\frac{\partial E_y}{\partial x}\right)+\left(\varepsilon k^2-\beta^2\right)E_y=0
\end{aligned} \tag{5.1}$$

In the paraxial scalar approximation, the second part in (5.1) can be neglected, yielding the following scalar wave equation [88]:

$$\nabla^2 E_T(x,y)+(k^2\varepsilon(x,y)-\beta^2)E_T(x,y)=0 \tag{5.2}$$

This leads to a scaling law similar to the one used in standard fiber analyses. It is natural to strive for a result similar to the V-parameter known from standard fibers. Consider the fiber structure with only pure silica and air holes, with air holes of diameter d are arranged on a triangular grid with a pitch, Λ . A directly translation is not

straightforward since no wavelength-independent core- or cladding index can be defined. But it is useful to define a V number for a PCF by [92]:

$$V_{PCF} = 2\pi \frac{\Lambda}{\lambda} \sqrt{n_{FM}^2(\lambda) - n_{FSM}^2(\lambda)} \tag{5.3}$$

where $n_{FM}(\lambda)$ is the wavelength dependent effective index of the fundamental mode (FM) and $n_{FSM}(\lambda)$ is the corresponding effective index of the first cladding mode in the infinite periodic cladding structure often denoted the fundamental space filling mode (FSM). The higher-order mode cut-off can be associated with a value of $V_{PCF} = \pi$ [92]. A common method for solving Eq. (5.1) employs a Fourier expansion to create a basis set of plane waves for the filed, which reduces the problem to the inversion of a matrix equation suitable for numerical computation [93],[94],[95]. Ref. [88] gives more detailed information of the related numerical techniques.

For us who are dealing with femtosecond lasers, the most important advantage of PCF will be the capability of manipulating GVD of the fiber. For the solid core PCF the air holes make the core becomes more and more isolated, the zero-dispersion point of the fundamental guided mode can be shifted to wavelengths in visible [96]. Of course, it is obvious that hollow-core PCF (HC-PCF) has extremely small GVD and holds promising applications in ultrashort optics too [97].

Due to the special dispersion characteristics of PCF, the nonlinear behavior can be much enhanced now. One such phenomenon which has attracted considerable attention is the recently demonstrated generation of an extremely broadband supercontinuum (SC) covering more than two octaves pumped by low-energy (1 nJ) pulses with an initial duration 100 fs [98],[99]. The analogous effect has also been observed in tapered fibers made by heating and stretching a standard fiber to form a narrow thread of silica surrounded by air. In comparison, SC generation in standard fibers requires more than 2 orders of magnitude higher initial peak intensities. The dramatic spectral broadening of relatively low-intensity pulses in PCFs is an interesting

phenomenon and has already been used in several fascinating applications including frequency metrology [31],[80].

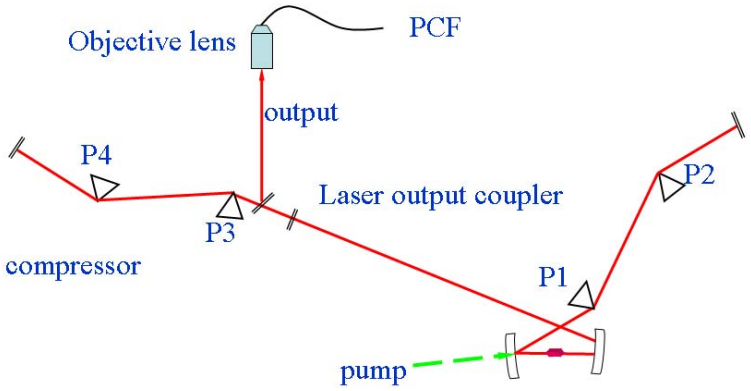

Fig. 5-1. The setup of dispersive waves generation in PCF with Ti:sapphire laser oscillator. The Ti:sapphire laser is same as Fig. 4-1. P3 and P4 are the dispersion compensation prisms to compensate dispersion of the optical elements outside the laser cavity, and we couple the femtosecond laser into a piece of PCF with microscopy objective lens.

However, some of the most interesting progress in nonlinear applications has not involved broadband spectral generation at all, but rather the generation of narrowband frequency components. It will be appreciated to have energy efficiently transferred to the wavelength needed with less complicated system. We have shown in previous section that we are able to tune the femtosecond RDWs in a Ti:sapphire laser, benefiting from the width of the gain spectrum but also being limited by it [75],[76]. Since the mechanism is general, there is a chance to apply this nonlinear process into a PCF system. Moreover, with the help of the freedom to engineer PCF for desired purpose, we are hoping that PCF may have even more brilliant results. In the previous work with Ti:sapphire laser, we obtain tunable multiple wavelength femtosecond lasers via changing the dispersions of the lasers cavity. While, with a piece of PCF already being made, we can not change the dispersion easily like what we did with the Ti:sapphire laser cavity. On the other hand, if we can change the group velocity of soliton, then we are going to able to tune the wavelengths of dispersive waves being generated. A

straightforward strategy will be tune the center wavelength of soliton to change the group velocity of soliton to excite different dispersive waves. Below, I will present some experimental result on this issue. To make a simpler expression, the femtosecond laser coupled into the PCF is called as pump light.

The pump laser source is the same mode locked femtosecond Ti:sapphire oscillator (Kapteyn-Murnane Labs, TS laser kit) we used in previous section, with tunable bandwidth and center wavelength, and a repetition rate of 85 MHz. A pair of external fused silica prisms is used to compensate the dispersions of optics outside the cavity, including a 20× microscope objective lens used to couple the laser pulses into the HC-PCFs, shown in Fig. 5-1. The pump laser power is 150 mW before the objective lens (coupling efficiency 10%-15%), and the pulse duration is 30 fs before the fiber. The output spectra are recorded by a fiber-coupled spectrometer (Ocean Optics, HR4000CG-UV-NIR) for the visible and an FT-IR Spectrometer (Nexus 870) for the infrared spectral range. The fiber under study is a Kagome HC-PCF shown in Fig. 5-2. Instead of coupling the laser beam into the hollow core, we couple it into the knots of the cladding, the size of each knot is about 1 μm shown in Fig. 5-2.

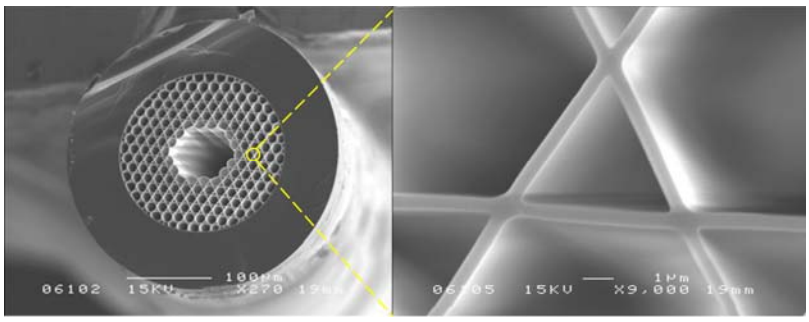

Fig. 5-2. Scanning electron microscope image of the hollow core PCF (left) and close-up of the knot of the PCF cladding (right). (Photographs courtesy of F. Benabid and F. Couny.)

We couple the compressed femtosecond laser pulses into the cladding of a 3.2 cm-long PCF, and record output spectra shown in Fig. 5-3. The GVD relation with the wavelength is shown in Fig. 5-4 for two perpendicular polarizations marked as 1 and 2 as well in the figure. Because of the limitations imposed by phase matching, the soliton

transfers energy only to a certain range of wavelengths, and only for the optimal polarization (axis 1 marked in Fig. 5-4). We observe generation of two RDWs placed on the blue and red sides of the soliton central wavelength (around 450 and 1800 nm respectively). We choose this relatively short fiber length, so that the infrared RDW does not experience too much material absorption, whilst keeping the level of RDW generation sufficiently high. Finally, we keep our pulse energy to a certain range so the nonlinear processes are dominated by the formation of the fundamental soliton and its RDW emission (only one on each side is generated). This is made possible thanks to dispersion of the fiber. The measured power of blue RDW shown in Fig. 5-3 is larger than 10% of the total output power. As seen here, we observe two RDWs on both sides of the soliton, which again is caused by the perturbation of the FOD.

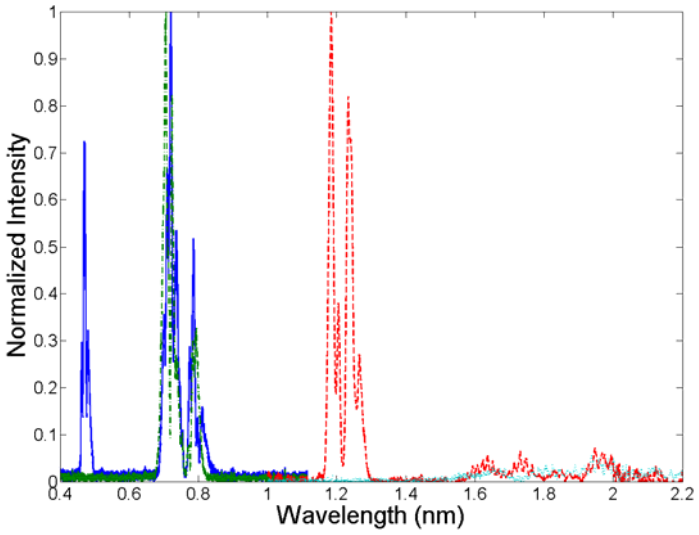

Fig. 5-3. By coupling the compressed femtosecond laser output into the cladding of a 3.2 cm long PCF, two sample spectra are shown in here for two orthogonal polarizations. The spectra are recorded by two different spectrometers.

As we just mentioned, we can change the RDW wavelength by changing the soliton wavelength because of the varying of GVD for different wavelength. With the tuning of pump light wavelength (from 740~830 nm) we can tune both wavelengths of

the blue and infrared RDW. Here we show experimental results in Fig. 5-5. The triangles correspond to the dispersive waves generation by polarized pump light along axis 2, and the square correspond to the dispersive waves generation by the polarization along axis 1 pump light and they are in excellent agreement with the theoretical simulations [100].

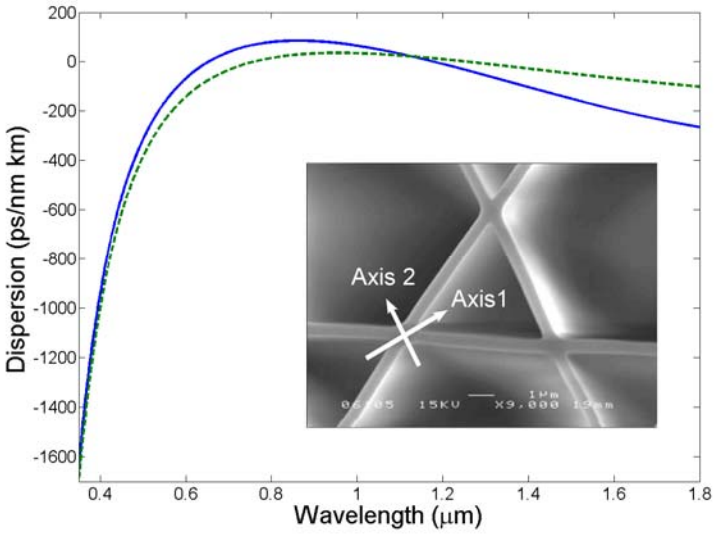

Fig. 5-4. The GVD as a function of the wavelength for two orthogonal polarizations in a sample knot of the cladding. The dispersion for polarization along the long axis (marked as axis 1) of the knot is shown in blue solid line, and the orthogonal one (marked as axis 2) is shown in green dashed line. The inset presents scanning electron microscopy image of the cladding.

We have shown that both visible and infrared RDWs can be tuned in a large spectral range by tuning the pump light wavelength. In practice however, this implies that the tuning range of the RDW is limited by the tuning range of the Ti:sapphire laser. However, we know that the different propagation modes in the same fiber will have totally different dispersion characteristics. This means the RDWs will be excited at other wavelengths for the same pump wavelength because phase-matching condition is changed. If we change the couple condition so that we can excite different propagation modes, and at the same time we tune the pump light wavelength. In that case, we are able to extend the tuning range of the RDW generation, and obtain extremely large tuning range that other method can not achieve with only an oscillator.

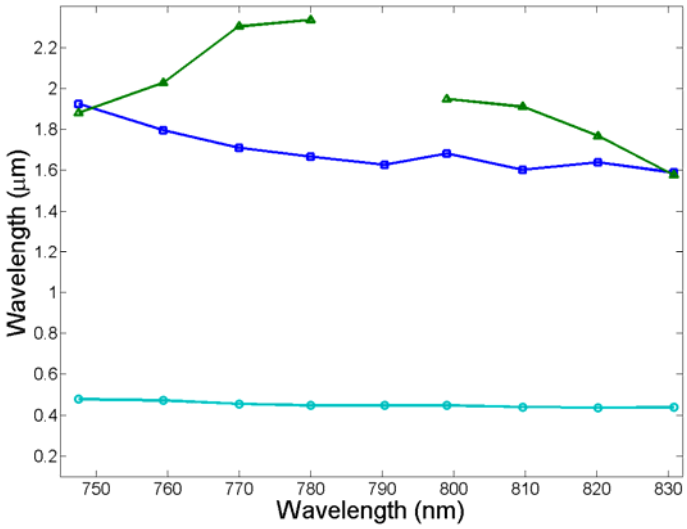

Fig. 5-5. Tuning of the dispersive wavelengths via the tuning of the pump light wavelength: the blue triangles and blue squares correspond to the IR and blue dispersive waves generated by same polarized pump light respectively, and the pink triangles correspond to the IR dispersive waves generated by the other perpendicular polarization pump light.

In Fig. 5-6 we show how the RDW wavelength changes when we couple the pump light into different knots of the PCF cladding. At the same time, we can easily fine-tune the RDW wavelength by tuning the pump light wavelength. The generation efficiency for the longer wavelengths RDWs (blue-detuned) is larger than that in the previous case. By changing the coupling conditions (either by coupling into a different knot or by coupling into different PCF modes in the same knot), and in addition by tuning the pump wavelength, we achieve an RDW tuning range covering the whole visible spectrum. In order to cover the entire visible spectra, only three knots are needed, even though we give more than enough examples of RDWs in Fig. 5-6. To our knowledge, this is the largest reported tuning range for efficient nonlinear optical frequency conversion obtained with a simple and un-amplified femtosecond laser.

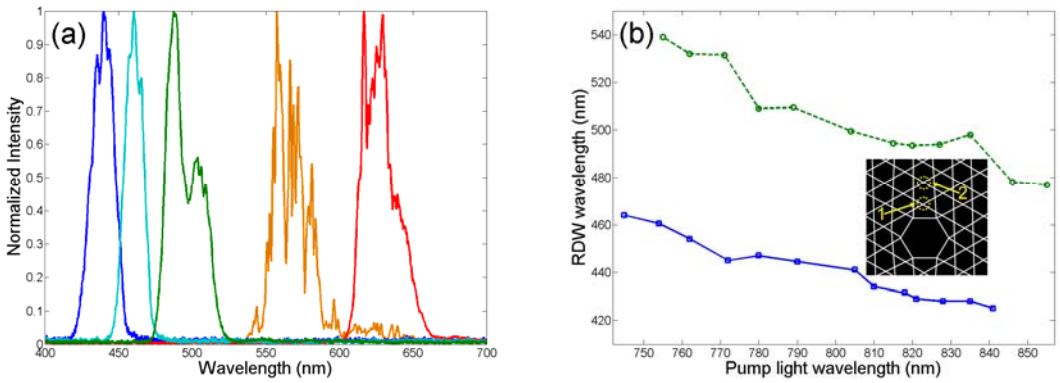

Fig. 5-6. The output after PCF via changing the coupling condition of PCF, with same input femtosecond pulse after Ti:sapphire oscillator (a). Tuning of the RDWs via the tuning of the pump light wavelength: the blue circles and green squares correspond to blue RDWs generated in different knots of the PCF cladding (b).

Ideally, the phase matching condition for soliton and RDW indicates that they propagate at the same group velocity, like what we have seen in the Ti:sapphire case. Then the generated RDWs should also be femtosecond pulses too. However this is slightly different in the PCF from the Ti:sapphire laser. In my previous experiment with Ti:sapphire laser, there is a pump source. So that all the energy lost due to the RDW generation will be made up by the pump source. In the steady state, the soliton and RDWs will share same group velocity. On the other hand, there is no out source at all in the case of the PCF. The soliton will shred energy to RDW due to the perturbation of the high order dispersions, and it will find a new equilibrium state during this process. Meanwhile, the group velocity of the soliton will change too since the steady state solution of the soliton has the group velocity related with both the amplitude and the GVD (see section 3). Actually, this new equilibrium building process is really fast. In experiments, I find this progress can be shorter than 1 mm in propagation length. So in principle the generated RDWs are ultrashort pulses too, but the output duration will be determined by the dispersion characteristics of the PCF.

Then it is important to confirm experimentally the ultrashort pulse duration of the generated frequency-tunable RDW, as well as to check their temporal delay with respect

to the pump pulse. As we just discussed that the femtosecond RDWs are expected to stretch considerably while propagating through dispersive media. However, thanks to highly efficient RDW generation, short propagation length, and good dispersion characteristics (shown in Fig. 5-4), the blue-shifted RDW pulses are not stretched too severely. I perform a cross-correlation measurement for the RDW and pump pulses with an autocorrelator (APE, Pulse Check). Fig. 5-7 shows the auto/cross-correlation trace for the RDW (at 470 nm wavelength) and the pump pulse. The trace has standard double-pulse auto/cross-correlation appearance, where the central peak corresponds to an autocorrelation trace of the pump pulse (our device can not measure direct autocorrelation of the RDW because its second harmonic is out of the working range). The side-peak separation corresponds to the delay between the two pulses, and two side peaks represent the cross-correlation between the RDW and the pump pulse. Because the frequency difference between the main soliton and RDW is so large, the optics dispersion after the fiber contributes to the measured 1 ps delay between the two pulses (for example 1 cm thick fused silica will cause a relative delay about 0.4 ps between these two wavelengths). The cross-correlation measurement confirms that after the 3.2 cm long PCF, a 40× objective lens and neutral density filters, the pulse duration of the 470 nm RDW is less than 160 fs (assuming a Gaussian pulse) without any dispersion compensation. Pulse stretching is also caused by dispersion in the aforementioned optics, and then shorter pulses can be obtained by adding extra dispersion compensation elements after the fiber output coupler. The reason of the specific wavelength (470 nm) used here because the GVD of the PCF under study has much larger (positive) value at shorter wavelength. So I want to check with the wavelength of RDW as shorter as possible, then all the other RDWs will have shorter pulse durations. However, as mentioned in the text the measurement is limited by the equipment, mainly the filter and the detector. If the wavelength of the RDW is too short then it will pass through the filter to saturate the detector, at the same time the frequency of the SHG or SFG of the RDW and the pump light will be out of the detection range. So in our case, the limit we can measure is at the wavelength of 470 nm, and the result here is supporting my prediction

made earlier.

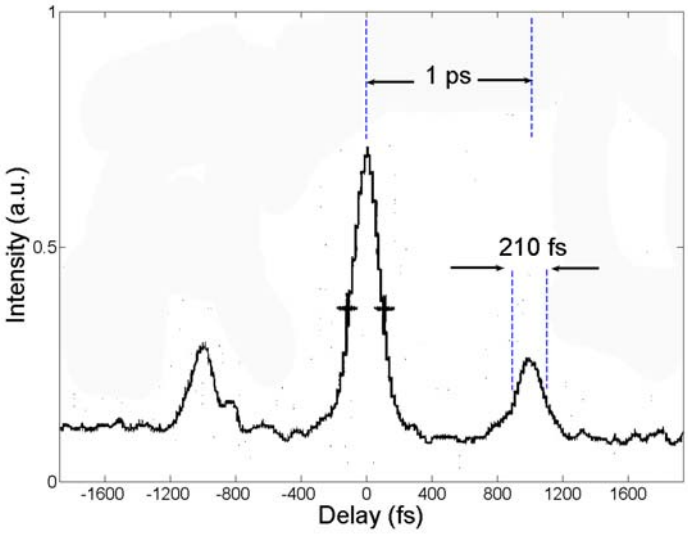

Fig. 5-7. Auto/cross-correlation traces of the pump pulse and the 470 nm RDW. The 1 ps separation between the peaks corresponds to the delay between the two pulses. The two side-peaks correspond to cross-correlation traces between the RDW pulse and the pump pulse, and it shows that the pulse duration of the 470 nm RDW is less than 160 fs (Gaussian pulse assumed) after PCF and other optics (no dispersion compensation being used).

As we have mentioned above, when 4OD dominates, the other (conjugate) RDW is generated in the infrared region (as shown in Fig. 5-3), and is expected to possess tuning and temporal features similar to the visible RDW. Compare our PCF dispersion in the infrared with that in the visible region (Fig. 5-4), we conclude that the output infrared pulse should be even shorter than the (measured, 160 fs) blue RDW pulse. Therefore, our method can possibly be used to produce tunable femtosecond pulses in the near- to mid-infrared spectral range. A numerical simulation confirms this prediction too.

We show the RDWs generation in PCF is a great method for generation of tunable femtosecond pulse with little energies, and it is also strongly different from general cases where it is mainly mediated by TOD and negligible. At the same time, we shall investigate more about its behavior with changing of physical parameters. The

compressor (P3 and P4) right after the output coupler of the oscillator is used to compensate the dispersions for all optical elements outside the laser cavity. Meanwhile, we can also use it to adjust the pulse duration by introducing different amount dispersion, which causes chirping for sure. This time we couple the laser pulse into a 9 cm long Kagome PCF. We also measure the pulse duration after the objective lens with the autocorrelator, so all the pulse durations mentioned below are those coupled into the fiber.

First, we launch a 20 fs optical pulse, with its central wavelength located at 800 nm. The output spectrum is shown in Fig. 5-8. The spectrum shows a broadening due to SPM and solitons self-frequency shift around the pump wavelength, and an RDW around 400 nm. The unusually large peak of this RDW indicates a strong energy transfer from the soliton body to the resonant radiation. One of key features of RDW generation is that the RDW wavelength is mainly determined by the phase matching condition but largely independent from the pump light intensity. This is a great advantage in that the tunability is achieved without sacrificing the pump intensity like in some other cases present in the literature [101], and with good stability. We gradually decrease the pump power without changing the pulse duration, and record the peak power wavelengths of both residual pump light and RDW, as showed in Fig. 5-9 (a). To make the variations clearer and to compare the effects on both pump light and RDW light, we normalize the frequencies to their maximum value. The figure shows clearly that the peak power frequency of the RDW actually shifts a little bit to higher frequencies at higher power because of the SPM resulted self frequency shift, but it is stable in most cases. When the power is smaller than 80 mW the RDW amplitude is so small that the peak wavelengths can not give accurate information. In general, it shows clearly that the RDW wavelength is mainly determined by the phase matching condition but may be affected by the pump power in a small range. This is an important property for the nonlinear optical frequency converter that output frequency is independent of the fluctuation of pump laser power.

Compared with the case of the RDW generation in Ti:sapphire laser oscillator, where the external pump source used, the efficiency of the RDW generation is affected

by the gain spectrum of the system [75],[76]. On the other hand, the efficiency for PCF is strongly dependent on the pump laser. We sample out part of the output to compare the peak power change for the two spectral regions, the pump light and RDW light. This is illustrated in Fig. 5-9 (b), where the red curve corresponds to the peak power of the residual pump light and the blue curve corresponds to the peak power in of the RDW. Again, we normalize the output intensity by being divided by the maximum value of each wavelength of the residue infrared and RDW respectively. It shows that after reaching a certain value of the pump power the RDW intensity increases almost linearly with the pump power. The intensity of RDW is strong enough to induce other nonlinear effects, like SPM, that extend its bandwidth further. While changing the power, the pulse duration is fixed, so that only intensity is changed. We can see clearly, the peak power of the residual IR changes almost linearly with the pump power at low pump power, but aberrates at higher power (>90 mW). It indicates a considerable energy being transferred to RDW, and there is threshold for such efficient RDW generation.

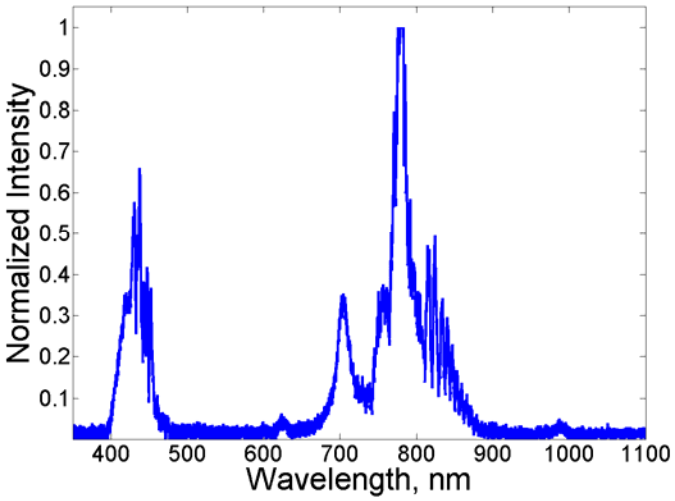

Fig. 5-8. The output spectrum of standard RDW, with pump pulse wavelength centered at 800 nm.

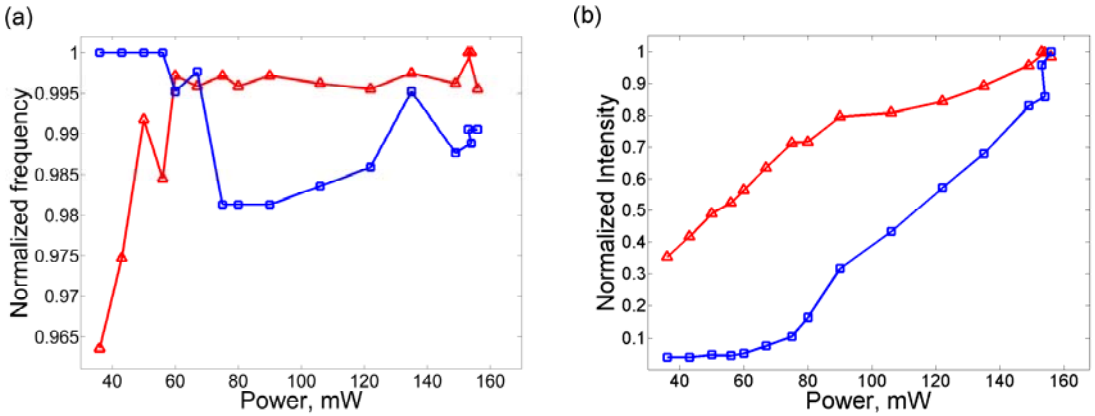

Fig. 5-9. Relations of normalized peak power frequency and pump power for residual IR (in red) and RDW (in blue) (a); The normalized intensity of residue pump light (in red) and RDW (in blue) change vs. pump power (b).

Then, we set pump power fixed at 200 mW. We start with the pulse duration 20 fs with a little bit negative chirped, and change the pulse durations by inserting prism further into the laser beam to introduce positive chirping. The intensity of pump light decreases gradually, but the peak intensity of the resonant RDW does not decrease during this progress. Meanwhile, the spectrum of the resonant RDW is getting broader and broader, and new wavelengths are generated with this stretching of pump pulse, shown in Fig. 5-10.

This spectrum broadening of RDW is not caused by the RDW itself but by this pump pulse. Because of the positive chirp, the pulse duration is stretched longer but the group velocity of soliton is not changed [102], then the RDW is excited at the same wavelength. At the same time, the longer pulse can form several solitons instead of just one with the amplitude of input pulse large enough [44]. Each soliton will excite different wavelengths of resonant RDW due to the different phase matching conditions that have to be satisfied for each soliton in fibers. By introducing this positive chirp, the pulse is stretched longer with blue part lagged. At the same time, the blue part of pulse may form new solitons in the PCF, which will excite different RDW wavelength due to the GVD of the PCF. In our case, it is shown clearly in Fig. 5-10. that longer wavelength of RDWs are generated due to these stretched pulses because of the GVD properties of

the studied PCF, which consists with the tunability previous theoretical and experimental results. For this PCF under study, when we increase the pump wavelength, the RDWs wavelength (blue side) decreases because of the dispersion characteristic of the PCF.

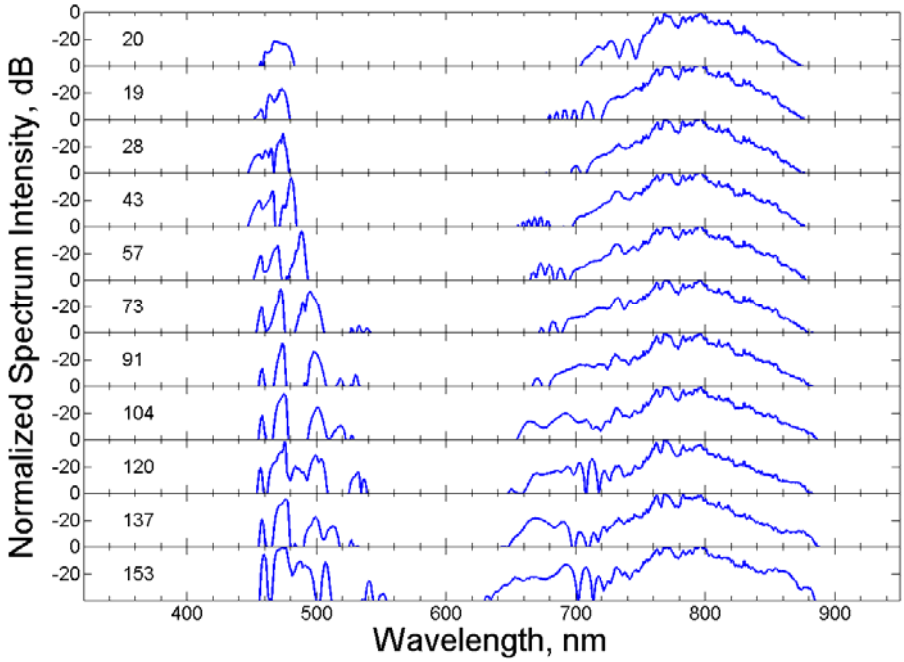

Fig. 5-10. The evolution of spectrum with changing the pump pulse durations, which are marked on the left side of the spectrum, which increase from 20 fs (negative chirped) to 153 fs (positive chirped). To make the weak components of the spectra easier to read, the spectra are in scale of logarithm.

As we discussed above the RDW generation has great advantage in generating frequency tunable femtosecond pulse, but it will be interesting to see if this tuning range can be extended by a cascaded RDW generation. Here, we show experimental results that may support this idea. The spectrum shown in Fig. 5-11 (a) is different from what we see in Fig. 5-8 with three peaks correspond to the pump light and two blue shift generations. It is clear that most energy of the pump light is transferred to the first blue shift generation in spectral range centered at 600 nm. This light intensity is even stronger than residual pump light. Meanwhile there is another blue shift light centered at 430 nm.

To make the relations between them clear, we check how the pump light power affects these blue shift generations shown in Fig. 5-12. How the peak frequency changes with pump power is shown in Fig. 5-12 (a). Red curve stands for infrared, and yellow and blue curves stand for first and second blue-shifted lights respectively. Compared to the yellow one, the intensity of the blue line is much smaller. We observe that both frequencies of pump and blue light do not change much during the process, so that we can conclude that light generated around 430 nm is a RDW. On the other hand, the frequency of yellow light does change at a linear rate. To show this dependency more clearly, what we show in the figure is not the absolute frequency, but the normalized frequency change. Meanwhile, we show a guided line of normalized frequency change for SPM in green curve, which has linear relation with pump power $\Delta\omega_{\max} \simeq \frac{\omega_0 n_2 I_0}{\tau}\frac{L}{c}$ where ω_0 is the laser carrier frequency, n_2 is the Kerr coefficient, I_0 is the intensity, L is the propagation length, τ is pulse duration and c is the speed of light. The calculated line, shown in Fig. 5-12 (a), fits very well with the first blue shift frequency change, so that we can conclude that SPM causes this strong energy transfer from infrared to yellow. We also sample part of the output, and record the power changes for each frequency and normalized them shown in Fig. 5-12 (b), where red, yellow and blue curves stand for each color output. It is noticed that the yellow curve changes almost at cubic rate of pump power, but the blue RDW changes at much faster rate compared with Fig. 5-9 (b). It is reasonable to say that SPM causes strong energy transfer from pump light to blue shift frequency, and this new light is so strong that they can form solitons inside the studied PCF. These solitons again excite blue shift RDW with phase matching conditions satisfied.

For this kind of cascaded frequency conversion we show one example that the generated RDW wavelength is even shorter than the second harmonic of pump laser, shown in Fig. 5-11 (b). It shows that there is possibility that RDW tunability can be extended after other strong nonlinear frequency shift with proper dispersion properties needed, and the peak intensity wavelength of the cascaded RDW free of the pump power fluctuation too.

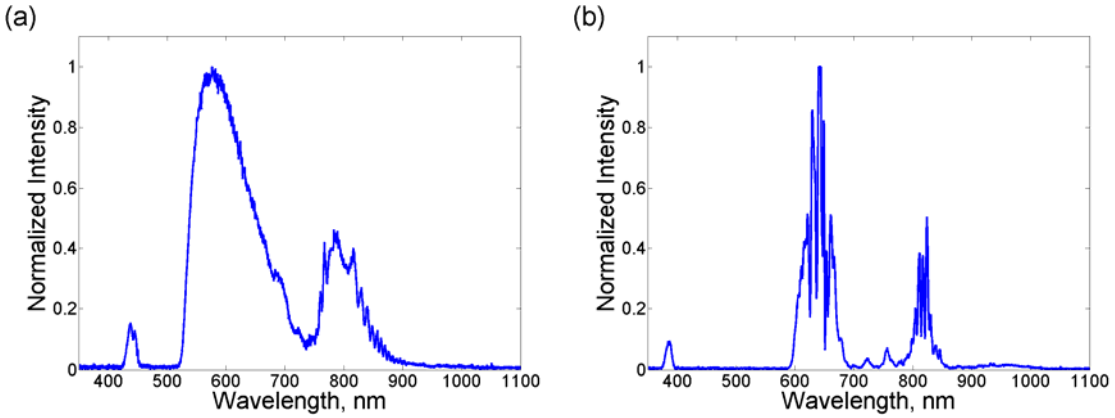

Fig. 5-11. The cascaded RDW generation by a SPM-resulted frequency-shifted soliton. In some case this cascaded RDW wavelength can exceed the second harmonic of pump laser, where pump laser wavelength is 820 nm, but the RDW wavelength is 380 nm.

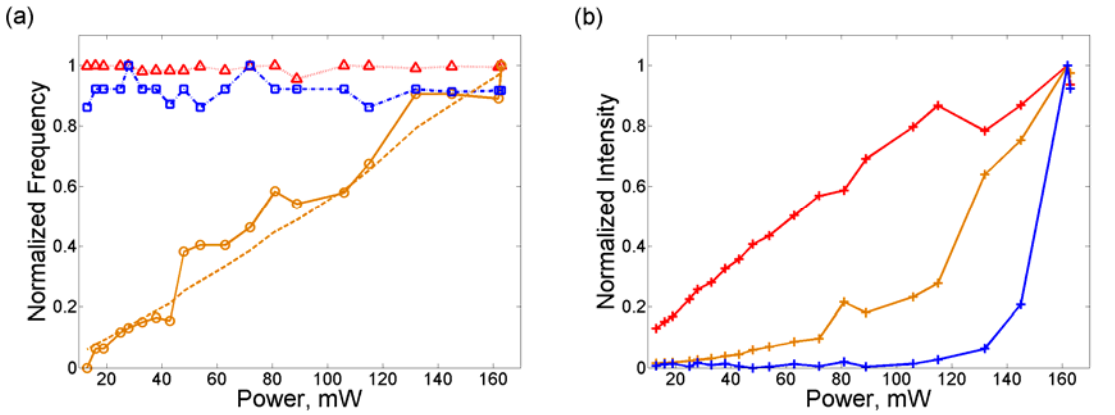

Fig. 5-12. The SPM generation peak frequency of dispersive wave generated in PCF(a), and The SPM generation peak power of dispersive wave generated in PCF.

We show above with a series of experimental results that the RDW generation can be very effective in the Kagome PCF under study. The generation is mainly determined by the GVD properties of the PCF, but not by the fiber length or pump light. This offers good tunable light sources without the need of sacrificing pump power, or a required specific length of the fiber. In our experiments, we found that the RDWs generating processes only evolve after a couple of millimeters of fiber, and this makes possible to think of applications based on compact devices. Based on the experimental

results, depending on the particular application, there are different suitable pump light pulses. For a broader RDW spectrum, a higher power and longer pulse is needed in order to extend the spectrum by means of SPM and high order solitons RDW generation. On the other hand, for a narrower bandwidth and a good tunability, a non-chirped pulse is needed. Moreover, the RDW intensity must be controlled in order not to introduce too much SPM, which is also related to the structure of PCF. For this application, a larger core size but closer dispersive character PCF will be favorable. Furthermore, we show that extremely strong SPM resolved frequency shift can be found in the studied Kagome PCF. This special interstitial feature of a Kagome-lattice PCF offers a broad variety of applications in nonlinear optics, and may cause cascaded RDWs generation.

As we mentioned that it is now well known and we have shown here that femtosecond pulses of light propagating along photonic PCFs can generate a broad optical supercontinuum [99], [103]. The resultant octave-spanning coherent light source can be applied to metrology [80], telecommunication [104] and spectroscopy [105]. In addition, we show the RDWs generation in PCF can be used to obtain tunable femtosecond pulse in an extremely large spectral range. However, in all of these experiments (supercontinuum, and wide-range frequency conversion) PCFs of many centimeters or even meters-long were used, and the processes were well-understood [98],[103].

In contrast to all the previous work, now we show that a supercontinuum or a smoothly-tunable femtosecond pulse can be obtained with extremely short fused silica PCF pumped by a femtosecond laser oscillator. Later, we will discuss these results release that the previously proposed generation mechanisms can not give fully explanations and it requires an alternative explanation or a better understanding of these processes.

It is generally believed that the enhanced nonlinear generation in PCFs owes to the small core (of a few-micrometer diameter) surrounded by a photonic crystal cladding with the geometry designed to have zero group-velocity dispersion at a desired wavelength. As a result, the femtosecond laser pulses can be strongly guided within a

small area and propagate over a considerable length without being stretched by dispersion [86],[88]. The fundamental nonlinearity is provided by the core material. The commonly accepted physical principles underlying supercontinuum generation are high-order soliton emissions combined with four-wave mixing, Raman-induced soliton self-frequency shift, and RDW generation mediated by solitons [98],[106],[107]. Recently, the generation of blue and violet light from infrared femtosecond pump pulses was explained by the effect of radiation trapping in a gravity-like potential created by accelerating solitons [108]. Among these experiments and numerical models using the generalized nonlinear Schrödinger equation, fibers with lengths from centimeters to meters were studied, but little work was done on fibers of sub-centimeter length. We note that supercontinuum generation was obtained with a 5.7 mm long soft-glass (Schott SF6) PCF, and the authors claimed this was due to the high nonlinearity of the material [109] (to our knowledge, the shortest fiber reported was 4 mm [110]). Here we focus on experiments with short PCFs made of fused silica (low nonlinearity material), and try to isolate the initial stages of supercontinuum generation.

Again, in these experiments we use same mode locked femtosecond Ti:Sapphire oscillator (Kapteyn-Murnane Labs, TS laser kit) with tunable bandwidth and center wavelengths, and a repetition rate of 85 MHz. A pair of external fused silica prisms is used to compensate the dispersions of optics outside the cavity, including a $20\times$ microscope objective lens used to couple the laser pulses into the PCFs. The laser power can be adjusted by tuning a neutral density filter placed in the beam.

We couple it into the knots of the cladding which have the size of about 1 μm shown in Fig. 5-2 [111]. The input pulse has the center wavelength of 806 nm and pulse duration $<$ 25 fs (for a Gaussian pulse). The focal spot of the laser beam is about 5 μm. We observe the output spectrum gradually broadening with increasing input power, as shown in Fig. 5-13 (a) (see Supplementary Information, GIF. S1) for a 3.1 mm-long fiber, and Fig. 5-13 (b) (see Supplementary Information, GIF. S2) for a 5.9 mm-long fiber. Compared with a common supercontinuum, these spectra are smoother. When the power is large enough for the blue spectral wing to expand and reach the frequency of

the RDW [52],[112], we see that the spectrum stops broadening (in the visible range), and the peak of the RDW gets stronger.

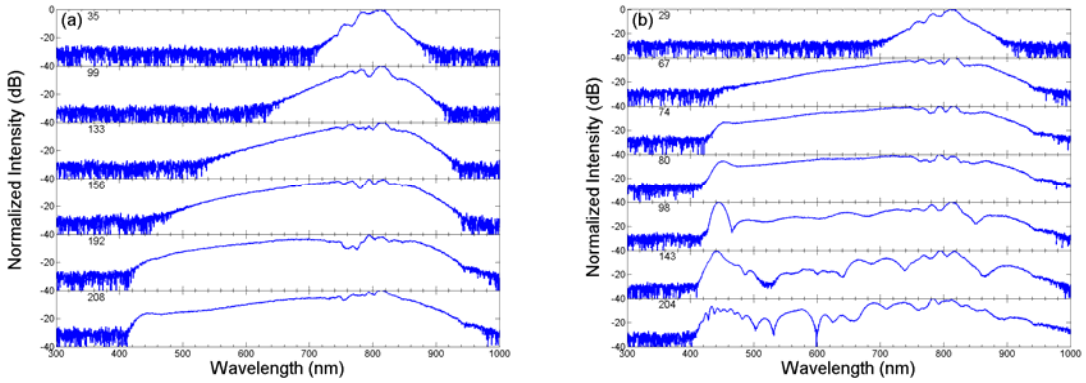

Fig. 5-13. Supercontinuum generation in 3.1 mm PCF (a) (also see Supplementary Information, GIF. S1), and 5.9 mm PCF (b) (Supplementary Information, GIF. S2), for varying pump power (which is marked on the left side of the spectral curves).

Under slightly different coupling conditions, we achieve generation of different blue-shifted wavelength-tunable femtosecond pulses; which correspond to different RDWs. In this case, we excite different modes in the same knot. Fig. 5-14 (a) shows an example, where same as previous results the tunability is achieved by tuning the wavelength of our Ti:sapphire laser oscillator. Again, the tuning is governed by the dispersion characters of the fiber, and when we decrease the input laser frequency the RDW frequency increases (somewhat counterintuitively) shown here and in Fig. 5-6. For a longer (20 mm) fiber, in addition to the blue-shifted RDW we observe the other conjugate IR-shifted RDW [100], with a peak wavelength at around 1.8 μm, as shown in Fig. 5-14 (b); however, for a short (5.9 mm) fiber, we do not observe any wavelength longer than 1.4 μm in infrared.

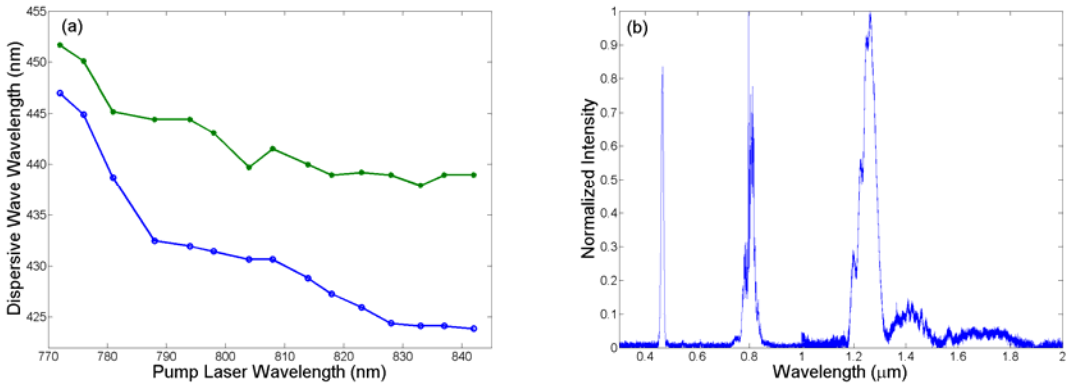

Fig. 5-14. Fine tunability of the resonant dispersive waves with changing the pump laser wavelength. Blue and green curves are output spectra with identical laser pulses coupled to the same PCF cladding knot but slightly different coupling conditions (a). The output spectrum for a 20 mm long PCF (b) (data from two spectrometers is combined). The peaks around 450 nm, 800 nm and 1300 nm correspond to the blue resonant dispersive wave, pump laser, and Raman generation respectively. The peak around 1800 nm may be related to the other (IR) resonant dispersive wave.

The observed supercontinuum generation is highly sensitive to the polarization of input laser beam because of the birefringent structure of the knot in the PCF cladding: When the polarization plane is rotated (by a half-wave plate specified for 780 nm), the generated bandwidth can be reduced substantially, compared with the situation when the polarization is optimal (Fig. 5-15).

The experiments here show that both the supercontinuum and the RDW generation are strongly polarization-dependent, which means they can be easily used for a polarization optical switch and integrated with other fibers.

We give the experimental results with fiber length of 3.1 mm here, but it is for sure that fiber as short as 2 mm can still work with our low energy laser. One of the important appliation of such PCF is the ultrashort pulse generation based on RDW, and we showed above how short pulse people can obtain with cm long fiber. For such short (mm long) fiber, even shorter pulses can be obtained because the pulses will suffer less dispersion.

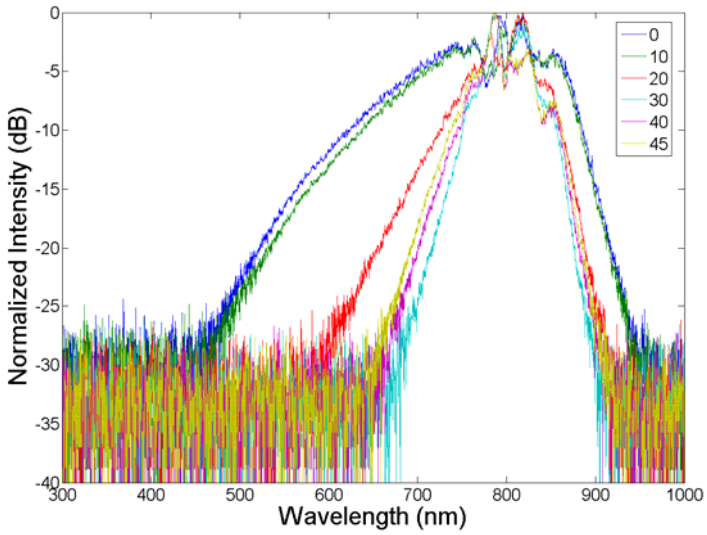

Fig. 5-15 The spectra of supercontinuum generation for different input laser polarizations. For each curve, the rotation angle of the half-wave plate is given (see text for detail).

An important issue is the mechanism behind the extraordinary phenomena described above. With short fibers, the most important nonlinear process will dominate among other complicated processes involved. For a 3.1 mm fiber, the SPM of light propagating in the fiber can not result in such a huge frequency shift [98]. The maximum frequency shift that can be achieved with SPM is $\Delta\omega_{\max} \simeq \omega_0 n_2 I_0 \frac{L}{c}$ [44], which we have observed in a longer fiber and shown earlier. One possible argument is that if the speed of the optical pulse is reduced, then this nonlinearity is enhanced. We use a photodiode to compare the time delay with and without the fiber, but do not observe any obvious change of the timing. So we conclude that the nonlinearity is not enhanced in this way. Furthermore, both Fig. 5-13 (a) and Fig. 5-13 (b) show asymmetric spectral broadening which is different from the theoretical result of Ref. [103]. On the other hand, the dispersion distance for this fiber $L_D = \tau^2 / |\beta_2|$ [44] is much larger than 3.1 mm at 800 nm. It would be hard to have formation of stable optical solitons, as pointed out in Ref. [109]. Besides, we do not observe the IR RDW with short fibers but the blue RDW is generated.

Thus this RDW generation is different from the modulation instability in conventional fibers [113]. When we change the polarization, the output power does not change much, which implies that the intensity in the fiber is actually the same. The polarization-dependent supercontinuum was observed before, but our experimental results show much stronger dependence compared with previous results [114], [115].

Another important issue is the carrier-envelope phase of the SC or RDW. Base on our experimental results with Ti:sapphire shown in Fig. 4-10, it shows clearly that there is no restriction that RDW generated far from pump light will keep exactly same carrier-envelope phase, in other words the offset frequency. However it is crucial part of the metrology of optical frequency with PCF. In Fig. 5-13, we can see clearly that the SC always happens earlier than the RDW generation and seeds the RDW generation. Then it is possible the SC keeps the same offset frequency. If SC happens earlier than RDW, then there is no good explanation for the SC in such short PCF yet.

Apparently, the micron-scale structure itself (that of a laser-guiding knot in the PCF cladding) contributes to the increased nonlinearity. Then, the key to understanding the spectral composition of the generated light must be the physics of intrinsic (polarization-dependent) PCF modes excited by the input laser beam [116]. Our results clearly show that as soon as this broadened spectrum hits the frequency of the RDW, phase matching then allows energy efficiently transferred into this wave's spectral region and the spectra of supercontinuum stop broadening. As the intensity of the RDW increases, new modes are excited. With the increased propagation length, more complicated nonlinear propagation process become significant, and this is the reason why complicated structures start showing in the output spectra [103][117].

One can engineer PCF dispersion by designing the structure and changing the silica-to-air ratio, or alternatively adjust the coupling conditions as talked above, thus adjust the wavelength of the RDW. Since this wave's frequency determines the bandwidth of the supercontinuum, as shown by the above results, with short enough fibers (and high enough input intensity) one can therefore achieve smooth spectral supercontinuum with the desired bandwidth

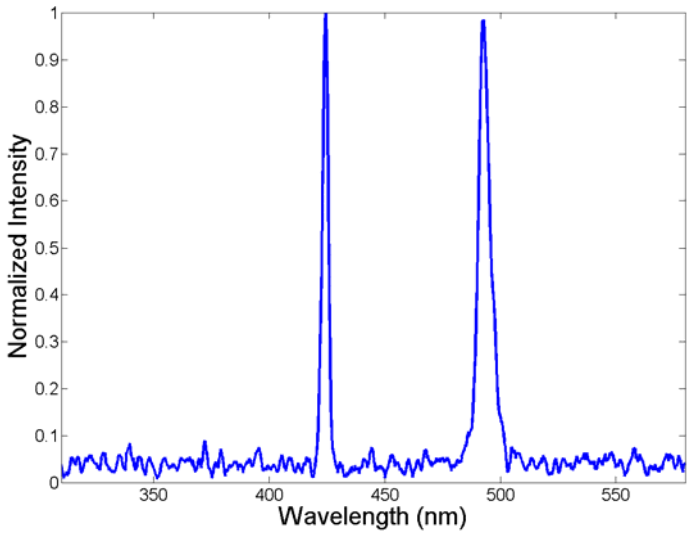

Fig. 5-16 The output spectrum of a 10 cm long PCF with pump laser wavelength at 1500 nm. The peak around 500 nm is the third harmonic of the pump laser, and the peak around 425 nm is the dispersive wave generation.

In addition to the production of a controlled supercontinuum, we always call the attention to the RDW generation. We show this process can be used for broad-range tunable frequency conversion of femtosecond pulses. With a reasonably short fiber length, we have confirmed that the blue-shifted output is a rather clean narrow-bandwidth femtosecond pulse. As an example of an extremely large frequency shift that can be obtained in such a converter, we show generation of a RDW whose frequency exceeds that of a third harmonic radiation for a fundamental wavelength at 1500 nm, as shown in Fig. 5-16 (we use 50 fs pulses obtained from an optical parametric amplifier and a 10 cm long PCF).

In summary, we show that efficient frequency conversion in PCF is not necessarily associated with large propagating length or high material nonlinearity. Supercontinuum generation can be obtained with extremely short fused silica PCFs by using a mode-locked oscillator only. Besides, the RDWs play an important role in various processes in such fibers: First, they determine the bandwidth of the generated

supercontinuum; Second, they can be used for efficient frequency conversion. With a proper selection of fiber length and pump intensity, the output can be a clean narrower-bandwidth femtosecond pulse. Compared with a conventional supercontinuum [118] and parametric frequency conversion processes [41],[119], the RDW generation in PCF offers extra degrees of control. This advantage will make it useful in many applications including all-fiber nonlinear optical components. Last, we point out that the well-studied processes such as soliton fission and SPM can not fully explain the nonlinear process at the initial stages of supercontinuum generation. A more detailed study is needed, which may elucidate the role of microstructures in producing high optical nonlinearity and help to make fully use of this advantage.

This is huge impact on the nonlinear optics because in the conventional nonlinear optics the nonlinearity relies on the material energy states or microscopic periodic inner structure [40],[44],[120]. However, we see in our experiments, for the low nonlinearity material -fused silica, the macroscopic periodic structure greatly enhanced the nonlinearity. This characteristic of PCF and photonic crystal will be able to deeply impact the application of nonlinear optics because the extra freedom to control the nonlinear optical materials (or structures).

6. APPLICATIONS IN COHERENT RAMAN MICROSPECTROSCOPY

Optical microscopy is a key technology for materials science and biological research. Coherent anti-Stokes/Stokes Raman scattering (CARS/CSRS) microscopy allows to obtain high-resolution imaging with chemical contrast, based on the vibrational Raman spectra of the sample molecules [121],[122],[123], and it extends a lot the applications of the microscopy. At the same, with all the lasers involved, there are more channels for the nonlinear frequency generation even at the same wavelength shown in Fig. 6-1. When the femtosecond lasers are applied to such experiments, on one hand the real time detection capability of CARS is enhanced [5], on the other hand the non-resonant contributions are also increased, which may distort the CARS signal and decrease the signal-to-background ratio [40],[44].

Recently, a so called hybrid CARS technique has been developed [124] and applied to micro-spectroscopy and imagine with a simplified system based on a femtosecond Ti:sapphire laser oscillator [125]. In addition, related techniques have been developed and used on a number of samples [125],[126],[127],[128], and a special emphasis has been made on the enhancement obtained through preparation of a substantial molecular coherence [129],[130],[131].

In this section, we demonstrate that the oscillator-based hybrid CARS micro-spectroscopy with both forward- and epi-detection (back-scattering) configuration. We show that this simple technique can be applied to obtain high chemical contrast combined with near diffraction-limited spatial resolution, and may have potential implications on opaque samples where the forward-propagating signal can not be collected. Compared with CARS experiments using the amplifier femtosecond laser system, the oscillator-based system has advantages of high repetition rate (~ 100 MHz) and sample friendly low energy (~ 3 nJ), which is crucial for live samples.

As we talked about in the Section 3, we can “roughly” separate the nonlinear optical processes involved in generation of non-resonant background and Raman-resonant signal as parametric and nonparametric processes. Because the non-resonant

background differs from the Raman signal in that it does not introduce population into real energy states but to some virtual levels. However, it is possible that a non-parametric process is involved if the two-photon absorption coincides with a real level. When several optical fields are involved, a parametric process can typically occur only if the laser pulses are overlapped in time within the nonlinear media. Because of its extremely fast behavior, a parametric process can be exploited in order to amplify femtosecond laser pulses while eliminating pre- and post-pulses [132],[133]. Moreover, one may utilize this behavior to eliminate unwanted parametrically-generated background, by applying time-delayed pulses to a sample. At the same time, the resonant signal can survive, due to the intrinsic memory associated with real energy levels. In particular, virtually un-attenuated background-free resonant Raman signal can be produced with short-pulse excitation and time-delayed probing of Raman coherence, as long as the probe pulse delay is less than the coherence lifetime.

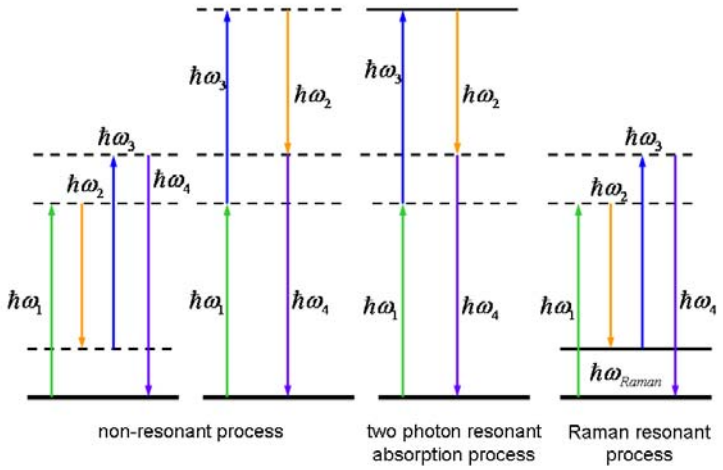

Fig. 6-1. Four photon process may contribute to the signal. The dashed line presents a virtual state and the solid line stands for the real energy state. The non-resonant processes give rise to the non-resonant susceptibility.

In the present work we utilize impulsive Raman excitation, with pump pulse

duration comparable to half the molecular period (and a correspondingly broad pump bandwidth so as to excite high-frequency molecular vibrations coherently). In this case, the Raman signal is [134]

$$S_{ICRS}(\tau) = \left|\chi_{\alpha\alpha}(\tau)\right|^2, \tag{6.1}$$

where $\chi_{\alpha\alpha}(t) \equiv -\frac{i}{\hbar}\left\langle\left[\alpha(t),\alpha(0)\right]\rho_g\right\rangle$ is the linear response function associate with polarizability, $\alpha(t)$ is the operator of polarizabilty, ρ_g ground state density operator and $\hbar = h/2\pi$ h is the Plank constant. If the pump and probe pulses overlap in time, it can not be expressed in such a simple way because all the 24 terms of third order nonlinearity need be taken into account due to the large bandwidth of the impulsive pump laser [40],[44].

We use the same mode-locked Ti:sapphire laser oscillator. The spectral bandwidth coverage can be extended to more than 2000 cm^{-1} [75],[76]. The oscillator output is focused onto a 5-mm thick LBO crystal (CASTECH) to generate the probe light via SHG, where the SHG spectrum is <1 nm because of the phase-matching constraint. Then the laser beam is collimated to send through a four-prism system, as shown in Fig. 6-2. The prisms are used to separate and then re-combine the pump and probe beams, and more importantly, to compensate the dispersions the pump pulse experiences through optical elements outside the laser cavity (including the first microscope objective lens Ob1). With the dispersions compensated, the pump pulse duration at the sample is less than 20 fs. The probe pulse duration is about 1 ps after all optics. The probe pulse is sent through an adjustable translation stage, which controls the relative timing between the pump and probe pulses. We also use a bandpass filter (BPF; F03-405.4-4, CVI-Melles Griot) to suppress the spectral wings of the probe pulse within the spectral windows corresponding to CARS and CSRS.

Then the infrared and SHG beams are collinearly coupled into an achromatic objective lens (Ob1, 20×, NA = 0.4, LOMO) and focused on the sample, which is a

benzene drop on microscope slide covered with a thin cover glass. Extra lenses are used to bring focuses of both pump and probe beams into the same plane. The measured input powers of the pump and probe beam before Ob1 are 110 mW and 1 mW respectively. Without inserting the optics shown in the dashed box of Fig. 6-2, the light after the sample is collected via the second objective lens (Ob2). After filtering off the pump and probe light, it is coupled into an imaging spectrograph (Chromex, Bruker Optics) with a TE-cooled CCD (iDus, Andor) attached. The resolution of the spectrometer is set to be better than 0.5 nm. The spectrograph and the translation stages for the probe pulse delay and for the sample holder are all motorized and computer-controlled.

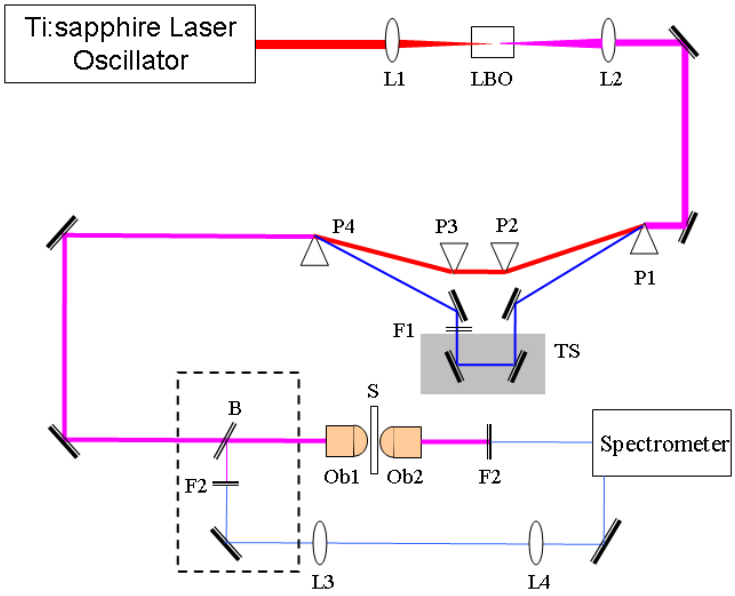

Fig. 6-2. Experimental setup schematics. L1,2, lenses, 200-mm focal length; LBO, lithium thiborate; P1-4, prisms; F1, bandpass filter centered at 405 nm (F03-405.4-4, CVI-Melles Griot); TS, translation stage; Ob1,2, microscope objective lenses. Sample is liquid benzene layer on microscope slide covered with thin cover glass. F2, Notch Filter (RNF-405.0, CVI-Melles Griot); B, beam splitter (a microscope glass slide). L3,4, lenses are used to image the sample onto the spectrograph and to eliminate unwanted background with iris. First, the parts in dashed box are not put in optical beam, and the light is collected through Ob2 at the forward direction. Then the parts in the dashed box are put in the optical beam, and the light will be collected at the backward direction (epi-detection) through lenses L3,4.

The resulting spectrogram for a neat solution of benzene is shown in Fig. 6-3. The trace around 405 nm corresponds to the residual probe light after the filter (RNF-405.0, CVI-Melles Griot). Clearly, the strong broadband signal at zero probe delay is the mixture of both resonant signal and the non-resonant background. The non-resonant contribution is spectrally broad. Due to its instantaneous nature, non-resonant FWM rapidly decays when the delay between the two pulses is increased. The long-living resonant contribution, on the other hand, stands out. Two narrowband blue- and red-shifted profiles are CARS and CSRS components of the scattered radiation, corresponding to the ring-stretching mode at 992 cm^{-1}. Even though the time delay of the probe pulse is accompanied by attenuation of the coherent Raman signal, it drastically improves the signal-to-background ratio.

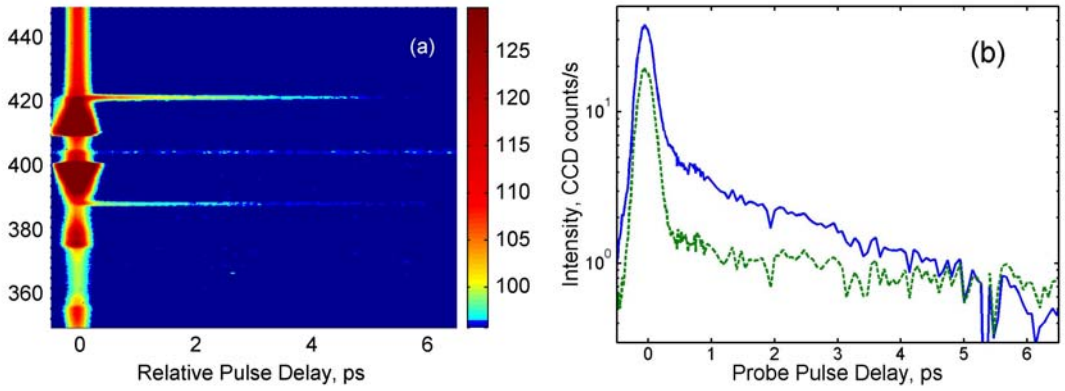

Fig. 6-3. CARS-CSRS spectrogram, obtained on a neat solution of benzene: (a) Spectrum of the scattered light is plotted as a function of the probe pulse delay. The probe pulse contribution is removed by a notch filter (RNF-405.0, CVI-Melles Griot); (b) Cross-sections of the spectrogram along the probe pulse delay at the peak of CARS (blue solid curve) and CSRS (green dotted curve). Ring-breathing mode at 992 cm^{-1} is excited.

Fig. 6-4 shows a similar spectrogram taken for a neat solution of pyridine. Due to the interference between two closely spaced ring-breathing modes, 992 and 1031 cm^{-1}, which are not resolved spectrally within the probe pulse bandwidth, one observes a modulation of the recorded CARS and CSRS signal as a function of the probe pulse

delay at the difference frequency between the two Raman modes. These oscillations, common for time-resolved CARS, are referred to as quantum beats.

To demonstrate imaging capabilities of the setup, we put a drop of benzene in a water drop on a microscope slide and covered with cover glass, which makes a liquid layer with thickness less than 100 μm. We record the intensity of the acquired CARS signal as a function of the focus displacement at the benzene-water interface. We scan an area with 100 μm by 100 μm with 2-μm steps for each axis, shown in Fig. 6-5. One can clearly see the interface between the two different liquids with the resolution of the beam focal spot size. We also plot the curve for the signal intensity versus the horizontal displacement of the bottom line in the image, shown below the image.

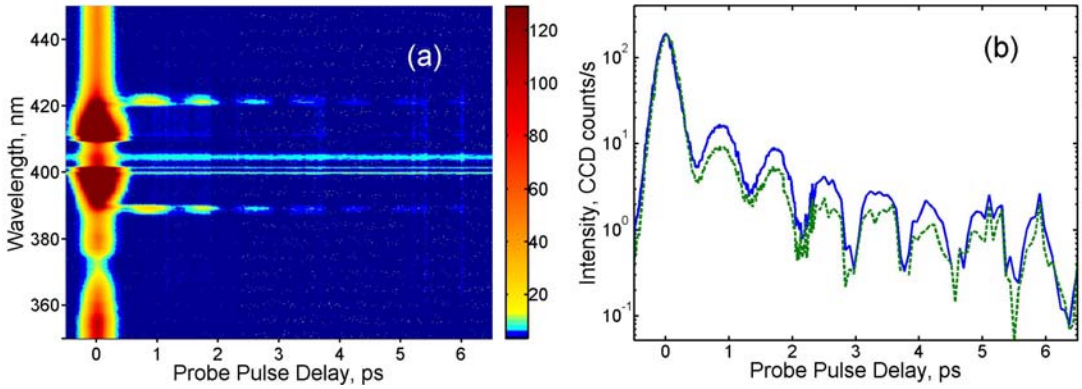

Fig. 6-4. CARS-CSRS spectrogram, obtained on a neat solution of pyridine: (a) Spectrum of the scattered light as a function of the probe pulse delay. The probe pulse contribution is removed by a notch filter (RNF-405.0, CVI-Melles Griot); (b) Cross-sections of the spectrogram along the probe pulse delay at the peak of CARS (blue solid curve) and CSRS (green dotted curve). The beating pattern is a result of interference between two excited Raman modes of pyridine, 992 and 1031 cm^{-1}.

In our experiment, we employ the impulsive excitation method so that all the modes that falling into the pump laser spectral bandwidth could be excited at the same time. Then, this means that we are not looking at specific Raman lines but certain range of Raman lines. This is great advantage if mixed sample with different chemicals is needed to be diagnosed, and those chemicals may be found in a single measurement.

Such a sample is shown in Fig 6-6, where we mixed the benzene and acetone together and obtain the CARS/CSRS spectrum with a single measurement. We see clearly that we are able to identify these two chemical at the same time without needing tuning the laser wavelength.

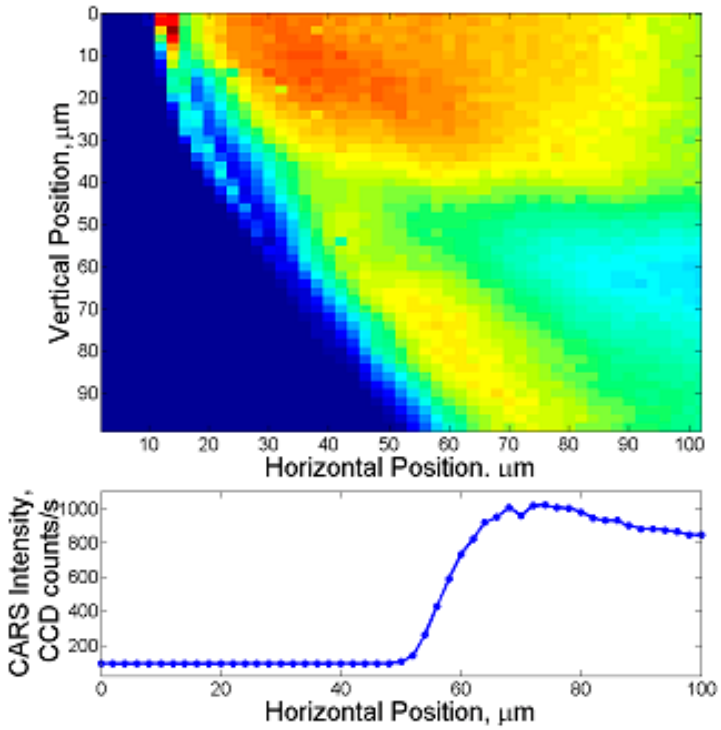

Fig. 6-5. Normalized CARS signal as a function of the focus displacement across the benzene-water boundary. Inset: 2D CARS image of the interface between water (down) and benzene (up).

Now we record the signal spectrum as a function of probe pulses delay in a much larger range, as shown in Fig. 6-7 (a). The positive delay means probe pulse lags the pump pulse; conversely the negative delay represents the probe pulse leads the pump pulse. Clearly, the strong broadband signal at zero delay is mainly due to the nonlinear generation through parametric process. As we mentioned earlier, Stokes and anti-Stokes Raman generation is produced by the coherence prepared by the pump laser, and therefore we do not expect any coherent Raman scattering when the probe pulse arrives

earlier than the pump pulse. However, we observe CARS and CSRS signal for negative probe delays, when the probe pulse goes ahead of the pump pulse on their path to the sample. With the help of the instances of parametric signal generation for two (negative) values of the probe pulse delay, we conclude that those signals correspond to the first and the second back-reflection of the probe pulse at glass-air interfaces. The CARS/CSRS signal generated for probe pulse delays ranging from -6 ps to -0.5 ps can be seen as generation with counter-propagating pump and probe pulses in an epi-detection configuration [135].

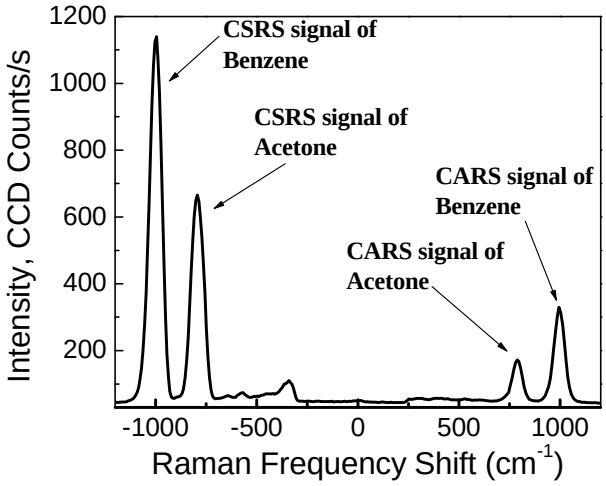

Fig. 6-6. CARS-CSRS spectrogram, obtained from the benzene mixture of benzene and acetone, showing that the impulsive excitation method has the advantage of monitoring all species with the Raman shift frequencies falling into the bandwidth of the pump laser.

Furthermore, to have a more detailed comparison, we plot the CARS and CSRS signal intensities on a natural logarithm scale [Fig. 6-7 (b)]. In addition, we pick one frequency between the anti-Stokes and Stoke lines and one frequency outside this range. We observe drastically different temporal behavior for resonant and non-resonant signal components. Meanwhile, we see that even in the epi-detection configuration, the CARS/CSRS signal is sufficiently strong. The difference between the back-generated

signal intensity and the forward-generated intensity is due to the small reflection coefficient (~ 4%). At the same time, this epi-detected signal is much larger than the signal produced by the second reflection; this indicates that the epi-detected signal is truly propagating in the backward direction with respect to the probe (but not the pump) pulse.

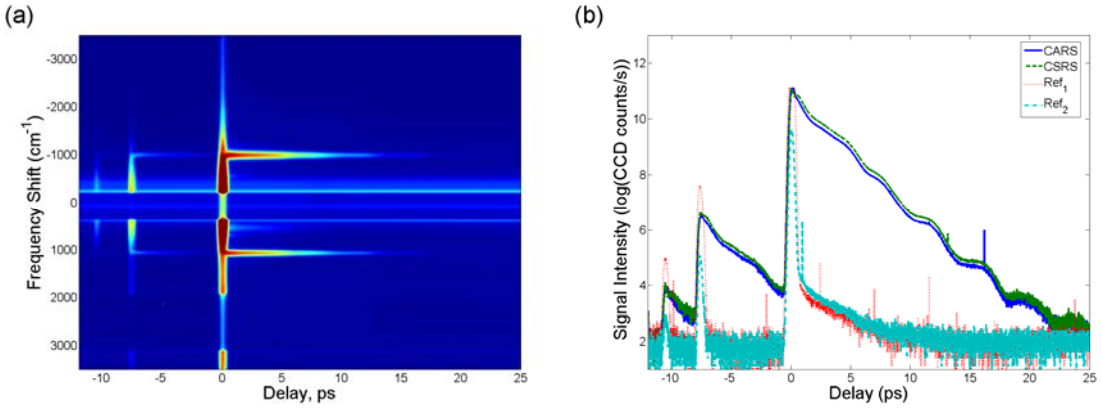

Fig. 6-7. CARS-CSRS spectrogram, obtained from the benzene sample: (a) Spectrum of the scattered light is plotted as a function of probe pulses delay. The probe pulse contribution is removed by a notch filter (RNF-405.0, CVI-Melles Griot); (b) Cross-sections of the spectrogram along the probe pulse delay at the peak of CARS (blue solid curve), CSRS (green dashed curve). The red dotted curve and cyan dashed-dotted curve are two references curves with the frequency between and outside CARS and CSRS respectively. The intensities are on the natural logarithm scales.

Then, we insert the beam splitter (which in our case is just a microscope slide) into the laser beam. Now, we have both pump and probe pulses propagating in the same direction, but detect the CARS signal in the backward direction (as shown in Fig. 6-2). The signal [Fig. 6-8 (a)] shows the same temporal behavior as in Fig. 6-7 (a). Fig. 6-8 (b) is the measured spectrum at ~ 1 ps probe pulse delay; the frequency shift of Stokes and anti-Stokes lines is in good agreement with the Raman spectrum of benzene. These experimental results confirm that the hybrid CARS micro-spectroscopy can be used in epi-detection configuration and potentially applied to opaque media [136],[137]. One thing is needed to clarify that we did not optimize the setup for epi-detection because of the limitation on optics components (*e.g.* beam splitter and mirrors), but the results here

show that much better results will be obtained with optimized design.

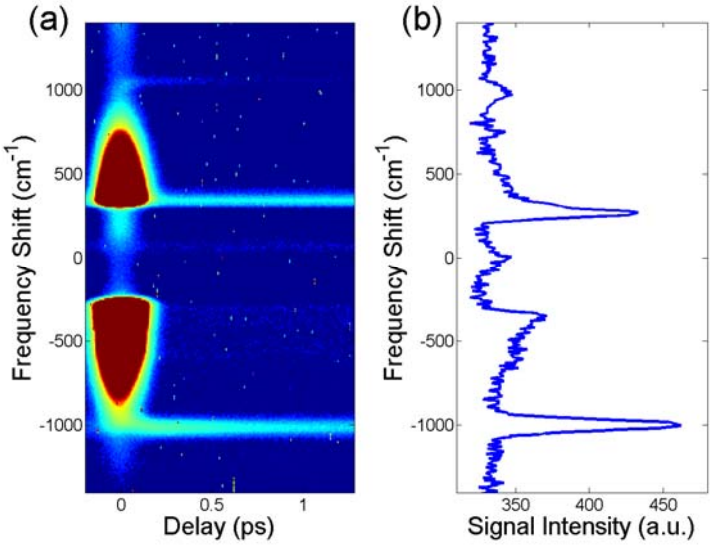

Fig. 6-8. CARS-CSRS spectrogram, obtained with epi-detection: (a) Spectrum as a function of the relative timing between probe and pump pulses (similar to Fig. 6-6 (a)). (b) The measured spectrum at ~ 1 ps probe pulse delay, and the frequency shift of Stokes and anti-Stokes lines are in good agreement with the Raman spectrum of benzene. At the same time, we compare the spectrum with the ones we obtained with water drops on the back side of the slide, and do not see a big change of the signal. This confirms that the signals obtained here are truly scattered at backward direction, not reflections at the air-glass interface.

We have demonstrated a simple, cost-effective setup and efficient epi-detected, which can be utilized for CARS microscopy. It is a feasible alternative to other oscillator-based systems, considered recently. Please note that the scheme does not require a pulse shaper. The employed four-prism system can, in principle, be replaced with a compact set of chirped mirrors. One can also fine-tune the optical elements to compensate for higher orders of dispersion (beyond the linear chirp) acquired by the ultrashort pump pulse before reaching the sample. At last, the described implementation can be further extended, *e.g.*, to different probe wavelengths if SHG is replaced by RDWs generation in a PCF.

We have shown the experimental results showing good application opportunities. Meanwhile, the nonlinear process is a little more complex than normal cases. Now we take a little bit theoretical look. The excitation process of stimulated Raman can be described by the stimulated scattering equation of motion for a damped nondispersive vibrational mode,

$$\frac{d^2Q}{dt^2}+2\gamma\frac{dQ}{dt}+\omega_v^2Q=\frac{1}{2m}\left(\frac{d\alpha}{dQ}\right)\left\langle E_iE_j\right\rangle, \tag{6.2}$$

where Q is the normal vibrational coordinate, m is the reduced mass density or moment of inertia, ω_v is the natural undamped frequency, γ is the dephasing rate of the mode, and α is the polarizability of a molecule. The driving force is the product contains difference-frequency terms $E_iE_j \sim \cos(\Omega t-\vec{k}\cdot\vec{r}) \sim Q(\vec{r},t)$ [40],[44],[138], where $\Omega=\sqrt{\omega_v^2-\gamma^2}$. With the impulsive excitation (*i.e.* delta function) taken into account, $E_iE_j \sim \delta(t)\cos\left(\vec{k}\cdot\vec{r}\right)\sim\delta(t)\left[\delta\left(\vec{k}+\vec{k}'\right)+\delta\left(\vec{k}-\vec{k}'\right)\right]$. This produces a standing-wave vibrational response:

$$Q(\vec{k},t)\propto a_{ij}\left[\delta\left(\vec{k}+\vec{k}'\right)+\delta\left(\vec{k}-\vec{k}'\right)\right]G^Q(t), \tag{6.3}$$

where $G^Q(t)$ is the impulsive response function (Green's function) given for underdamped modes by:

$$G^Q(t)=e^{-\gamma t}\sin(\Omega t)/m\Omega. \tag{6.4}$$

For an underdamped vibrational mode, it shows that

$$I(t)\propto e^{-2\gamma t}\sin^2(\Omega t)\propto e^{-2\gamma t}\left[1-\cos(2\Omega t)\right]. \tag{6.5}$$

Impulsive stimulated Raman scattering signal show oscillations at twice the vibrational frequency and decay at twice the vibrational dephasing rate. The dephasing time of benzene was measured to be around 5.1~5.3 ps [139], and our experiments (*i.e.* Fig. 6-7) show that about 2.5~2.6 ps in good agreement with the prediction.

7. CONCLUSIONS AND FUTURE WORK

Solitary waves have been the subject of intense theoretical and experimental studies in many different fields, including hydrodynamics, nonlinear optics, plasma physics, and biology. The temporal optical solitons are widely applied in optical communications and ultrashort laser systems as discussed in the introductions. We have shown in previous sections that when there is perturbation acting on a soliton (*e.g.* by a localized loss in the fiber or modified parameters in the laser cavity), a soliton will reshape its form and shed the excess energy into RDW. The interaction between a soliton and a dispersive wave was considered to be a parasitic effect and the prior work on RDW *per se* was kept marginal relative to the soliton dynamics. Indeed, in all the soliton-related applications, the RDW generation was a source of dissipation of the soliton energy, which affected the performance of soliton-based telecommunication system, and limited the pulse duration in a soliton laser.

However, I show in this dissertation the RDW generation is quite efficient when the FOD dominates. It is used to produce tunable femtosecond pulses both in a mode-locked Ti:sapphire laser and the small features of a PCF.

With the RDW generation in Ti:sapphire laser, we achieve multi-wavelength operation with tunable frequency difference between the main soliton and the RDW. Furthermore, because of the balance of the XPM and the negative GDD inside the cavity, the generated RDW behaviors like a soliton inside the laser cavity. The generated RDW holds ultrashort pulse duration, and is confirmed by our autocorrelation measurement. Other than the applications discussed earlier *e.g.* Raman spectroscopy, such dual- or multi-wavelength operation Ti:sapphire laser shows possible application in generating tunable mid-infrared femtosecond pulses. However, we do not have nonlinear crystal working in this spectral range, and no suitable detector either. This possibility is not confirmed with experiment in this dissertation, but doable with equipments requirement satisfied.

At the same time, there are still some works need to be done to fully understand then to fully make use such physical phenomena. It is really surprising to see the soliton behavior in the laser cavity is so stable under the cavity dispersion variation. The soliton makes itself adjusted quickly with those changes. We need have more detailed information of the pulse energy, pulse duration changes with dispersion changes, then we are able to have a better understanding the dynamics of Ti:sapphire laser mode locking.

Moreover, the idea of RDW generation is extended into the PCF, and we obtain tunable femtosecond pulses with the frequency tuning range covering the entire visible spectrum. Slightly different from Ti:sapphire laser, the pulse duration is kept short not because of the soliton-like behavior but the good dispersion properties of the PCF under study. It is same as the case in Ti:sapphire laser the nonlinear frequency conversion process is very efficient, and even larger than earlier theoretical estimations. In our experiments less than 1 nJ of input energy is needed. We achieve the largest tuning range for efficient nonlinear optical frequency conversion with such a simple and low energy femtosecond laser (not only the visible light but also the infrared light, Fig 5-5).

At the same time, I want to point out that the experimental results not only are the best ones up to date, but also indicate the mechanism of such efficient nonlinear process is not so clear at this moment. As pointed out in the Ref. [98],[103] that the mechanism of the conventional supercontinuum -SPM- can’t result in such large frequency shift, and they conclude the soliton fission is responsible for such large frequency expansion. In our experiments with longer fiber (~9 cm), we clearly show we can obtain the SPM resulted frequency shift and its frequency is power dependent. Meanwhile, we also show its frequency shift is much smaller compared with RDW generation in blue in the same output. This confirms that the SPM is not the mechanism of the supercontinuum in PCF. However, we cannot easily draw the conclusion that the RDW generation is responsible for the supercontinuum either. It is probably true for the cases when people use longer fiber and longer pulse. The longer fiber will help the

propagation features dominate in the total effects, and the longer pulse will result in the high order soliton generation and then more RDWs will come out as well.

In our short PCF experiment, we observe very smooth supercontinuum spectrum compared with those in Ref. [98]. In our experiment, we employ much shorter pulse on purpose so that no high order solitons involved. Meanwhile, our experimental results show very clearly the supercontinuum generation happens on an earlier stage compared with the generation of the RDW. Actually, it turns out that the supercontinuum seeds the RDW generation. This indicates that the RDW generation is not the mechanism of supercontinuum, but will dominate with longer pulses and longer fibers. At the same time, our results raise more questions and call for further studies in order to have a better understanding of the supercontinuum in PCF.

I point out that the solving of NSE – the envelope equation can't give fully picture of the supercontinuum. One such example is the so called f-2f method applied into the optical metrology. There is no any physics limit imposed on the frequency components generated by such equations, and I show that the RDW generated in Ti:sapphire laser may holds different offset frequency compared with the main soliton. However, f-2f experiment after PCF is confirmed by scientists by solid experiments that the supercontinuum frequency components all hold same offset frequency. With all experimental results here, we can see that the supercontinuum spectrum gradually increases with the pump power without any spectrum gap. It is reasonable to think those frequency components are generated gradually with reference to each other. If all these frequency combs are generated by the third order nonlinearity (we may think as a four-wave mixing process but with other limitation too), then such offset frequency is kept same for all frequency components. In other words, we present good experimental results show great application capability of such RDW and supercontinuum generations in PCF, but the mechanism still needs further development.

In the RDW generation in the PCF, it shows much more efficient nonlinear optical frequency conversion comparable with conventional nonlinear optical crystals, and it has the advantages of larger tuning range, higher damage threshold, less energy

requirements and many others as well. With the discussion just made above, it shows immediately a possible application other than mentioned earlier because this special offset frequency characteristic.

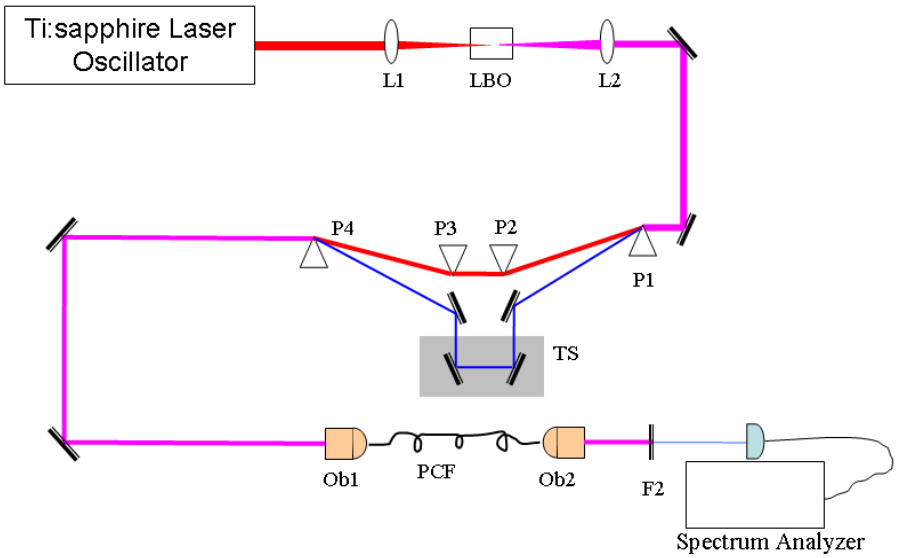

Fig. 7-1. Simple setup for the offset frequency measurement of the resonant dispersive wave generated in PCF.

For example, we mentioned that the supercontinuum can be used to measure the offset frequency in the optical metrology. However most of the supercontinuum energy is wasted in those experiments. Here we can improve a lot by directly employing the RDW instead of supercontinuum, shown in Fig. 7-1. We can fully make use the laser energy by only concentrate on the wavelength interested.

In the common f-2f experiments, what people used the frequency components are the two generated after supercontinuum in PCF, and the energy is extremely low ~ fJ. In our setup, I am able to generate the wavelength wanted with much higher energy ~ 10 pJ. Then people will have a chance to improve the signal to noise ratio about 100 times. For metrology, this should be a really good number. One such result is shown in Fig. 7-2, where (a) shows the fundamental spectrum, and (b) shows the SHG generation in blue

dashed line and the RDW generated in PCF in green solid line. The red dashed-dotted line shows the total spectrum on the detector.

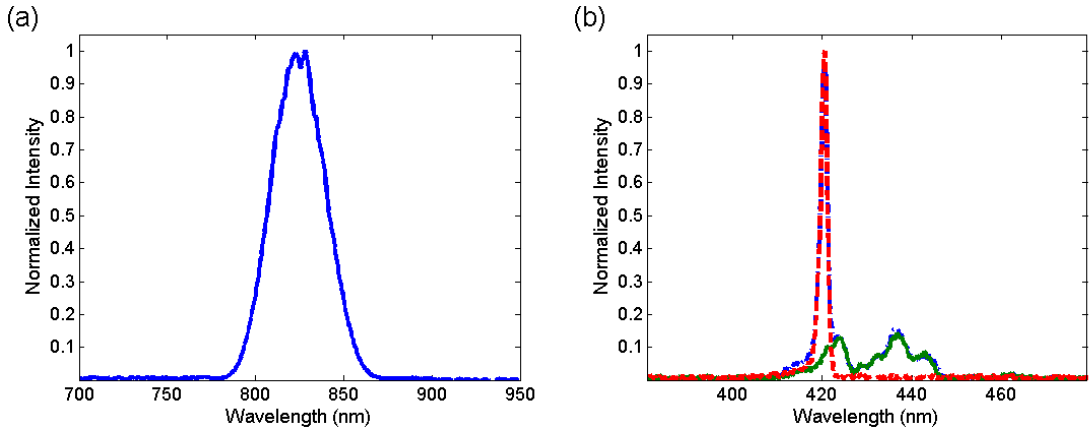

Fig. 7-2. The comparison of the spectrum output of the SHG and the RDW at 420 nm.

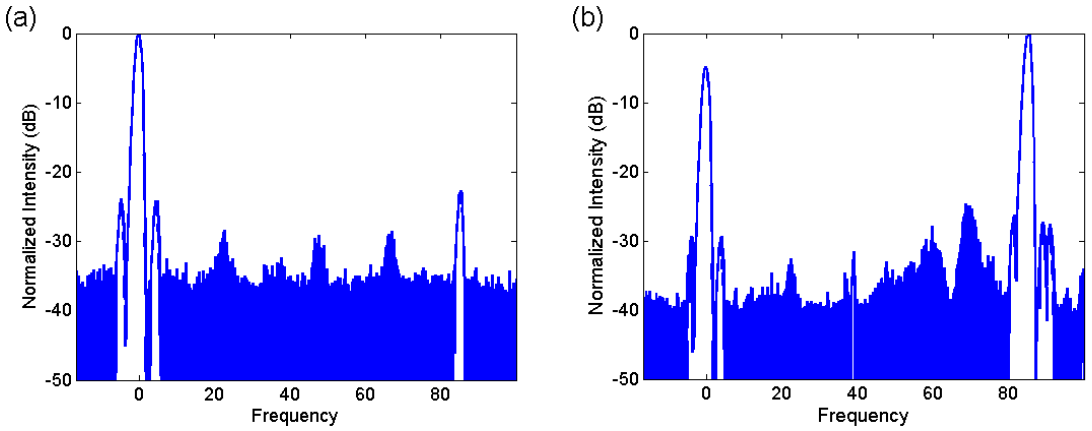

Fig. 7-3. The beating signal obtained from the f-2f measurement. The signal is obtained with a low frequency band pass, and the beating signal shows clearly at the low frequency part. The signal at high frequency (85 MHz) is the repetition rate (a); the signal is obtained without extra electronics, and the beating signal shows up around repetition rate (b). The radio frequency around repetition rate is some signal always observed on the campus of the Aggieland.

The f-2f beating results are shown in Fig. 7-3 (a). The signal is obtained with a low frequency bandpass, and the beating signal shows clearly at the low frequency part. The signal at high frequency (85 MHz) is the repetition rate; (b) the signal is obtained without extra electronics, and the beating signal shows up around repetition rate. The

radio frequency around repetition rate is some signal always observed on the campus of the Texas A&M University (maybe a campus radio station). Here I just want to give a principle prove experimental result in that all our optical components in the setup are not optimized. For instance we only have a mall amount power of the SHG coupled into the detector and the wavelength of the RDW is not tuned to best position either. Meanwhile the resolution is set at 1 MHz, so better signals can be obtained at better resolution. However, it is still surprising to see the very clear and very stable beating signal, since our laser cavity is not stabilized with external electronics. This is for sure confirm our claim above, but more important the good RDW characteristic shows here will make it favorable in more applications.

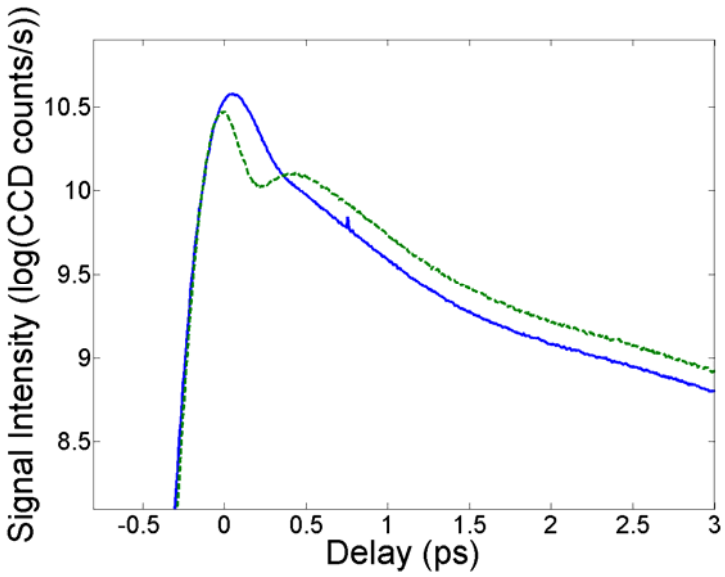

Fig. 7-4. A closer look at the CARS (blue solid line)/CSRS (green dashed line) signals in a shorter time period. The pump and probe lasers are overlapped in time range -0.5 ps to 0.5 ps. Clearly they show different temporal behavior in this short time period. The sample under study is benzene.

With a simple femtosecond-oscillator-based system, I demonstrate that it can be applied in coherent Raman microscopy, and the non-resonant background is eliminated by using a hybrid technique, which combines laser pulse shaping and timing with frequency-resolved detection, and is based on the different temporal behavior of

parametric and nonparametric processes. I show that this simple technique can be applied to obtain high chemical contrast and high resolution images, and it can be used for backward detection as well.

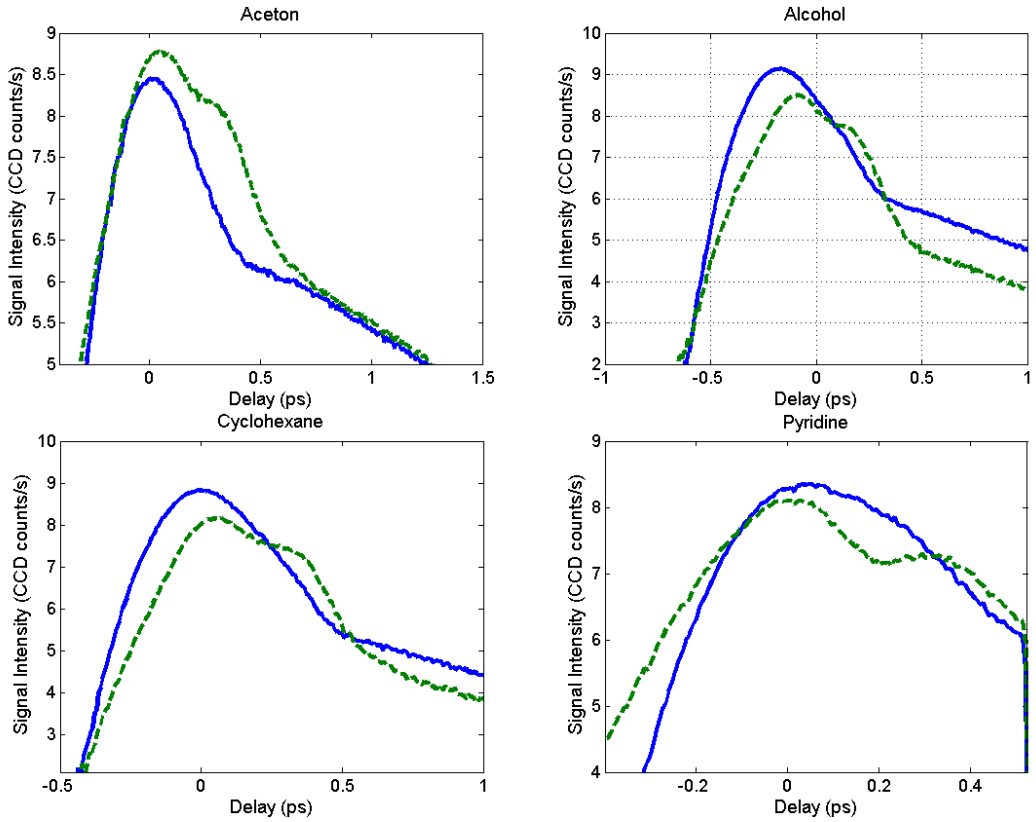

Fig. 7-5. A closer look at the CARS (blue solid line)/CSRS (green dashed line) signals for different chemicals: acetone, alcohol, cyclohexane and pyridine, and they all show similar behaviors.

At the same time, we can also improve the CARS experiments. First, we showed that the Ti:sapphire laser spectrum coverage can be extend to be larger than 2000 cm^{-1} by the RDW generation, but we did not give such experimental results only because the samples used in this dissertation do not have that large Raman frequency shift. It is interesting to see that we are able to direct observe glucose Raman signals with the same setup. This could be great help for glucose diagnoses since the light around 800 nm can penetrate human skins. There is also a chance that such laser system can be applied to

mixed gasses detection with the HC-PCF, which we used to generate RDWs. With numerical estimation, it shows this should be a sound application. Meanwhile the great tunability the PCF offers will help to extend the CARS spectroscopy to much larger spectral range.

Besides all these, I also find interesting fast temporal behavior of the CARS/CSRS signals for benzene, shown in Fig. 7-4. In the figure, it shows that the Stokes and anti-Stokes lines both have similar behavior in a large time scale, but vary in the ultrashort time scale. The Stokes line shows some dip, but the anti-Stokes does not. This phenomenon is also confirmed with other samples as well, shown in Fig. 7-5. As we pointed out in the text that the difference between the parametric and non-parametric processes. This difference may actually shows the life time of the virtual state we mentioned there, or it may be a method to look at the virtual state. The fast population removing from the ground state affects these two different frequency components. Further research on this will help to understand the ultrashort laser interaction with medium. At the same time, this temporal character can be used to diagnose the femtosecond laser pulse as well.

In this dissertation, I present some of our up to date research results. The first proposed and confirmed tunable femtosecond RDW generation starts drawing attentions of optics society [140]. The femtosecond CARS microscopy itself is really hot topic right now [141]. In addition, I also present more possible applications in this section, which also show that deeper studies are need for better understandings of both the supercontinuum in PCF and the fast CARS/CSRS temporal characteristics. In turn, they will burst the future applications too. In summary, the results shown in this dissertation are important to the femtosecond optics applications, and future developments of these techniques and fundamental physics can be achieved based on our work presented here.

REFERENCES

[1]. G. Steinmeyer, D. H. Sutter, L. Gallmann, N. Matuschek, and U. Keller, "Frontiers in ultrashort pulse generation: Pushing the Limits in Linear and Nonlinear Optics," Science **286**, 1507-1512(1999).

[2]. P. B. Corkum and Z. Chang, "The attosecond revolution," OPN **19**, 24-29 (2008).

[3]. F. Krausz and M. Ivanov, "Attosecond physics," Rev. Mod. Phys. **81**, 163-234 (2009).

[4]. F. Träger, *Springer Handbook of Lasers and Optics* (Springer, 2007).

[5]. M. O. Scully, G. W. Kattawar, R. P. Lucht, T. Opatrny, H. Pilloff, A. Rebane, A. V. Sokolov, and M. S. Zubairy, "FAST CARS: Engineering A Laser Spectroscopic Technique for Rapid Identification of Bacterial Spores," Proc. Natl. Acad. Sci. **99**, 10994-11001 (2002).

[6]. U. Keller, "Recent developments in compact ultrafast lasers," Nature **424**, 831-838 (2003).

[7]. V. Yanovsky, V. Chvykov, G. Kalinchenko, P. Rousseau, T. Planchon, T. Matsuoka, A. Maksimchuk, J. Nees, G. Cheriaux, G. Mourou, and K. Krushelnick, "Ultra-high intensity- 300-TW laser at 0.1 Hz repetition rate," Opt. Express **16**, 2109-2114 (2008).

[8]. E. I. Moses, R. L. McCrory, D. D. Meyerhofer, and C. J. Keane "A new era for high-energy-density physics," OPN **20**, 42-47 (2009).

[9]. Cl. Rulli`ere, *Femtosecond Laser Pulses: Principles and Experiments* 2nd Edition (Springer, 2005).

[10]. G. Cerullo and S. De Silvestri, "Ultrafast optical parametric amplifiers," Rev. Sci. Instrum. **74**, 1-18 (2003).

[11]. T. H. Maiman, "Stimulated optical radiation in ruby," Nature **187**, 493-494 (1960)

[12]. B. E. A. Saleh and M. C. Teich, *Fundamentals of Photonics* 2nd Edition (Wiley-Interscience, 2007).

[13]. A. E. Siegman, *Lasers* (Oxford University Press, 1986).

[14]. O. Svelto, *Principles of Lasers* (Plenum Press, 1998).

[15]. D. H. Auston, “Transverse mode-locking,” IEEE J. Quantum Electron. QE-**4**, 420-422 (1968).

[16]. D. H. Auston, “Forced and spontaneous phase locking of the transverse modes of a He-Ne laser,” IEEE J. Quantum Electron. QE-**4**, 471-473 (1968).

[17]. M. Piché and P.-A. Bélanger, “Transverse mode-locking by short pulse injection in large aperture TEA CO_2 oscillators,” Appl. Opt. **19**, 127-135 (1980).

[18]. A. G. Fox and T. Li, “Resonant modes in an optical maser,” Proc. IRE(Correspondence), **48**, 1904-1905, (1960); “Resonant modes in a maser interferometer,” Bell .Sys. Tech. J., **40**, 453-488, (1961).

[19]. H. Kogelnik and T. Li, “Laser beams and resonators,” Appl. Opt. **5**, 1550-1567 (1966).

[20]. A. E. Siegman, “Unstable optical resonators,” Appl. Opt. **13**, 353-367 (1974).

[21]. E. Goulielmakis, M. Uiberacker, R. Kienberger, A. Baltuska, V. Yakovlev, A. Scrinzi, Th. Westerwalbesloh, U. Kleineberg, U. Heinzmann, M. Drescher, and F. Krausz, “Direct measurement of light waves,” Science **305**, 1267-1269 (2004).

[22]. K. L. Sala, G. A. Kenney-Wallace, and G. E. Hall, “CW autocorrelation measurements of picosecond laser pulses,” IEEE J. Quantum Electron. **16**, 990-996 (1980).

[23]. R. Trebino, *Frequency-Resolved Optical Gating* (Kluwer Academic, 2002).

[24]. C. Iaconis and I. A. Walmsley, “Spectral phase interferometry for direct electric-field reconstruction of ultrashort optical pulses,” Opt. Lett. **23**, 792-794 (1998).

[25]. K. C. Chu, J. P. Heritage, R. S. Grant, K. X. Liu, A. Dienes, W. E. White, and A. Sullivan, “Direct measurement of the spectral phase of femtosecond pulses,” Opt. Lett. **20**, 904-906 (1995).

[26]. M. A. Franco, H. R. Lange, J.-F. Ripoche, B. S. Prade, and A. Mysyrowicz, “Characterization of ultrashort pulses by cross-phase modulation,” Opt. Comm. **140**, 331-40 (1997).

[27]. H. Lange, M. Franco, J-F. Ricpoche, B. Prade, P. Rousseau, and A. Mysyrowicz, "Reconstruction of the time profile of femtosecond laser pulses through cross-phase modulation," IEEE J. Sel. Top. Quantum Electron. **4**, 295-300 (1998).

[28]. C. W. Siders, J. L. W. Siders, F. G. Omenetto and A. J. Taylor, "Multi-pulse interferometric frequency resolved optical gating," IEEE J. Quantum Electron. **35**, 432-440 (1999).

[29]. M. E. Anderson, L. E. E. de Araujo, E. M. Kosik, and I. A. Walmsley, "The effects of noise on ultrashort-optical-pulse measurement using SPIDER," Appl. Phys. B **70**, S85-S93 (2000).

[30]. T. Brabec and F. Krausz, "Nonlinear optical pulse propagation in the single-cycle regime," Phys. Rev. Lett. **78**, 3282-3285 (1997).

[31]. S. T. Cundiff, "Phase stabilization of ultrashort optical pules," J. Phys. D: Appl. Phys. **35**, R43-R59 (2002).

[32]. J. Ye and S. T. Cundiff, *Femtosecond Optical Frequency Comb: Principle, Operation, and Applications* (Springer, 2004).

[33]. F Gires and P Tournois, "Interferometre utilisable pour la compression d'impulsions lumineuses modulees en frequence," C R Acad Sci Paris **258**, 6112-6115 (1964).

[34]. J. A. Giordmaine, M. A. Duguaym, and J. W. Hansen, "Compression of optical pulse," IEEE J. Quantum Electron. **4** 252-255 (1968).

[35]. F. X. Kaertner, *Few-Cycle Laser Pulse Generation and Its Applications*, Vol. 95 of Topics in Applied Physics (Springer, 2004).

[36]. E. B. Treacy, "Compression of picosecond light pulses," Phys. Lett. A **28**, 34-35 (1968).

[37]. R. L. Fork, O. E. Martinez, and J. P. Gordon, "Negative dispersion using pairs of prisms," Opt. Lett. **9**, 150-152 (1984).

[38]. R. Szipocs, K. Ferencz, C. Spielmann, and F. Krausz, "Chirped multilayer coatings for broadband dispersion control in femtosecond lasers," Opt. Lett. **19**, 201-203 (1994).

[39]. W. Koechner and M. Bass, *Solid-State Lasers: A Graduate Text* (Springer-Verlag, 2003).

[40]. Y. R. Shen, *The Principles of Nonlinear Optics* (Wiley, 1984).

[41]. P. A. Franken, A. E. Hill, C. W. Peters, and G.Weinreich, "Generation of optical harmonics," Phys. Rev. Lett. **7**, 118-119 (1961).

[42]. C. V. Raman, "A new radiation," Indian J. Phys. **2**, 387 (1928); C. V. Raman and K. S. Krishnan, "A new type of secondary radiation," Nature **121**, 501-502 (1928).

[43]. A. Kastler, "Optical methods for studying hertzian resonances," Science **158**, 214-221 (1967).

[44]. R. W. Boyd, *Nonlinear Optics* (Academic Press, 2003).

[45]. J. D. Jackson, *Classical Electrodynamics* (Wiley, 1998).

[46]. L. D. Landau and E. M. Lifshitz, *Electrodynamics of Continuous Media* (Addison-Wesley, 1960).

[47]. M. Born and E. Wolf, *Principles of Optics* 7th Edition (Cambridge University Press, 1999).

[48]. T. Dauxois and M. Peyrard, *Physics of Solitons* (Cambridge University Press, 2006).

[49]. L. F. Mollenauer, R. H. Stolen, and J. P. Gordon, "Experimental observation and picosecond pulse narrowing and solitons in optical fibers," Phys. Rev. Lett. **45**, 1095-1098 (1980).

[50]. J. C. Bronski, M. Segev and M. I. Weinstein, "Mathematical frontiers in optical solitons," Proc. Natl. Acad. Sci. USA **98**, 12872-12873 (2001).

[51]. P. K. A. Wai, C. R. Menyuk, Y. C. Lee, and H. H. Chen, "Nonlinear pulse propagation in the neighborhood of the zero-dispersion wavelength of monomode optical fibers," Opt. Lett. **11**, 464-466 (1986).

[52]. N. Akhmediev and M. Karlsson, "Cherenkov radiation emitted by solitons in optical fibers," Phys. Rev. A **51**, 2602-2607 (1995).

[53]. A. Newell and J. Moloney, *Nonlinear Optics* (Westview Press, 2003).

[54]. W. Koechner, *Solid-State Laser Engineering* 6th Edition (Springer, 2006).

[55]. J. Yao, *Nonlinear Optical Frequency Conversion and Laser Tuning Technology* (Science Press, 1995) (in Chinese).

[56]. http://www.coherent.com/downloads/FAPandVerdiWhitepaperfinal.pdf

[57]. P. F. Moulton, "Spectroscopic and laser characteristics of Ti:Al_2O_3," J. Opt. Soc. Am. B **3**, 125-133 (1986).

[58]. H. A. Haus, "Mode-locking of laser," IEEE J. Sel. Top. Quantum Electron. **8**, 1173-1185 (2000).

[59]. R. L. Fork, C. H. Brito Cruz, P. C. Becker, and C. V. Shank, "Compression of optical pulses to six femtoseconds by using cubic phase compensation," Opt. Lett. **12**, 483-485 (1987).

[60]. S. E. Harris, "Electromagnetically induced transparency," Phys. Today **50**, 36-42 (1997).

[61]. M. O. Scully and M. S. Zubairy, *Quantum Optics* (Cambridge University Press, 1997).

[62]. S. Ruhman, A. G. Joly, and K. A. Nelson, "Coherent molecular vibrational motion observed in the time domain through impulsive stimulated Raman scattering," IEEE J. Quantum Electron. **24**, 460-469 (1988).

[63]. A. Leitenstorfer, C. Fürst, A. Laubereau, and W. Kaiser, "Femtosecond carrier dynamics in GaAs far from equilibrium," Phys. Rev. Lett. **76**, 1545-1548 (1996).

[64]. A. Schülzgen, R. Binder, M. E. Donovan, M. Lindberg, K. Wundke, H. M. Gibbs, G. Khitrova, and N. Peyghambarian, "Direct observation of excitonic Rabi oscillations in semiconductors," Phys. Rev. Lett. **82**, 2346-2349 (1999).

[65]. M. Dantus, M. J. Rosker, and A. H. Zewail, "Real-time femtosecond probing of 'transition states' in chemical reactions," J. Chem. Phys. **87**, 2395-2397 (1987).

[66]. M. R. X. de Barros and P. C. Becker, "Two-color synchronously mode-locked femtosecond Ti:sapphire laser," Opt. Lett. **18**, 631-633 (1993).

[67]. H. Y. Shen, R. R. Zeng, Y. P. Zhou, G. F. Yu, C. H. Huang, Z. D. Zeng, W. J. Zhang, and Q. J. Ye, "Comparison of simultaneous multiple wavelength lasing in

various neodymium host crystals at transitions from $^4F_{3/2}$–$^4I_{11/2}$ and $^4F_{3/2}$–$^4I_{13/2}$," Appl. Phys. Lett. **56**, 1937-1938 (1990).

[68]. C. Tian, T. Walther, R. Nicolaescu, X. J. Pan, Y. Liao, and E. S. Fry, "Synchronous, dual-wavelength, injection-seeded amplification of 5-ns pulses in a flash-lamp-pumped Ti:sapphire laser," Opt. Lett. **24**, 1496-1498 (1999).

[69]. Z. Zhang and T. Yagi, "Dual-wavelength synchronous operation of a mode-locked Ti:sapphire laser based on self-spectrum splitting," Opt. Lett. **18**, 2126-2128 (1993).

[70]. G. Imeshev, M. M. Fejer, A. Galvanauskas, and D. Harter, "Generation of dual-wavelength pulses by frequency doubling with quasi-phase-matching gratings," Opt. Lett. **26**, 268-270 (2001).

[71]. A. Leitenstorfer, C. Fürst, and A. Laubereau, "Widely tunable two-color mode-locked Ti:sapphire laser with pulse jitter of less than 2 fs," Opt. Lett. **20**, 916-918 (1995).

[72]. C. J. Zhu, J. F. He, and S. C. Wang, "Generation of synchronized femtosecond and picosecond pulses in a dual-wavelength femtosecond Ti:sapphire laser," Opt. Lett. **30**, 561-563 (2005).

[73]. C. Lin, H. Kogelnik, and L. G. Cohen, "Optical-pulse equalization of low-dispersion transmission in single-mode fibers in the 1.3 - 1.7-Mu m spectral region," Opt. Lett. **5**, 476-478 (1980).

[74]. J. Zhou, G. Taft, C.-P. Huang, M. M. Murnane, H. C. Kapteyn, and I. P. Christov, "Pulse evolution in a broad-bandwidth Ti:sapphire laser," Opt. Lett. **19**, 1149-1151 (1994).

[75]. J. Peng and A. V. Sokolov, "Simple technique for spectral and temporal control of a mode-locked Ti:Sapphire oscillator," J. Mod. Opt. **54**, 2689-2698 (2007).

[76]. J. Peng, F. Zhu, and A. V. Sokolov, "High-order dispersion-resulted tunable multiwavelength femtosecond laser," Opt. Lett. **33**, 1620-1622 (2008).

[77]. H. Qasmi, J. Barre, and T. Dauxois, "Links between nonlinear dynamics and statistical mechanics in a simple one-dimensional model," cond-mat/0407662v1.

[78]. I. P. Christov, M. M. Murnane, H. C. Kapteyn, J. Zhou, and C. Huang, "Fourth-order dispersion-limited solitary pulses," Opt. Lett. **19**, 1465-1467 (1994).

[79]. J. Yao, W. Sheng, and W. Shi, "Accurate calculation of the optimum phase-matching parameters in three-wave interactions with biaxial nonlinear-optical crystals," J. Opt. Soc. Am. B **9**, 891-902 (1992).

[80]. S. T. Cundiff and J. Ye, "Femtosecond optical frequency combs," Rev. Mod. Phys. **75**, 325-342 (2003).

[81]. A. V. Sokolov, D. R. Walker, D. D. Yavuz, G. Y. Yin, and S. E. Harris, "Raman generation by phased and antiphased molecular states," Phys. Rev. Lett. **85**, 562-565 (2000).

[82]. J. D. Joannopoulos, S. G. Johnson, J. N. Winn, and R. D. Meade, *Photonic Crystals: Molding the Flow of Light* 2nd Edition (Princeton University Press, 2008); online version: http://ab-initio.mit.edu/book/.

[83]. E. Yablonovitch and T. J. Gmitter, "Photonic band structure: The Face-centered-cubic Case," Phys. Rev. Lett. **63**, 1950-1953 (1989).

[84]. E. Yablonovitch, "Photonic crystals: What's in a Name?," OPN, **18**, 12-13 (2007)

[85]. Lord Rayleigh, "On the maintenance of vibrations by forces of double frequency, and on the propagation of waves rhrough a medium endowed with a periodic structure," Phil. Mag. S.5. **24** (147), 145-159 (1887).

[86]. Lord Rayleigh, "On the remarkable phenomenon of crystalline reflexion described by Professor Stokes," Phil. Mag. S.5. **26** (160), 256-265 (1888).

[87]. P. St. J. Russell, "Photonic crystal fibers," Science **299**, 358-362 (2003).

[88]. P. St. J. Russell, "Photonic crystal fibers," J. Lightwave. Technol. **24**, 4729-4749 (2007).

[89]. E. Yablonovitch, "Photonic band-gap structures," J. Opt. Soc. Am. B **10**, 283-295 (1993).

[90]. P. Yeh, A. Yariv, and E. Marom, "Theory of Bragg fiber," J. Opt. Soc. Am. **68**, 1196-1201 (1978).

[91]. T. A. Birks, P. J. Roberts, P. S. J. Russell, D. M. Atkin, and T. J. Shepherd, "Full 2-D photonic bandgaps in silica/air structures," Electron Lett., **31**, 1941-1943 (1995).

[92]. M. D. Nielsen and N. A. Mortensen, "Photonic crystal fiber design based on the V- parameter," Opt. Express, **11**, 2762-2768 (2003).

[93]. B. T. Kuhlmey, R. C. McPhedran, and C. M. de Sterke, "Modal cutoff in microstructured optical fibers," Opt. Lett. **27**, 1684 (2002).

[94]. A. Ferrando, E. Silvestre, J. J. Miret, P. Andrs, and M. V. Andrs, "Full-vector analysis of a realistic photonic crystal fiber," Opt. Lett. **24**, 276-278 (1999).

[95]. T. A. Birks, J. C. Knight, and P. S. J. Russell, "Endlessly single-mode photonic crystal fiber," Opt. Lett. **22**, 961-963 (1997).

[96]. J. C. Knight, J. Arriaga, T. A. Birks, A. Ortigosa-Blanch, W. J. Wadsworth, P. St. J. Russell, "Anomalous dispersion in photonic crystal fiber," IEEE Photon. Technol. Lett. **11**, 674-676 (1999).

[97]. F. Benabid, J.C. Knight, G. Antonopoulos, and P. St. J. Russell, "Stimulated Raman scattering in hydrogen-filled hollow-core photonic crystal fiber," Science **298**, 399-402 (2002).

[98]. J. Herrmann, U. Griebner, N. Zhavornokov, A. Husakow, D. Nickel, J. C. Knight, W. J. Wadsworth, P. St. J. Russell, and G. Korn, "Experimental evidence for supercontinuum generation by fission of higher-order solitons in photonic fibers," Phys. Rev. Lett. **88**, 173901 (2002).

[99]. J. K. Ranka, R. S. Windeler and A. J. Stentz, "Visible continuum generation in air-silica microstructure optical fibers with anomalous dispersion at 800 nm," Opt. Lett. **25**, 25-27 (2000).

[100]. F. Benabid, F. Biancalana, P. S. Light, F. Couny, A. Luiten, P. J. Roberts, J. Peng, and A. V. Sokolov, "Fourth-order dispersion mediated solitonic radiations in HC-PCF cladding," Opt. Lett. **33**, 2680-2682 (2008).

[101]. N. Ishii, C. Y. Teisset, S. Koehler, E. E. Serebryannikov, T. Fuji, T. Metzger, F. Krausz, A. Baltuska, and A. M. Zheltikov. “Widely tunable soliton frequency shifting of few-cycle laser pulses,” Phys. Rev. E **74**, 036617 (2006).

[102]. C. Desem and P. L. Chu, “Effect of chirping on solution propagation in single-mode optical fibers,” Opt. Lett. **11**, 248-250 (1986).

[103]. J. M. Dudley, G. Genty, and S. Coen, “Supercontinuum generation in photonic crystal fiber,” Rev. Mod. Phys. **78**, 1135-1184 (2006).

[104]. S. V. Smirnov, J. D. Ania-Castanon, T. J. Ellingham, S. M. Kobtsev, S. Kukarin, and S. K. Turitsyn, “Optical spectral broadening and supercontinnum generation in telecom applications,” Opt. Fiber Technol. **12**, 122-147 (2006).

[105]. A. M. Zheltikov, “Microstructure-fiber frequency converters,” Laser Phys. Lett. **1**, 220-233 (2004).

[106]. K. M. Hilligsøe, H. N. Paulsen, J. Thøgersen, S. R. Keiding, and J. J. Larsen, “Initial steps of supercontinuum generation in photonic crystal fibers,” J. Opt. Soc. Am. B **20**, 1887-1893 (2003).

[107]. D. V. Skryabin, F. Luan, J. C. Knight, P.St.J. Russell, “Soliton self-frequency shift cancelation in photonic crystal fibers,” Science **301**, 1705-1708 (2003).

[108]. A. V. Gorbach, D. V. Skryabin, “Light trapping in gravity-like potentials and expansion of supercontinuum spectra in photonic-crystal fibres,” Nature Photon. **1**, 653-657 (2007).

[109]. F. G. Omenetto, N. A. Wolchover, M. R. Wehner, M. Ross, A. Efimov, A. J. Taylor, V. V. R. K. Kumar, A. K. George, J. C. Knight, N. Y. Joly, and P. St. J. Russell, “Spectrally smooth supercontinuum from 350 nm to 3 μm in sub-centimeter lengths of soft-glass photonic crystal fibers,” Opt. Express **14**, 4928-4934 (2006).

[110]. A. Apolonski, B. Povazay, A. Unterhuber, W. Drexler, W. J. Wadsworth, J. C. Knight, and P. St. J. Russell, “Spectral shaping of supercontinuum in a cobweb photonic-crystal fiber with sub-20-fs pulses,” J. Opt. Soc. Am. B **19**, 2165-2170 (2002).

[111]. F. Couny, F. Benabid, P.J. Roberts, P.S. Light, and M.G. Raymer, “Generation and photonic guidance of multi-octave optical-frequency combs,” Science **318**, 1118-1121 (2007).

[112]. W. H. Reeves, D. V. Skryabin, F. Biancalana, J. C. Knight, P. St. J. Russell, F. G. Omenetto, A. Efimov and A. J. Taylor, “Transformation and control of ultra-short pulses in dispersion-engineered photonic crystal fibres,” Nature **424**, 511-515 (2003).

[113]. A. Hasegawa and W. F. Brinkman, “Tunable coherent IR and FIR sources utilizing modulation instability,” Quantum Electron. Lett. **16**, 694-697 (1980).

[114]. A. Proulx, J.-M. Ménard, N. Hô, J. Laniel, R. Vallée, and C. Paré, “Intensity and polarization dependences of the supercontinuum generation in birefringent and highly nonlinear microstructured fibers,” Opt. Express **11**, 3338-3345 (2003).

[115]. M. Tianprateep, J. Tada, and F. Kannari, “Influence of polarization and pulse shape of femtosecond initial laser pulses on spectral broadening in microstructure fibers,” Opt. Rev. **12**, 179–189 (2005).

[116]. P. St. J. Russell, “Bloch wave analysis of dispersion and pulse propagation in pure distributed feedback structures,” J. Mod. Opt. **38**, 1599-1619 (1991).

[117]. C.-M. Chen, and P. L. Kelley, “Nonlinear pulse compression in optical fibers: scaling laws and numerical analysis,” J. Opt. Soc. Am. B **19**, 1961-1967 (2002).

[118]. R. R. Alfano, *The Supercontinuum Laser Source* 2nd Edition (Springer-Verlag, 1989).

[119]. R.L.Byer and R.L. Herbst, *Parametric Oscillation and Mixing* in: Y.R. Shen (Ed.), Topics in Applied Physics, Nonlinear Infrared Generation, 16, (Springer, 1977).

[120]. Yu. A. Il’inskii and L. V. Keldysh, *Electromagnetic Response of Material Media* (Plenum, 1994),

[121]. R. Leonhardt, W. Holzapfel, W. Zinth, and W. Kaiser, “Terahertz quantum beats in molecular liquids,” Chem. Phys. Lett. **133**, 373-377 (1987).

[122]. M. D. Duncan, J. Reintjes, and T. J. Manuccia, “Scanning coherent anti-Stokes Raman microscope,” Opt. Lett. **7**, 350-352 (1982).

[123]. M. Muller and A. Zumbusch, “Coherent anti-Stokes Raman scattering microscopy,” ChemPhysChem **8**, 2157-2170 (2007).

[124]. D. Pestov, R. K. Murawski, G. O. Ariunbold, X. Wang, M. C. Zhi, A. V. Sokolov, V. A. Sautenkov, Y. V. Rostovtsev, A. Dogariu, Y. Huang, and M. O. Scully, “Optimizing the laser-pulse configuration for coherent Raman spectroscopy,” Science **316**, 265-268 (2007).

[125]. J. Peng, D. Pestov, M.O. Scully, and A.V. Sokolov, “Simple setup for hybrid coherent Raman microspectroscopy,” J Raman Spectrosc. **40,** 795-799 (2009).

[126]. G. I. Petrov, V. V. Yakovlev, A. V. Sokolov, and M. O. Scully, “Detection of *Bacillus subtilis* spores in water by means of broadband coherent anti-Stokes Raman spectroscopy,” Opt. Express **13**, 9537-9542 (2005).

[127]. S. Roy, T. R. Meyer, and J. R. Gord, “Time-resolved dynamics of resonant and nonresonant broadband picosecond coherent anti-Stokes Raman scattering signals,” Appl. Phys. Lett. **87**, 264103 (2005).

[128]. B. D. Prince, A. Chakraborty, B. M. Prince, and H. U. Stauffer, “Development of simultaneous frequency- and time-resolved coherent anti-Stokes Raman scattering for ultrafast detection of molecular Raman spectra,” J. Chem. Phys. **125**, 044502 (2006).

[129]. H. Kano and H. Hamaguchi “Dispersion-compensated supercontinuum generation for ultrabroadband multiplex coherent anti-Stokes Raman scattering spectroscopy,” J Raman Spectrosc. **37**, 411-415 (2006).

[130]. G. I. Petrov, R. Arora, V. V. Yakovlev, X. Wang, A. V. Sokolov, and M. O. Scully, “Comparison of coherent and spontaneous Raman microspectroscopies for noninvasive detection of single bacterial endospores,” Proc. Natl. Acad. Sci. USA **104**, 7776-7779 (2007).

[131]. A. V. Sokolov, M. Y. Shverdin, D. R. Walker, D. D. Yavuz, A. Burzo, G. Y. Yin, and S. E. Harris, "Generation and control of femtosecond pulses by molecular modulation," J. Mod. Opt. **52**, 285-304 (2005).

[132]. I. N. Ross, P. Matousek, M. Towrie, A. J. Langley, and J. L. Collier, "The prospect for ultrashort pulse duration and ultrahigh intensity using optical parametric chirped pulse amplifiers," Opt. Commun. **144**, 125-133 (1997).

[133]. X. Yang, Z. Xu, Y. Leng, H. Lu, L. Lin, Z. Zhang, R. Li, W. Zhang, D. Yin, and B. Tang, "Multiterawatt laser system based on optical parametric chirped pulse amplification," Opt. Lett. **27**, 1135-1137 (2002).

[134]. S. Mukamel, *Principles of Nonlinear Optical Spectroscopy* (Oxford University Press, 1995).

[135]. J.-X. Cheng, A. Volkmer, and X. S. Xie, "Theoretical and experimental characterization of coherent anti-Stokes Raman scattering microscopy," J. Opt. Soc. Am. B. **19**, 1363-1375 (2002).

[136]. A. Volkmer, J.-X. Cheng, and X. S. Xie, "Vibrational imaging with high sensitivity via epidetected coherent anti-Stokes Raman scattering microscopy," Phys. Rev. Lett. **87**, 023901 (2001).

[137]. A. Weippert, J.-M. Funk, A. Materny, and W. Kiefer, "Experimental verification of backscattering CARS spectroscopy on opaque media," J Raman Spectrosc. **24**, 705-708 (1993).

[138]. K. A. Nelson and E. P. Ippen, "Femtosecond coherent spectroscopy," in I. Prigogine and S.A. Rice (Ed.), Adv. in Chem. Phys. **LXXV**, 1-35 (1988).

[139]. T. Joo, M. A. Dugan and A. C. Albrecht, "Time-resolved coherent Stokes Raman spectroscopy (CSRS) of benzene," Chem. Phys. Lett. **177**, 4-10 (1991).

[140]. S. Roy, S. K. Bhadra, and G. P. Agrawal, "Effects of higher-order dispersion on resonant dispersive waves emitted by solitons," Opt. Lett. **34**, 2072-2074 (2009).

[141]. A. Volkmer, P. P. Radi, A. M. Zheltikov, and A. Zumbusch, "New trends and recent advances in coherent Raman microscopy and nonlinear optical

spectroscopy: Introduction to the special issue," J Raman Spectrosc. **40**, 712-713 (2009).

VITA

Name: Jiahui Peng

Address: Texas A&M University, Physics Department,
College Station, TX 77843-4242

Email Address: pengjiahui@tamu.edu

Education: B.S., Applied Optics, Nankai University, 1998
M.S., Optics, Shanghai Institute of Optics & Fine Mechanics, 2002

Memberships: Optical Society of America
Institute of Electrical and Electronics Engineers

Awards: First Prize, National Science and Technology Progress Award 2004
First Prize, Shanghai Science and Technology Progress Award 2003

Publications:

1. J. Peng, D. Pestov, M.O. Scully, & A.V. Sokolov, "Simple setup for hybrid coherent Raman microspectroscopy," Journal of Raman Spectroscopy **40,** 795-799 (2009).
2. J. Peng, F. Zhu & A.V. Sokolov, "High-order dispersion-resulted tunable multiwavelength femtosecond laser," Optics Letters **33,** 1620-1622 (2008).
3. F. Benabid, F. Biancalana, P. S. Light, F. Couny, A. Luiten, P. J. Roberts, J. Peng, & A.V. Sokolov, "Fourth-order dispersion mediated solitonic radiations in HC-PCF cladding," Optics Letters **33**, 2680-2682 (2008).
4. J. Peng & A.V. Sokolov, "Simple technique for spectral and temporal control of a mode-locked Ti:Sapphire oscillator," Journal of Modern Optics **54,** 2689-2698 (2007).
5. J. Peng, D. Pestov, M.O. Scully, & A.V. Sokolov, "Coherent Raman Micro-Spectroscopy with a Mode-Locked Ti:Sapphire Oscillator," CLEO/QELS 2008 (paper CThE6) (*Optical Society of America Incubic/Milton Chang Student Travel Award*).
6. J. Peng & A.V. Sokolov, "Double Femtosecond Pulses Mode-Locked Ti:Sapphire Oscillator," Frontiers in Optics 2007/Laser Science XXIII (in Laser Science, OSA Technical Digest (CD) (Optical Society of America, 2007), paper LTuJ2).